



National Library
of Canada

Bibliothèque nationale
du Canada

Canadian Theses Service

Services des thèses canadiennes

Ottawa, Canada
K1A 0N4

CANADIAN THESES

NOTICE

The quality of this microfiche is heavily dependent upon the quality of the original thesis submitted for microfilming. Every effort has been made to ensure the highest quality of reproduction possible.

If pages are missing, contact the university which granted the degree.

Some pages may have indistinct print especially if the original pages were typed with a poor typewriter ribbon or if the university sent us an inferior photocopy.

Previously copyrighted materials (journal articles, published tests, etc.) are not filmed.

Reproduction in full or in part of this film is governed by the Canadian Copyright Act, R.S.C. 1970, c. C-30. Please read the authorization forms which accompany this thesis.

**THIS DISSERTATION
HAS BEEN MICROFILMED
EXACTLY AS RECEIVED**

THÈSES CANADIENNES

AVIS

La qualité de cette microfiche dépend grandement de la qualité de la thèse soumise au microfilmage. Nous avons tout fait pour assurer une qualité supérieure de reproduction.

S'il manque des pages, veuillez communiquer avec l'université qui a conféré le grade.

La qualité d'impression de certaines pages peut laisser à désirer, surtout si les pages originales ont été dactylographiées, à l'aide d'un ruban usé ou si l'université nous a fait parvenir une photocopie de qualité inférieure.

Les documents qui font déjà l'objet d'un droit d'auteur (articles de revue, examens publiés, etc.) ne sont pas microfilmés.

La reproduction, même partielle, de ce microfilm est soumise à la Loi canadienne sur le droit d'auteur, SRC 1970, c. C-30. Veuillez prendre connaissance des formules d'autorisation qui accompagnent cette thèse.

**LA THÈSE A ÉTÉ
MICROFILMÉE TELLE QUE
NOUS L'AVONS REÇUE**



54

National Library
of CanadaOttawa, Canada
K1A 0N4Bibliothèque nationale
du Canada

TC -

IS

0-315-23252-8

CANADIAN THESES ON MICROFICHE SERVICE - SERVICE DES THÈSES CANADIENNES SUR MICROFICHE

PERMISSION TO MICROFILM - AUTORISATION DE MICROFILMER

• Please print or type - Écrire en lettres moulées ou dactylographier

AUTHOR - AUTEUR

Full Name of Author - Nom complet de l'auteur

GLEN WARREN ROVANG

Date of Birth - Date de naissance

March 27, 1960

Canadian Citizen - Citoyen canadien

☒ Yes / Oui☐ No / Non

Country of Birth - Lieu de naissance

Canada

Permanent Address - Résidence fixe

Box 722
Peace River, Alberta
T0H 2X0

THESIS - THÈSE

Title of Thesis - Titre de la thèse

An Experimental Investigation of a closed-Loop
Two-Phase Thermosyphon System for Low Grade
Heat Recovery from Liquid Heat SourcesDegree for which thesis was presented
Grade pour lequel cette thèse fut présentée

M. Sc. Mechanical Engineering

Year this degree conferred
Année d'obtention de ce grade

1985

University - Université

University

Name of Supervisor - Nom du directeur de thèse

K.C. Cheng

AUTHORIZATION - AUTORISATION

Permission is hereby granted to the NATIONAL LIBRARY OF CANADA to
microfilm this thesis and to lend or sell copies of the film.The author reserves other publication rights, and neither the thesis nor exten-
sive extracts from it may be printed or otherwise reproduced without the
author's written permission.L'autorisation est, par la présente, accordée à la BIBLIOTHÈQUE NATIONALE
DU CANADA de microfilmer cette thèse et de prêter ou de vendre des ex-
emplaires du film.L'auteur se réserve les autres droits de publication; ni la thèse ni de longs ex-
traits de celle-ci ne doivent être imprimés ou autrement reproduits sans
l'autorisation écrite de l'auteur.

ATTACH FORM TO THESIS - VEUILLEZ JOINDRE CE FORMULAIRE À LA THÈSE

Signature

Date

Glen Rovang

JUL 12 / 85

NL-91 (r. 84/03)

Canada

3
THE UNIVERSITY OF ALBERTA

6
An Experimental Investigation of a Closed-Loop Two-Phase
Thermosyphon System for Low Grade Heat Recovery from Liquid
Heat Sources

by



Glen W. Rovang

A THESIS

SUBMITTED TO THE FACULTY OF GRADUATE STUDIES AND RESEARCH
IN PARTIAL FULFILMENT OF THE REQUIREMENTS FOR THE DEGREE
OF Master of Science

Department of Mechanical Engineering

EDMONTON, ALBERTA

Fall 1985

THE UNIVERSITY OF ALBERTA

RELEASE FORM

NAME OF AUTHOR Glen W. Rovang
TITLE OF THESIS An Experimental Investigation of a
Closed-Loop Two-Phase Thermosyphon
System for Low Grade Heat Recovery from
Liquid Heat Sources

DEGREE FOR WHICH THESIS WAS PRESENTED Master of Science

YEAR THIS DEGREE GRANTED Fall 1985

Permission is hereby granted to THE UNIVERSITY OF ALBERTA LIBRARY to reproduce single copies of this thesis and to lend or sell such copies for private, scholarly or scientific research purposes only.

The author reserves other publication rights, and neither the thesis nor extensive extracts from it may be printed or otherwise reproduced without the author's written permission.

(SIGNED)

Glen W. Rovang.....

ADDRESS: Box 722

Peace River, Alberta

T0H 2X0

DATED June 14, 1985

THE UNIVERSITY OF ALBERTA

FACULTY OF GRADUATE STUDIES AND RESEARCH

The undersigned certify that they have read, and recommend to the Faculty of Graduate Studies and Research, for acceptance, a thesis entitled An Experimental Investigation of a Closed-Loop Two-Phase Thermosyphon System for Low Grade Heat Recovery from Liquid Heat Sources submitted by Glen W. Rovang in partial fulfilment of the requirements for the degree of Master of Science.


.....*K. C. Cheng*.....
Supervisor

.....*Gerald W. Sadler*.....

.....*M. J. Anderson*.....

Date.....*June 14, 1985*.....

8



To My Parents
Don and Jessie Rovang

Abstract

The steady state operating and heat transfer characteristics of a closed loop thermosyphon system for low grade heat recovery are examined with three types of working fluid; liquid phase water, two-phase water, and two-phase refrigerant R-113. The effects of external operating parameters such as heat source temperature, cooling water flow rate, initial liquid charge level, and liquid-vapor separator are studied. Forced flow tests with the liquid phase system were carried out for comparison purposes.

Results presented include an evaluation of system performance and heat exchanger behaviour for each case tested. As well, evaporator convective boiling is discussed and flow visualization photographs of the flow regimes encountered in the evaporator tube and condenser shell are presented. Heat transfer results for the evaporator tube were found to correlate well with inverse Graetz parameter for liquid-phase and low quality two-phase water flow.

Overall results indicate that the refrigerant charged system offers the best performance for the low heat source temperature range tested. It was found to operate most efficiently when the flow at the evaporator exit was composed of saturated vapor - without superheating. Problems encountered which were detrimental to heat recovery were condenser flooding and primary loop flow restrictions.

Acknowledgement

The author wishes to express his sincere gratitude to Dr. K.C. Cheng, project supervisor, for his assistance during the course of this study, and for his enthusiasm towards this work.

Many hours of discussion with fellow graduate student Bjorn Ystad and his useful advice have contributed immeasurably to this study.

As always, the technical staff and machinists of the Department of Mechanical Engineering headed by Tom Villet and Al Muir provided work of excellent quality during the construction of the experimental apparatus. Special thanks go to Terry Nord for his assistance with electronic instrumentation.

Financial aid from the Natural Sciences and Engineering Research Council of Canada under a strategic grant is greatly appreciated.

Table of Contents

Chapter	Page
1. Introduction	1
1.1 Background	1
1.2 The Thermosyphon Principle and Applications	3
1.3 Scope of the Study	7
2. Closed Loop Single-Phase Water Thermosyphon and Forced Flow Tests	9
2.1 Introduction	9
2.2 Experimental Apparatus	10
2.3 Instrumentation	15
2.4 Experimental Procedure	17
2.5 Data Analysis	20
2.6 Thermosyphon Flow Results and Discussion	27
2.6.1 Overall System Characteristics	27
2.6.2 Lower Heat Exchanger	38
2.6.3 Upper Heat Exchanger	45
2.7 Forced Flow Results and Discussion	53
2.8 Conclusion	60
3. Closed Loop Two-Phase Water Thermosyphon Tests	65
3.1 Introduction	65
3.2 Experimental Apparatus and Instrumentation	66
3.3 Experimental Procedure	68
3.4 Data Analysis	69
3.5 Results and Discussion	72
3.5.1 Overall System Characteristics	72
3.5.2 Upper and Lower Heat Exchangers	80
3.5.3 Evaporator Convective Boiling	83

3.6 Conclusion	89
4. Closed Loop Two-Phase Refrigerant R-113 Thermosyphon Tests	91
4.1 Introduction	91
4.2 Experimental Apparatus and Instrumentation	92
4.3 Experimental Procedure	94
4.4 Data Analysis	96
4.5 Results and Discussion	98
4.5.1 Overall System Characteristics	98
4.5.2 System Efficiency	111
4.5.3 Evaporator Convective Boiling	115
4.5.4 Primary Loop Flow and Pressure Instabilities	118
4.5.5 Convective Boiling Pressure Drop	129
4.5.6 Flow Visualization	139
4.6 Conclusion	144
5. Concluding Remarks	155
References	159
Appendix I	163
Appendix II	171
Appendix III	173

List of Tables

Table	Page
2.1 Heat Exchanger Dimensions	15
4.1 Properties of Refrigerant R-113	92
4.2 Kandlikar Correlation Coefficients	99
4.3 Heat Recovery with Different Working Fluids	111

List of Figures

Figure	Page
2.1 Schematic diagram of experimental apparatus	11
2.2 Print of lower heat exchanger cross-section	14
2.3 Data acquisition flow chart	18
2.4 Relationship between heat extraction and heat input	29
2.5 Effect of system temperature difference on overall heat recovery	29
2.6 Effect of system temperature difference on total thermosyphon mass flow rate	32
2.7 Effect of average input heat flux on total thermosyphon mass flow rate	32
2.8 Total thermosyphon mass flux at lower heat exchanger inlet	33
2.9 Effect of working fluid Reynolds number at lower heat exchanger inlet on system effectiveness	35
2.10 Comparison of system heat recovery and effectiveness	35
2.11 System thermodynamic efficiency vs. working fluid Reynolds number	37
2.12 Effect of input heat flux on thermodynamic efficiency	37
2.13 Arithmetic mean overall heat transfer coefficient for lower heat exchanger	39
2.14 Logarithmic mean overall heat transfer coefficient for lower heat exchanger	39
2.15 Dean number effect on arithmetic mean overall heat transfer coefficient	41
2.16 Dean number effect on logarithmic mean overall heat transfer coefficient	41

Figure	Page
2.17 Effect of thermosyphon flow rate on heat exchanger effectiveness	42
2.18 Average Nusselt number vs. Dean number in lower heat exchanger coil	42
2.19 Comparison of Nusselt number with coiled tube correlation	44
2.20 Inverse Graetz number effect on average Nusselt number for thermosyphon flow in the lower heat exchanger	44
2.21 Correlation of Nusselt number with modified inverse Graetz parameter	46
2.22 Reynolds number vs Rayleigh number for flow regime determination	46
2.23 Arithmetic mean overall heat transfer coefficient for the upper heat exchanger	48
2.24 Logarithmic mean heat transfer coefficient for the upper heat exchanger	48
2.25 Dean number effect on arithmetic mean overall heat transfer coefficient	49
2.26 Dean number effect on logarithmic mean overall heat transfer coefficient	49
2.27 Effect of Dean number on tube side Nusselt number in the upper heat exchanger	50
2.28 Effect of inverse Graetz parameter on Nusselt number for tube side flow	50
2.29 Fin side heat transfer coefficient vs. thermosyphon mass flow rate for upper heat exchanger	52
2.30 Upper heat exchanger effectiveness vs. thermosyphon mass flow rate	52
2.31 Reynolds number vs. Rayleigh number for flow regime comparison	54
2.32 Ratio of curved to straight tube pressure drop for upper heat exchanger coil	54

Figure	Page
2.33 Relationship between heat recovery and heat input for forced flow conditions	56
2.34 Effect of system temperature difference on overall heat recovery	56
2.35 Effect of forced flow Reynolds number on system effectiveness	58
2.36 Effect of input heat flux on thermodynamic efficiency	58
2.37 System thermodynamic efficiency vs. forced flow Reynolds number	59
2.38 Arithmetic mean overall heat transfer coefficient for lower heat exchanger with forced flow conditions	59
2.39 Effect of forced flow Dean number on Nusselt number for inner coiled tube	61
2.40 Lower heat exchanger Nusselt number vs. modified inverse Graetz parameter for forced flow	61
2.41 Arithmetic mean heat transfer coefficient for upper heat exchanger	62
2.42 Fin side heat transfer coefficient vs. forced primary loop mass flow rate	62
3.1 Effect of cooling water flow rate on Q_2 vs. $T_h - T_c$ with 70% charge level and downcomer closed	75
3.2 Effect of charge level on Q_2 vs. $T_h - T_c$ with $V_c = 30$ ml/s and downcomer closed	75
3.3 Effect of downcomer on Q_2 vs. $T_h - T_c$ with 20% charge level and $V_c = 70$ ml/s	76
3.4 Evaporator tube inlet mass flux vs. wall heat flux with 20% charge level and open downcomer	76
3.5 Effect of charge level on G_1 vs. q_1 with $V_c = 10$ ml/s and closed downcomer	77

Figure	Page
3.6 Effect of downcomer on G_1 vs. q_1 with 20% charge level and $V_c = 70$ ml/s	77
3.7 Evaporator exit vapor quality vs. heat flux with 70% charge level and closed downcomer	78
3.8 Heat recovered vs. condenser shell side vapor quality with 70% charge level and closed downcomer	78
3.9 System efficiency vs. input heat flux with 70% charge level and open downcomer	79
3.10 Effect of charge level on η vs. q_1 with $V_c = 10$ ml/s and closed downcomer	79
3.11 Examples of fluctuating phenomena for 20% charge level, $T_h = 75^\circ\text{C}$, $V_c = 30$ ml/s, and downcomer open	81
3.12 Effect of charge level on U_1 vs. q_1 with closed downcomer and $V_c = 10$ ml/s	82
3.13 Effect of downcomer on U_1 vs. q_1 with 20% charge level and $V_c = 30$ ml/s	82
3.14 Effect of cooling water flow rate on U_2 vs. x_2 with 70% charge level and open downcomer	84
3.15 Effect of charge level on U_2 vs. x_2 with closed downcomer and $V_c = 70$ ml/s	84
3.16 Effect of downcomer on U_2 vs. x_2 with 70% charge level and $V_c = 70$ ml/s	85
3.17 Comparison of experimental evaporator heat transfer coefficient with single phase component correlation	85
3.18 Comparison of experimental evaporator heat transfer coefficient with Shah correlation	87
3.19 Comparison of experimental evaporator heat transfer coefficient with Shrock-Grossman correlation	87

Figure	Page
3.20 Two-phase water Nu_1 vs. Z_1 with all data and comparison with single phase results	88
3.21 Effect of cooling water flow rate on condenser shell side heat transfer coefficient vs. quality with 70% charge level and closed downcomer	88
4.1 Heat recovery vs. system temperature difference with 20% charge level	100
4.2 Heat recovery vs. system temperature difference with $V_c = 75$ ml/s	100
4.3 Total working fluid mass flux at evaporator inlet for 100% charge level	102
4.4 Effect of evaporator exit quality on total heat recovery for 100% charge level	102
4.5 Evaporator exit quality vs. wall heat flux with 65% charge level	103
4.6 Evaporator exit quality vs. wall heat flux with $V_c = 55$ ml/s	103
4.7 Effect of cooling water flow rate on vapor superheating at evaporator exit with 20% charge level	105
4.8 Effect of charge level on vapor superheating at evaporator exit with $V_c = 55$ ml/s	105
4.9 Evaporator exit quality vs. $(T_w - T_s)$ for $V_c = 55$ ml/s	107
4.10 Effect of $(T_w - T_s)$ on wall heat flux with $V_c = 55$ ml/s	107
4.11 Condenser shell side quality vs. evaporator exit quality for 100% charge level	108
4.12 Condenser shell side quality vs. evaporator exit quality for $V_c = 55$ ml/s	108
4.13 Effect of cooling water flow rate on Q_2 vs. x_2 for 100% charge level	110

Figure	Page
4.14 Effect of charge level on Q_2 vs x_2 with $V_c=55$ ml/s	110
4.15 Effect of cooling water flow rate and input heat flux on efficiency for 20% charge level	112
4.16 Effect of charge level and input heat flux on efficiency with $V_c=75$ ml/s	112
4.17 Effect of cooling water flow rate and flow quality on efficiency for 65% charge level	114
4.18 Effect of charge level and flow quality on efficiency with $V_c=75$ ml/s	114
4.19 Operating region of thermosyphon for isobaric conditions	116
4.20 Ratio of experimental to single phase turbulent evaporator tube heat transfer coefficient vs. inverse Martinelli parameter	117
4.21 Ratio of experimental to single phase turbulent evaporator heat transfer coefficient vs. Boiling number	117
4.22 Comparison of experimental evaporator heat transfer coefficient with Shah correlation	119
4.23 Comparison of experimental evaporator heat transfer coefficient with Shrock-Grossman correlation	119
4.24 Comparison of experimental evaporator heat transfer coefficient with Kandlikar correlation	120
4.25 Primary loop flow and pressure oscillations for 65% charge level, 65°C heat source temperature, and $V_c=25$ ml/s	122
4.26 Frequency spectrum of primary loop flow and pressure oscillations for 65% charge level, 65°C heat source temperature, and $V_c=25$ ml/s	123

4.27	Frequency of downcomer flow fluctuations for 100% charge level	126
4.28	Frequency of condensate flow fluctuations for 65% charge level	126
4.29	Frequency of system pressure fluctuations for 20% charge level	127
4.30	Variance of system pressure signal for 65% charge level	127
4.31	Variance of system pressure signal with evaporator exit quality, all data	128
4.32	Two-phase friction pressure drop through evaporator vs. heat flux for 100% charge level	133
4.33	Two-phase friction pressure drop through evaporator vs. heat flux for $V_c=55$ ml/s	133
4.34	Effect of evaporator exit quality on two-phase frictional pressure drop for 65% charge level	135
4.35	Effect of evaporator exit quality on two-phase frictional pressure drop for $V_c=55$ ml/s	135
4.36	Two-phase pressure drop vs. inverse Martinelli parameter for 100% charge level	137
4.37	Ratio of measured evaporator pressure drop to homogeneous model prediction vs. x_1 for 65% charge level	137
4.38	Ratio of measured evaporator pressure drop to homogeneous model prediction vs. inverse Martinelli parameter for 100% charge level	138
4.39	Transient boiling flow at the evaporator exit for 20% charge level, 85°C heat source, and $V_c=75$ ml/s	146
4.40	Effect of charge level and temperature on evaporator flow regimes with $V_c=25$ ml/s	148

4.41	Effect of cooling water flow rate on evaporator exit flow with 20% charge level and 85°C heat source	149
4.42	Pulsing flow at evaporator exit with 55°C heat source and $V_c = 75$ ml/s	150
4.43	Condenser flooding for 20% charge level and 85°C heat source	151
4.44	Condenser flooding for 100% charge level and 85°C heat source	152
4.45	Flooded condenser for 65% charge level, 85°C heat source, and $V_c = 75$ ml/s	153
4.46	Vapor injection into fully flooded condenser for 100% charge and 85°C heat source	154

Nomenclature

A	inside surface area of heat exchanger coils, m^2
Bo	Boiling number, q_{fg} / Gh_{fg}
Co	Convection number
C_{pl}	specific heat of liquid at constant pressure, $J/kg \text{ } ^\circ K$
C_{pv}	specific heat of vapor at constant pressure, $J/kg \text{ } ^\circ K$
d	inside diameter, m
F_c	curved tube friction factor
F_s	straight smooth tube friction factor, $64/Re$
Fr	Froude number, $G^2 / \rho^2 g d$
f_c	frequency of oscillation of condensate flow, c/s
f_D	frequency of oscillation of downcomer flow, c/s
f_P	frequency of oscillation of system pressure, c/s
f_{th}	homogeneous model two-phase friction factor
G	mass flux, $kg/m^2 s$
G_1	total working fluid mass flux at evaporator entrance, $kg/m^2 s$
Gr	Grashof number, $G \beta (\Delta T) d^3 / \nu^2$
g	gravitational constant, 9.81 m/s^2
h	average heat transfer coefficient, $W/m^2 \text{ } ^\circ C$
h_{exp}	experimentally determined heat transfer coefficient, $W/m^2 \text{ } ^\circ C$
h_{fg}	latent heat of vaporization, J/kg
h_o	fin side heat transfer coefficient of condenser, $W/m^2 \text{ } ^\circ C$
h_{pred}	heat transfer coefficient predicted by a correlation, $W/m^2 \text{ } ^\circ C$
h_s	modified Dittus-Boelter turbulent liquid phase heat transfer correlation, $W/m^2 \text{ } ^\circ C$

h_t	two-phase heat transfer coefficient, $W/m^2\text{ }^\circ C$
K^*	Dean number, $Re(r/R)^{0.5}$
k_f	thermal conductivity of liquid, $W/m\text{ }^\circ C$
l	tube length, m
\dot{m}_c	mass flow rate of cooling water, kg/s
\dot{m}_h	mass flow rate of heating water, kg/s
\dot{m}_1	mass flow rate of working fluid through lower heat exchanger, kg/s
\dot{m}_2	mass flow rate of working fluid through upper heat exchanger, kg/s
Nu	Nusselt number, hd/k
Pe	Peclet number, $RePr$
Pr	Prandtl number, $C_{p1} \mu_f / k_f$
ΔP	measured convective boiling frictional pressure drop
ΔP_t	homogeneous model prediction for convective boiling friction pressure drop
Q_1	rate of heat release by heating fluid, W
Q_2	rate of heat gain by cooling water, W
q	average wall heat flux, Q/A , W/m^2
q_{fg}	average wall heat flux based on latent heat only, W/m^2
R	radius of curvature of coiled tube, m
Ra	Rayleigh number, $GrPr(d/l)$
Re	Reynolds number, Gd/μ_f
r	radius of tube, m
r_h	hydraulic radius, m
s^2	raw variance of oscillating voltage signals, Volts ²
T	temperature, $^\circ C$
T_b	fluid bulk temperature, $^\circ C$

T_s	saturation temperature of working fluid, °C
T_w	wall temperature, °C
ΔT	characteristic temperature difference, °C
U	overall heat transfer coefficient based on arithmetic mean temperature difference, $W/m^2 \cdot ^\circ C$
U_{lm}	overall heat transfer coefficient based on logarithmic mean temperature difference, $W/m^2 \cdot ^\circ C$
V_c	cooling water volumetric flow rate, ml/s
v_p	variance of system pressure oscillations, kPa^2
$X_{t,t}$	Martinelli parameter
x_1	vapor mass quality at evaporator exit
x_2	condenser shell side vapor mass quality
Z	inverse Graetz number in curved tube, $(KPr d/l)^{-1}$
z	axial distance, m
β	coefficient of thermal expansion, $1/^\circ K$
ϵ	heat exchanger effectiveness
η	second law thermodynamic efficiency
μ	absolute viscosity, kg/ms
$\bar{\mu}$	homogeneous absolute viscosity, kg/ms
ν	kinematic viscosity, m^2/s
ρ	density, kg/m^3
$\bar{\rho}$	homogeneous density, kg/m^3

Subscripts

1,2	at evaporator and condenser, respectively
c	cooling stream
f	liquid
g	vapor
h	heating stream

i inlet
o outlet
s single phase
t two-phase

1. Introduction

1.1 Background

Concern with the efficient use of available energy resources has increased considerably since the energy crisis of the 1970's, which was sparked by the Arab oil embargo of 1973. When it was realized that man's incredible consumption of fossil fuels was rapidly depleting that resource, more emphasis was placed on nuclear fission reactors for the production of power.

Fossil and nuclear fuels are used to produce energy primarily in the form of high temperature heat, which in turn may be used as a heat source directly, to drive a mechanical device, or generate electricity. The high temperature application classifies them as *high grade energy sources*, where the driving force for heat transfer is large. High grade energy is easily utilized, and until recently has been the most profitable for its users. However, both nuclear and conventional energy sources are now suffering serious economic and environmental drawbacks. For this reason, attention has been drawn to ways of making processes more efficient, and to energy sources previously considered to yield insufficiently to merit serious investigation. Alternatives include wind, biogas, solar, and geothermal energy sources.

Before 1975, there was little extensive scientific research on alternative energy sources, but since then,

literally volumes have been produced [1] on the subject. Such novel ideas as generating electricity from the temperature stratification in the oceans have been proposed, and mathematical models developed to predict performance [2]. In experimental systems, gross production of more than 100 kilowatts has been achieved with temperature differences of only 22°C [3]. Geothermal deposits of hot water and solid media have long been used for space heating in France and Hungary, and a feasibility study of the use of Canada's large geothermal resource was conducted at Regina by Vandenberghe and Vigrasse [4]. Consistent hot water production in the region of 60°C was encountered.

Such energy sources are available mainly in the low temperature region - around 100°C. For this reason they are termed *low grade energy sources*, as it is difficult to transport heat over a small temperature difference. Included in this definition is perhaps the most popular "new" energy source, that of solar radiation. A recent application of solar energy is for domestic heating through the use of flat plate solar collectors. In this type of system, a working fluid is heated in the solar collector, and then circulated to heat an energy storage facility in the home for later use.

This work is concerned with the basic problem of transporting such low grade energy over a distance with a -----
numbers in square brackets denote references at the end of the thesis

small temperature difference between the heat source and sink. This might be encountered in several of the above examples, such as the geothermal well where hot water is pumped to the surface, or the flat plate solar collector system, where the working fluid is circulated between a low temperature heat source and a heat sink. The energy required in pumping a working fluid in this type of situation takes away from the net useable heat which may have been recovered. Therefore it is desirable in low grade energy applications to have a method of transporting heat over a distance without additional energy input.

1.2 The Thermosyphon Principle and Applications

Several devices are available which utilize capillary action, or body forces due to gravity or rotation to circulate working fluids between a heat source and heat sink, thus transporting energy. These are not new, and two which use the body force of gravity are closed tube thermosyphons, and closed loop thermosyphons, both of which may be operated with a single or two-phase working fluid. Although the work contained herein deals with the operating characteristics of a closed loop type system, it is useful to first discuss the principles of heat transport for a closed tube thermosyphon to provide a basis for comparison.

In its simplest form, the single phase closed tube thermosyphon is a tube sealed at both ends, filled with some working fluid. When the lower end is heated, and the upper

end cooled, colder, higher density fluid is located above warmer, lower density fluid in the gravity field. The temperature and density stratification causes buoyancy effects where the hot fluid rises and the cold fluid falls, thus transporting energy from the heat source to the heat sink. When the falling cold fluid encounters the rising warm fluid a complicated mixing zone is formed. The different modes of flow as well as the hydrodynamic coupling region between the heated and cooled zones are well discussed by Bayley and Lock [5].

The closed loop thermosyphon utilizes separate tubes to convey the rising hot fluid and the falling cold fluid, so that there is no interaction, and flow is in one direction only. Once natural circulation begins, the working fluid velocity increases until the overall buoyancy force is balanced by viscous friction in the loop.

It is possible to operate such systems with two-phase working fluids, so that heat transfer to and from the working fluid is in the form of latent heat. With the closed tube thermosyphon, the liquid is vaporized in the lower end, rises to the upper cool end, and rejects heat to the sink through condensation. The condensate flow returns to the heated portion down the wall of the tube. The closed tube two-phase thermosyphon has received some attention in the area of low grade energy transport. It has been proposed for such novel uses as constructing ice dams [6], and for solidifying permafrost foundations [7,8]. An extensive body

of literature exists for information on the heat transfer and operating characteristics of single and two-phase closed tube thermosyphons.

In the closed loop two-phase thermosyphon, the vaporized working fluid travels up the *riser line*, is condensed at the heat sink, and liquid returns to the evaporator section through a *condensate line*, with no interaction between the streams. Additionally, flow in the riser line may be passed through a liquid-vapor separator where the liquid component of the rising flow is separated off and returned to the evaporator section through a *downcomer line*. This enables the condensation section of the loop to receive higher vapor quality flow to improve the condensation efficiency.

The closed loop two-phase thermosyphon has recently found low grade application in phase-change refrigerant charged solar collector systems. Possible commercially available arrangements of such solar heating systems are discussed in [9,10,11]. Two extensive studies on the operating behaviour of these types of systems were done by Al-Tamimi [12] and Lee [13], and the feasibility of these arrangements for cold climates is discussed by Kissner [14], and Cheng [15].

The use of a closed loop thermosyphon need not be restricted to solar collector applications, however. Many industrial processes can be improved through transfer of waste heat from exhaust gases to incoming combustion

streams. Considerable amounts of ventilation air are required in factories, hospitals, swimming pools and air tight homes, and it would be desirable to preheat incoming fresh air with the hot exhaust, especially in winter. This is not difficult if the two fluid streams are close enough to be passed through a single heat exchanger. In some situations, physical limitations or contamination problems might cause the streams to be separated by some distance. To solve the problem in a conventional way, one might use two heat exchangers coupled with a pump and working fluid to achieve heat transfer. This is very versatile and can meet most physical requirements but involves the installation of pumps and controls.

If the heat source stream is not located above the heat sink stream in the gravity field, a closed loop two-phase thermosyphon device might be used to implement heat transfer. There are several advantages to such an arrangement. The thermosyphon is a very simple device which requires no pumps or controls, and is thus maintenance free, making it economically desirable. Heat transfer is one way only - if the upper end of the system becomes warmer than the lower, the working fluid will not flow and only minor heat transfer by conduction can occur. The heat source and heat sink are separated by a vertical and horizontal distance if desired, thus rerouting of ducts or pipes to achieve energy transport is not required. The two-phase systems offer an additional advantage over single phase

thermosyphons or forced flow arrangements in that the heat transfer coefficients associated with the boiling and condensation processes are very high, thus making the total system more efficient.

Some work has been done to determine the operating characteristics of closed loop two-phase thermosyphons in a low grade energy situation, such as by Cheng, et al [16], with refrigerant R-113 as the working fluid. A gas to gas system was constructed and tested by McDonald, et al [17], also using R-113 as the independent working fluid. However, there is a lack of complete information on the behaviour of closed loop two-phase thermosyphons for low-grade energy applications, and this provides the incentive for the present study.

1.3 Scope of the Study

An experimental system was constructed to investigate the operating and heat transfer characteristics of a closed loop two-phase thermosyphon for heat transfer from a low grade liquid heat source ($<100^{\circ}\text{C}$) to a liquid heat sink. The tests are conducted primarily for steady state operating conditions, with the short term time averaged temperatures and flow rates in the system constant over long time intervals.

The first series of tests deals with testing of the apparatus with liquid phase water as the working fluid (Chapter 2) to provide baseline data for two-phase tests.

Extensive information on the behaviour of the compact heat exchangers used in the system is provided at this point for future reference.

Chapter 3 deals with the operation of the system with two-phase water as the working fluid. This is achieved by maintaining a partial vacuum in the primary loop to lower the saturation temperature of the water. A study of the subcooled and low quality nucleate boiling heat transfer in the evaporator tube is also carried out.

Chapter 4 of this thesis is concerned with a high flow quality refrigerant R-113 system. Flow visualization studies are also performed on the flow from the evaporator, and in the condenser shell to provide better physical insight into the operating characteristics of the system.

Each chapter is basically an independent piece of work, but comparisons with the other types of systems is made throughout. Repetition between each section is avoided, and only changes in experimental apparatus, procedure, or data analysis from that given in Chapter 2 will be mentioned in subsequent chapters. The ultimate goal of this work is to provide experimental data for a wide range of external operating parameters in the low temperature regime, and to clarify the basic mechanisms of heat transport for the three different closed loop thermosyphon systems tested. The data is presented primarily in graphical form, and an attempt to provide insight into the processes involved will be made in the accompanying text.

2. Closed Loop Single-Phase Water Thermosyphon and Forced Flow Tests

2.1 Introduction

The steady state operating and heat transfer characteristics of a closed loop liquid-phase thermosyphon with water as the working fluid were studied to provide reference data for later study of two-phase systems. The simulated low grade heat source is liquid water at temperatures ranging between 55 and 95 degrees Centigrade, which classifies it as low grade. The heat sink temperature is approximately constant at 13-17°C, for a maximum system temperature difference of about 80 degrees.

The effects of various external operating parameters on the flow and heat transfer characteristics of the thermosyphon are studied to determine optimum operation for efficient small temperature difference and low grade energy recovery. The results are also compared to the operation of the primary loop in forced flow, which is the conventional method of transporting energy between a separated heat source and sink. A small centrifugal pump was installed in the primary loop for this series of tests. In addition to the performance of the overall system, the characteristics of the individual heat exchangers used are described.

The primary loop flow rates and temperatures will be constant in time provided that thermal conditions at the heat source and heat sink are also constant and this

characterises the steady state condition. With some geometries, steady state for the liquid phase ~~closed~~ loop thermosyphon cannot be achieved because of large oscillations in flow rate and pressure [18]. Over the range of operating parameters used for this system, such drastic behaviour was not encountered.

The single phase thermosyphon tested here may be classified as a long loop [19]. This means that local buoyancy forces in a flow cross-section are negligible compared to the overall buoyancy effect which drives the natural circulation process. In this situation, the heat exchangers feel the loop flow rate as if it were forced, quite unlike the natural convection encountered in a closed tube thermosyphon.

2.2 Experimental Apparatus

The test thermosyphon consists of three separate loops, diagrammed in Fig. 2.1. The actual closed loop thermosyphon or primary loop is composed of two heat exchangers, coupled on the working fluid sides by a network of copper tubing and fittings. Two secondary loops are required for heating and cooling, and the forced circulation of these fluids allows for control and measurement of such parameters as heat input and extraction. To allow for the inclusion of valves, flowmeters, and sight glasses, the copper tubing size in the primary loop varies from 1.27 cm (0.5 in) to 1.91 cm (0.75 in). The larger size is used wherever possible to

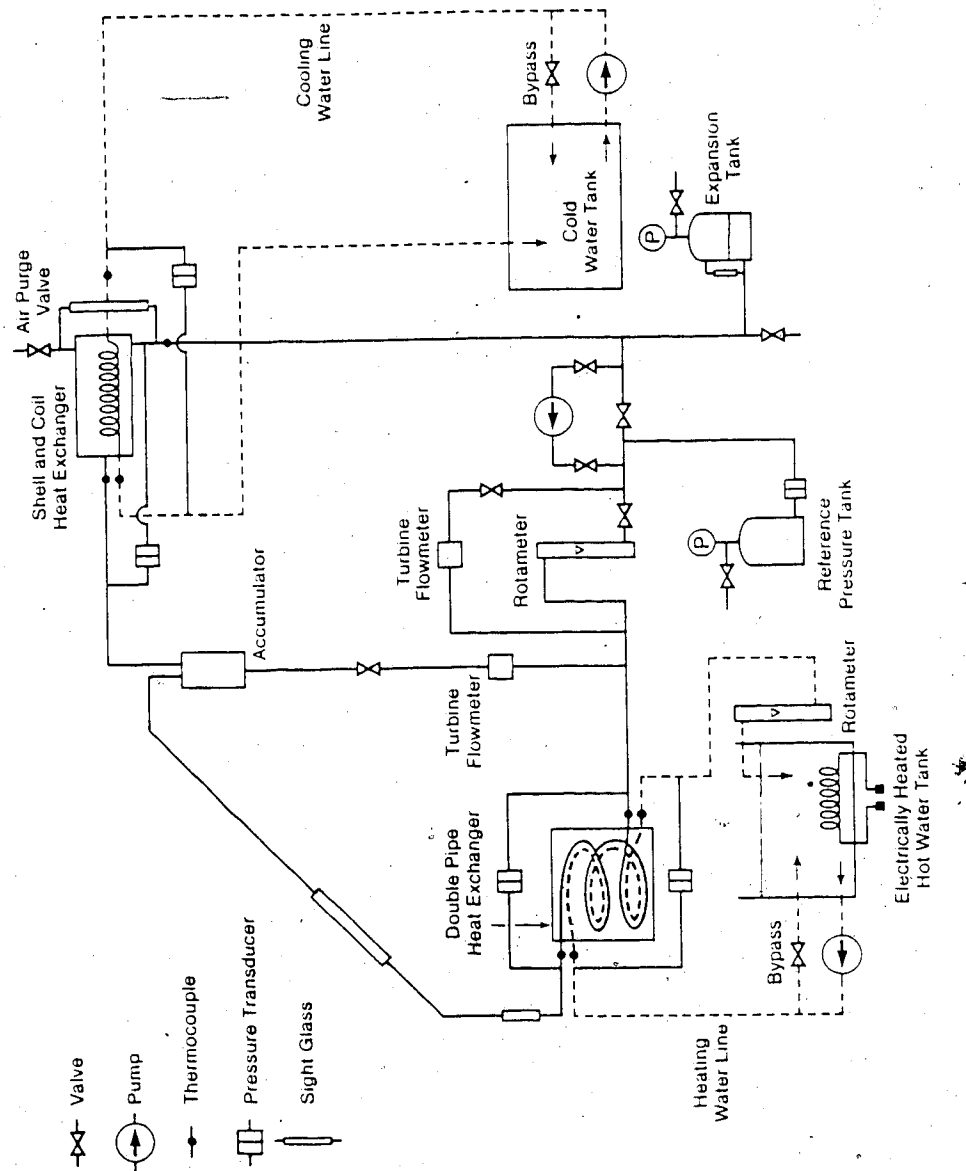


Fig. 2.1 Schematic diagram of experimental apparatus

reduce friction losses. The heat exchangers are separated by a vertical distance of 2.36 m (93 in.), measured from the inlet pipe of the lower heat exchanger to the horizontal axis of the upper heat exchanger. The horizontal separation of the two units is approximately 2.3 meters.

The heating loop, which supplies the lower heat exchanger, consists of an insulated, electrically heated hot water tank (389 l capacity) with a pump, rotameter, and by-pass for flow rate control. The heating elements and tank temperature are regulated by a PID temperature and power controller, with a maximum input of 3.7 kilowatts. Heat input to the primary loop is calculated from the flow rate and temperature change in the heating water as it passes through the lower heat exchanger.

The cooling loop consists of a cold water tank (1110 l cap.), pump, turbine flow meter, and by-pass setup. The tank temperature is kept fairly constant by continuously circulating cold tap water. The heat transported and recovered by the system is calculated from the flow rate and temperature change of the cooling water as it passes through the upper heat exchanger. Both the hot water and cold water loops are connected to the heat exchangers in the primary loop with rubber hoses and copper tubing.

The lower heat exchanger is a Packless Industries model CDAX-500 coiled double pipe unit with a three lobe twist ($1/3$ turn per inch) on the inner copper tube. A cross section of the tubes is shown in Fig. 2.2 and the outer

round pipe is steel. The upper heat exchanger is a Solar Research model 5835 shell and copper coil unit with continuous low integral fins (root radius 0.5 in., fin height 1/16 in., and 16 fins per inch). The physical dimensions of both heat exchangers are given in Table 1. Both the upper and lower units are operated in counterflow, with the working fluid flowing in the inner pipe in the lower heat exchanger, and in the shell side of the upper.

The distilled water in the working fluid loop was treated with Zeotec 5900² corrosion inhibitor at a concentration of 0.5% vol/vol of water. This provides a pH range of 8.5-10, and electrical conductivity range of 1000-2000 mmhos•cm, which prevented corrosion and scaling during the course of the tests. Large sight glasses constructed of Pyrex tubing with teflon seals and Swagelok fittings allowed visual inspection of the fluid level and clarity.

An expansion tank was used to keep the system pressure at about 10 psi over the course of the single phase tests. This was to prevent any dissolved gases from coming out of solution and forming gas pockets which would inhibit the syphoning effect in the tubes. The accumulator (liquid-vapor separator) was not required for the liquid-phase tests and this section was closed to the flow. A centrifugal pump (14.9 Watts, 3000 rpm) was installed in the working fluid loop for study of the system under forced flow conditions.

² nitrite, metaborate, polyacrylamide, and copper corrosion inhibitors

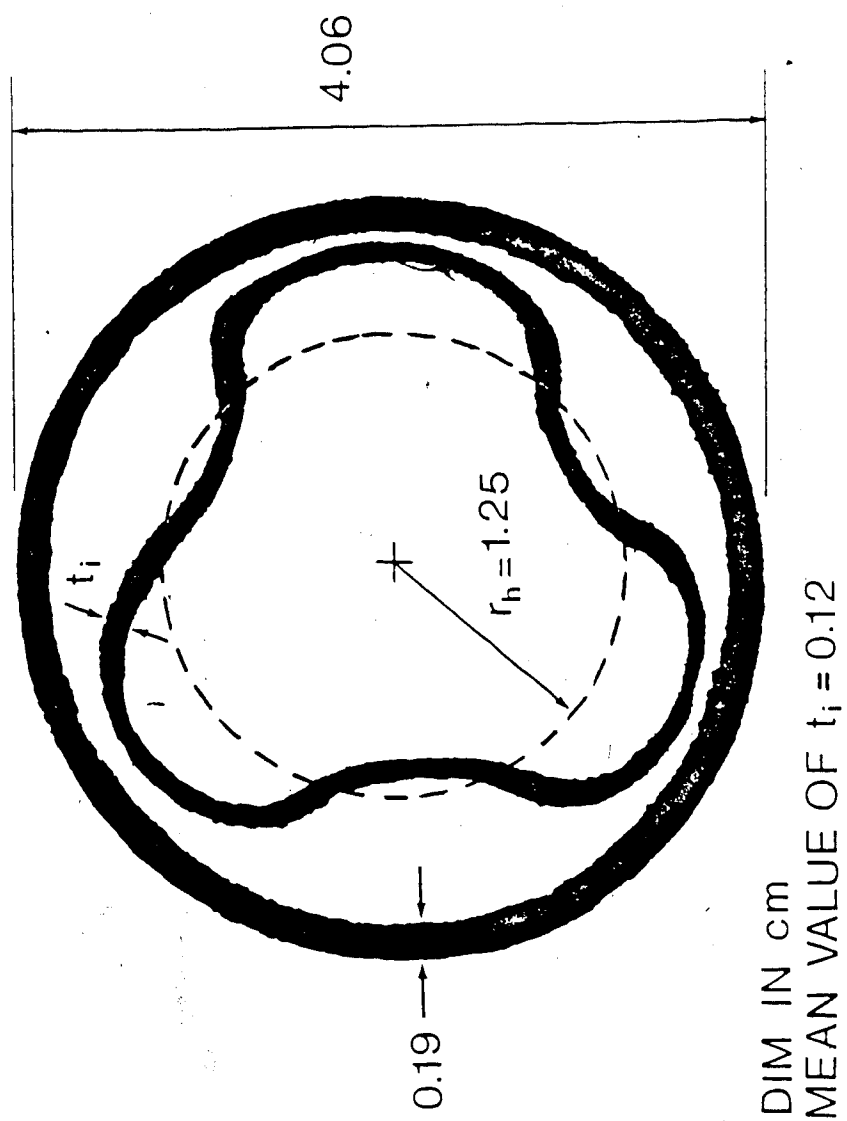


Fig. 2.2 Print of lower heat exchanger cross-section

Table 2.1 Heat Exchanger Dimensions

Type	Packless Industries CDAX 500 Double Pipe helical coil with 3 lobe inner spiral	Solar Research 5835 B Shell and Coil with continuous low integral fin
Application	Lower Heat Exchanger: heating	Upper Heat Exchanger: cooling
Inner Tube I.D. (m)	0.02494 (equiv.)	0.0127
Effective Length (m)	5.310	7.620
L/d ratio	213	600
Coil Radius of Curv. (m)	0.1743	0.053
r/R ratio	0.072	0.120
Number of Coils	4 1/2	21
Inner Heat Transfer Area (sq. m)	0.526	0.304
Outer Area of Inner Coil (sq. m)	0.572	0.952
External Dimensions	pipe: 4.06 cm O.D. 3.68 cm I.D.	shell: 15.24 cm O.D. 14.61 cm I.D.

2.3 Instrumentation

The geometry of the heat exchangers and piping promotes good mixing of the fluids in the primary and secondary loops, but additional wire meshes were installed upstream of the thermocouples to ensure bulk temperature measurement. The 1.6 mm outside diameter sheathed iron-constantan thermocouples were located at the inlets and outlets of the primary and secondary loops for both heat exchangers, and in the downcomer line. These were initially calibrated with ASTM mercury in glass thermometers with divisions of 0.1°C in a controlled temperature bath. The thermocouples were later recalibrated before installation with an HP-2807A quartz thermometer with an accuracy of 0.1°C , and were found not to wander appreciably. The maximum error using a linear correlation between voltage and temperature is estimated to be $\pm 0.3^{\circ}\text{C}$.

Pressure drops for the working, heating, and cooling fluids in both heat exchangers were measured with Validyne differential pressure transducers. The selection of diaphragm sensitivity was based on preliminary tests, and calibration was done with either inclined mercury or U-tube water manometers. The maximum error for the 5, 8, and 10 psi transducers (system pressure, cooling fluid, heating fluid) was ± 0.1 psi, and the error for the 0.5 psi transducers (working fluid, both heat exchangers) was ± 0.005 psi (1% of range).

A sensitive rotameter was used to measure the working fluid flow rate (range 2.8-36.6 ml/s) with an estimated error of ± 0.2 ml/s. A higher capacity rotameter (0-0.386 l/s range) was used to measure the heating fluid flow rate, and although it proved to be inaccurate, it was an acceptable guide for setting the heating fluid flow rate. The heat transferred in the lower heat exchanger is then calculated based on the more accurate working fluid flow rate, which is possible only for the single phase tests. The cooling water flow rate was monitored by a turbine flow meter (range 5-80 ml/s) with a maximum error of ± 0.3 ml/s over the range. The power supplies and signal conditioners of the flow meters and pressure transducers were set to give +10 volts full scale output.

All electrical output devices; thermocouples, pressure transducers, and turbine flow meters, were monitored by an Hewlett Packard 3497A data acquisition control unit and

Hewlett Packard 85 micro-computer. The flow chart for the data acquisition process is shown in Fig. 2.3. Reference for the thermocouples was provided by circuitry in the thermocouple cards of the acquisition unit. A Digital Decwriter IV printer provided the hard copy listing of the experimental results.

2.4 Experimental Procedure

The single-phase closed loop thermosyphon test schedule allowed for the manipulation of three external parameters: heating fluid temperature, heating fluid flow rate, and cooling fluid flow rate. This in turn varied the heat transfer coefficients of the heat exchangers, the input and extracted heat, and system effectiveness and efficiency.

The hot water tank temperature was varied from 55-95°C in increments of 10°C, while the flow rates used were 30, 40 and 50 ml/s. The cooling water flow rate ranged from 10-60 ml/s in increments of 10 ml/s and the temperature was approximately constant at 13-17°C. Other unaltered parameters were initial working fluid level in the primary loop (completely filled and air purged), and system pressure which was essentially constant at the start of all tests at 10 psi gauge. Room air temperature was very stable at 23.5°C, with an occasional half degree fluctuation.

All equipment, including the power supplies for pressure transducers and flowmeters, and the data acquisition unit were powered up at least 24 hours in advance of any

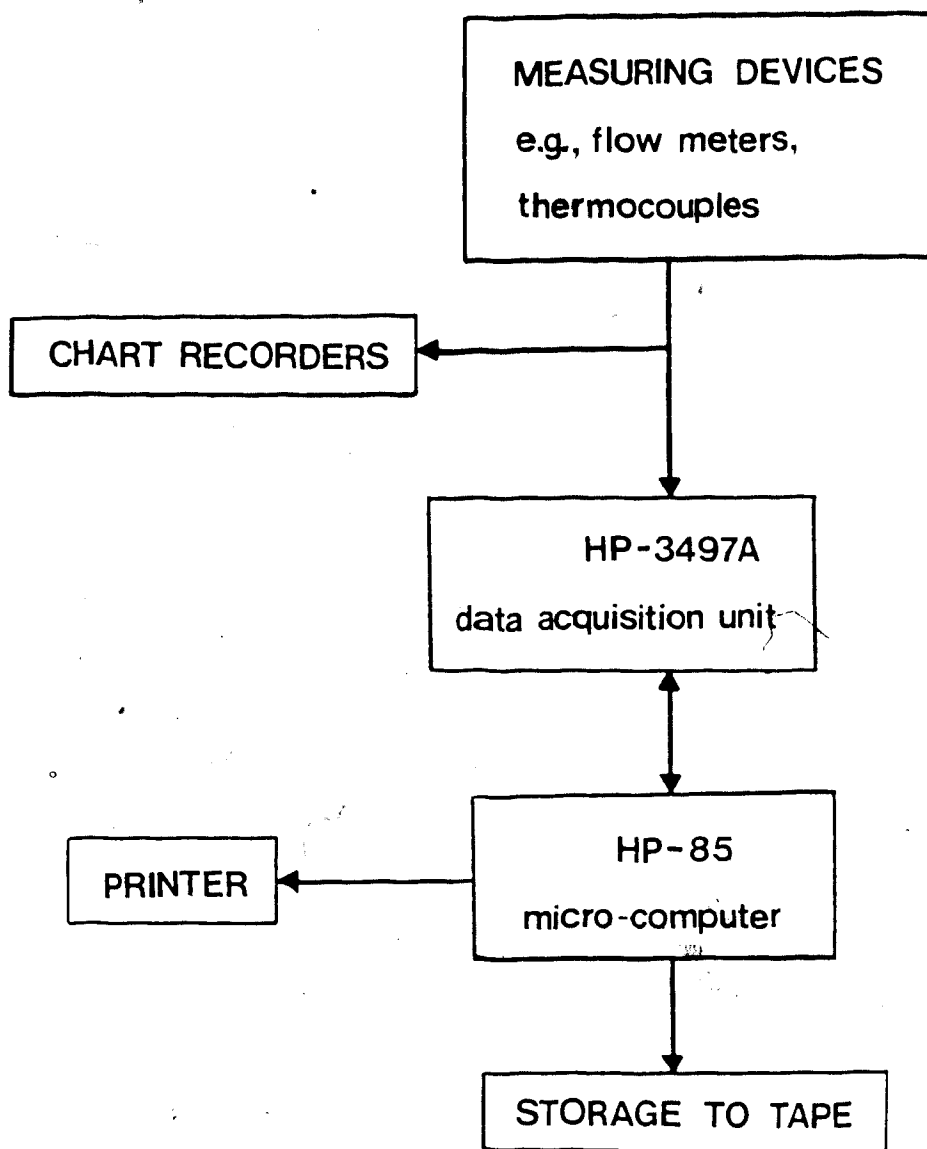


Fig. 2.3 Data acquisition flow chart

tests, and cold tap water was circulated in the cooling tank for several hours preceding a test to ensure a steady heat sink temperature. The heating water tank temperature was preset about four hours before a test to allow the electrical heaters to bring the large mass of the water in the heating tank to the correct temperature. The water was continuously agitated with a stirrer to protect the heating elements and provide a uniform tank temperature.

To start a test, the cooling water was first circulated and set to the desired flow rate. The heating water, already set at the proper temperature, was circulated and adjusted to the correct flow rate. Due to the relatively short height of the lower heat exchanger (~10 in.), it took an unreasonably long period of time for the water column above the unit to become hot enough to begin the natural circulation process. For this reason, the centrifugal pump in the primary loop was engaged for about 15 seconds to allow the heated working fluid to travel up the riser tube, and cold fluid to flow down the return line. The resulting density difference in the lines would allow natural circulation to begin, and the pump was no longer required.

The steady state condition was identified when short term averaged temperatures and flow rates were constant in time for all points in the system. The measured parameters for each test included flow rates in the primary and secondary loops, temperatures at the inlets and outlets of the streams passing through both heat exchangers, and

pressure drops across the heat exchangers. The computer acquired data was read consecutively 10 times, then averaged. The manually inputted rotameter readings were entered once, just before the automatic data acquisition process was begun. A sample data acquisition program listing for the micro-computer and control unit is included in Appendix I.

2.5 Data Analysis

Operating the thermosyphon in single phase greatly reduces the complexities of data analysis as compared to a two-phase system. Some very useful correlations for the properties of liquid water compiled by Fujii, Nosh and Honda [20] are used in the computer aided reduction of the raw data, and the FORTRAN library used for property calculations may be found in Appendix II. It is assumed that the slight pressurization of the working fluid does not cause significant error in the calculation of properties, as these are primarily temperature dependent for liquids.

In an experimental system of this nature, heat transport is of primary interest. The useful energy transferred by a fluid passing through a heat exchanger is given by

$$Q = \dot{m}(\Delta h) \quad (2.1)$$

with Δh being the total change in the intensive enthalpy of the fluid stream. The specific heat at constant pressure is

defined as [21]

$$C_{p1} = \left(\frac{\partial h}{\partial T} \right)_p \quad (2.2)$$

For liquids the specific heat is closely approximated by

$$C_{p1} = \left(\frac{\Delta h}{\Delta T} \right)_p \quad (2.3)$$

Transposing and substituting Eq.(2.3) into Eq.(2.1) one obtains

$$Q = \dot{m} C_{p1} (\Delta T) \quad (2.4)$$

for the total heat transferred to or from a liquid stream. The heat exchangers are well insulated so that heat losses to the surroundings are negligible, thus the heat released by one stream is equal to that gained by the other in the heat exchanger. The average wall heat flux in a heat exchanger is defined as

$$q = Q/A \quad (2.5)$$

with A being the effective heat transfer area of the inner tube. The heat transferred in a heat exchanger may also be written as

$$Q = UA(\Delta T) \quad (2.6)$$

with ΔT being the characteristic temperature difference and

U the overall heat transfer coefficient. It is necessary to define the overall heat transfer coefficient based on the type of temperature difference used. The simplest form is the arithmetic mean temperature difference (AMTD), which is given by

$$\Delta T = \frac{T_{hi} + T_{ho}}{2} - \frac{T_{ci} + T_{co}}{2} \quad (2.7)$$

When the total heat transferred is calculated from the cold stream, and Eq.(2.6) is combined with Eq.(2.4), the overall heat transfer coefficient based on an arithmetic mean temperature difference becomes

$$U = \frac{\dot{m}_c C_{pl} (T_{co} - T_{ci})}{\frac{A}{2} [(T_{hi} + T_{ho}) - (T_{ci} + T_{co})]} \quad (2.8)$$

Another common characteristic temperature difference is known as the logarithmic mean temperature difference (LMTD) which is easily derived [22] and is given by

$$\Delta T_{lm} = \frac{(T_{ho} - T_{ci})(T_{hi} - T_{co})}{\ln[(T_{ho} - T_{ci})/(T_{hi} - T_{co})]} \quad (2.9)$$

Substituting in Eq.(2.6) and combining with Eq.(2.4) the overall heat transfer coefficient based on a logarithmic mean temperature difference for a counterflow situation can be calculated from

$$U_{lm} = \frac{\dot{m}_c c_{pl} (T_{co} - T_{ci})}{A \left\{ \frac{(T_{ho} - T_{ci}) - (T_{hi} - T_{co})}{\ln(T_{ho} - T_{ci}) / (T_{hi} - T_{co})} \right\}} \quad (2.10)$$

It is interesting to compare the two definitions of heat exchanger characteristic temperature difference mathematically. Equating Eq.(2.7) to Eq.(2.9) and rearranging one obtains

$$\exp \left\{ \frac{2[(T_{ho} - T_{ci}) - (T_{hi} - T_{co})]}{(T_{hi} + T_{ho}) - (T_{ci} + T_{co})} \right\} = \frac{(T_{ho} - T_{ci})}{(T_{hi} - T_{co})} \quad (2.11)$$

It can be seen from Eq.(2.11) that the equality will be satisfied if $(T_{ho} - T_{ci})$ is equal to $(T_{hi} - T_{co})$. These quantities are the differences between the terminal temperatures of the separate streams of the heat exchanger. Actually, the exponential form of Eq.(2.11) is quite insensitive to differences in these two quantities and if $(T_{ho} - T_{ci})$ is not more than 50% greater than $(T_{hi} - T_{co})$, then the AMTD will agree with the LMTD within about 1% [23]. However, this condition is not met for the lower heat exchanger in single phase thermosyphon tests, so results will be shown with both definitions of temperature difference. For subsequent tests, only the arithmetic mean temperature difference is used as the results are in close agreement with those given by the logarithmic mean calculation.

Due to the geometries of the heat exchangers and the condition of having fluids flowing in both the heating and cooling streams of the units, no attempt was made to attach thermocouples along the tube walls to accurately determine the wall temperature profiles. For convenience and simplicity in interpreting the experimental results, the average wall temperature of the inner tubes of both heat exchangers (cold side flow) is taken to be the mean of the hot side inlet and outlet bulk temperatures to give

$$T_w = \frac{(T_{hi} + T_{ho})}{2} \quad (2.12)$$

The average bulk temperature of a cold stream passing through a heat exchanger is simply the mean of the measured inlet and outlet bulk temperatures which yields

$$T_b = \frac{T_i + T_o}{2} \quad (2.13)$$

The average heat transfer coefficient between a flowing fluid and a heated wall is defined as

$$h = q/\Delta T \quad (2.14)$$

with

$$\Delta T = T_w - T_b \quad (2.15)$$

The assumption given by Eq.(2.12) implies that the

calculation of the average inner heat transfer coefficients in the heat exchangers is the same as that for the overall heat transfer coefficient. This is rather coarse but necessary due to physical limitations, and it is of interest to carry out the analysis in this manner when calculating the average Nusselt number for a heat exchanger inner tube. The Nusselt number is defined as

$$Nu = h d / K_f \quad (2.16)$$

It was found that the Nusselt number for the flow in the inner tube of the lower heat exchanger correlated well with the dimensionless parameter inverse Graetz number. The Graetz number is often used in equations which estimate heat transfer in entry region flow and is defined here as

$$Gz = Re Pr d / \ell \quad (2.17)$$

The dimensionless group $(RePr)$ is often referred to as the Peclet number, so the inverse Graetz parameter may be written as

$$Gz^{-1} = Pe^{-1} (\ell / d) \quad (2.18)$$

By substituting the curved tube Dean number for Reynolds number, the dimensionless parameter Z is obtained:

$$Z = (K Pr d / \ell)^{-1} \quad (2.19)$$

The data was found to fit a simple power equation correlation in the form

$$Nu = a Z^b \quad (2.20)$$

It is also possible to compare the experimentally determined Nusselt number for the helically coiled inner tube of the lower heat exchanger with a correlation developed for coils with constant wall temperature and laminar flow [24] given by

$$Nu_{coil} = 3.65 + 0.08 [1 + 0.08(r/R)^{0.9}] R_e^B P_r^{1/3} \quad (2.21)$$

$$\text{with } B = 0.05 + 0.2903(r/R)^{0.194}$$

This correlation may also be used to calculate the tube side heat transfer coefficient of the upper heat exchanger coil. With this information, and the calculated overall heat transfer coefficient of the upper unit, it is possible to estimate the fin side coefficient h_o by employing the electrical analogy. The resistance of the thin copper wall is assumed negligible and this gives

$$h_o = \left[\frac{A_F}{U_2 A} - \frac{A_F}{h_{coil} A} \right] \quad (2.22)$$

where A_F is the fin side area = 0.952 m²
and A is the tube side area = 0.304 m².

Another method of evaluating heat exchanger performance is to calculate the effectiveness. This is defined as the ratio of actual heat transfer to maximum possible heat transfer between the streams in the heat exchanger [25]. For the lower unit, this would simply be

$$\epsilon_1 = \frac{T_{co} - T_{ci}}{T_{hi} - T_{ci}} \quad (2.23)$$

It is also possible to compute the effectiveness of the entire primary loop, treating it as one heat exchanger between the heat source and heat sink fluids. Using the same concept, the second law thermodynamic efficiency of the system may be calculated from an availability analysis [26] to give

$$\eta = \frac{\dot{m}_c c_{pl} [(T_{co} - T_{ci}) - T_r \ln(T_{co}/T_{ci})]}{\dot{m}_h c_{pl} [(T_{hi} - T_{ho}) - T_r \ln(T_{hi}/T_{ho})]} \quad (2.24)$$

Relations which are specific to a particular chapter will be discussed in the sections in which they occur.

2.6 Thermosyphon Flow Results and Discussion

2.6.1 Overall System Characteristics

During the four month period from September to December, 1983, a total of 120 tests were performed to determine the operating characteristics of the closed loop

single-phase water thermosyphon and its associated heat exchangers for a given set of external operating parameters. It was found that the variation of heating fluid flow rate did not greatly affect the graphically presented results, so only the data associated with a heating fluid flow rate of 40 ml/s will be presented to avoid repetition. This was chosen to be representative as it is the average of the three different flow rates used (30, 40, and 50 ml/s).

The overall performance of the system as a whole will be dealt with first. Fig. 2.4 illustrates the relationship between extracted and input energy for the system. The primary loop is behaving like a heat exchanger between the heat source and heat sink, and the only difference between input and extraction is heat loss. This is minimal in this system due to the relatively low temperatures involved and the insulation of the piping and heat exchangers.

Transferring heat with a low temperature driving force is difficult and the additional problem of mass transport in the primary loop is encountered for natural circulation flow. Fig. 2.5 shows the effect of the temperature difference between the heat source tank and heat sink tank on the total heat transport by the system. This primarily reflects the increase in heat source temperature, as the cooling water temperature is essentially constant for the tests. As is expected, the increase in temperature difference provides better overall performance, as this is an increase in the driving force for heat transfer. The

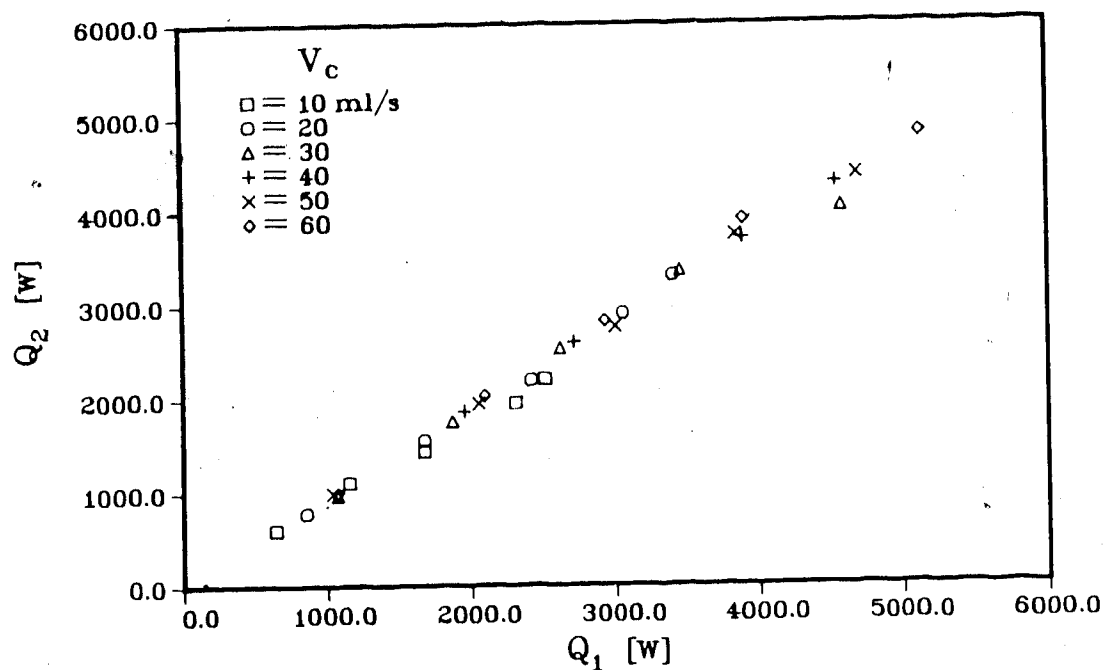


Fig. 2.4 Relationship between heat extraction and heat input

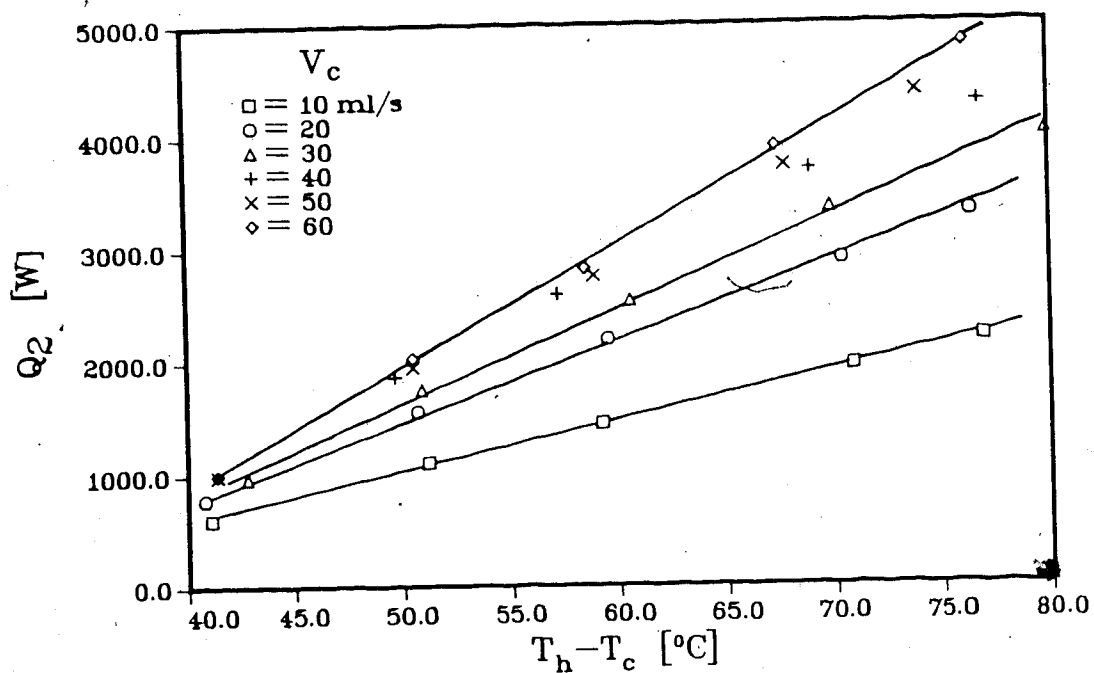


Fig. 2.5 Effect of system temperature difference on overall heat recovery

relationship between these parameters may be better envisioned by considering the entire primary natural circulation loop as one heat exchanger between the heating and cooling streams, as mentioned earlier. Examining Eq.(2.6), one can consider the system characteristic temperature difference to be that plotted on the abscissa of Fig. 2.5. Because total heat transferred is plotted on the ordinate of the graph, the slope of the graphed lines becomes the product of the system overall heat transfer coefficient and some characteristic heat transfer area (UA). Note that for the same temperature difference, an increase in the cooling water flow rate results in better heat transport and thus a higher overall heat transfer coefficient.

The effect of an increase in cooling water flow rate on system performance is twofold. First and most obvious, this will cause more heat to be extracted at the upper heat exchanger. Secondly, it lowers the temperature of the working fluid leaving the upper heat exchanger and increases its density. The increased density differences between the downflow and upflow sections of the primary loop causes the flow rate of the working fluid to rise, thus transporting mass and heat between the heat source and heat sink at a faster rate. Similarly, an increase in heat source temperature would also cause higher natural circulation rates by lowering the fluid density in the riser line.

This is substantiated by Fig. 2.6 which shows the working fluid mass flow rate plotted against the system temperature difference. The parameter which influences the natural circulation mass flow rate the most is heat source temperature, and the secondary effect is found by increasing the coolant flow rate.

In order to combine the effects of the temperature difference between the heat source and heat sink, and the cooling water flow rate, the mass flow rate may be plotted against average input heat flux as shown in Fig. 2.7. Increased flow rate corresponds to a higher heat flux. Conventionally, the mass flow rate in the primary loop is given in terms of mass flux, so the natural circulation mass flux at the entrance to the lower heat exchanger is shown in Fig. 2.8.

It should be mentioned here that the cooling water flow rates depicted in the legend are not exact as the flow rate would wander somewhat after initially set. They are very close, however, and the exact values are used in any calculations.

Another interesting aspect of system performance is the quality of the heat recovered. This refers to the temperature that the cooling water is heated to, which will be decreased for higher cooling water flow rates. This is reflected in the calculation of the overall effectiveness for the system, which is essentially the temperature change that the cooling water undergoes divided by the maximum

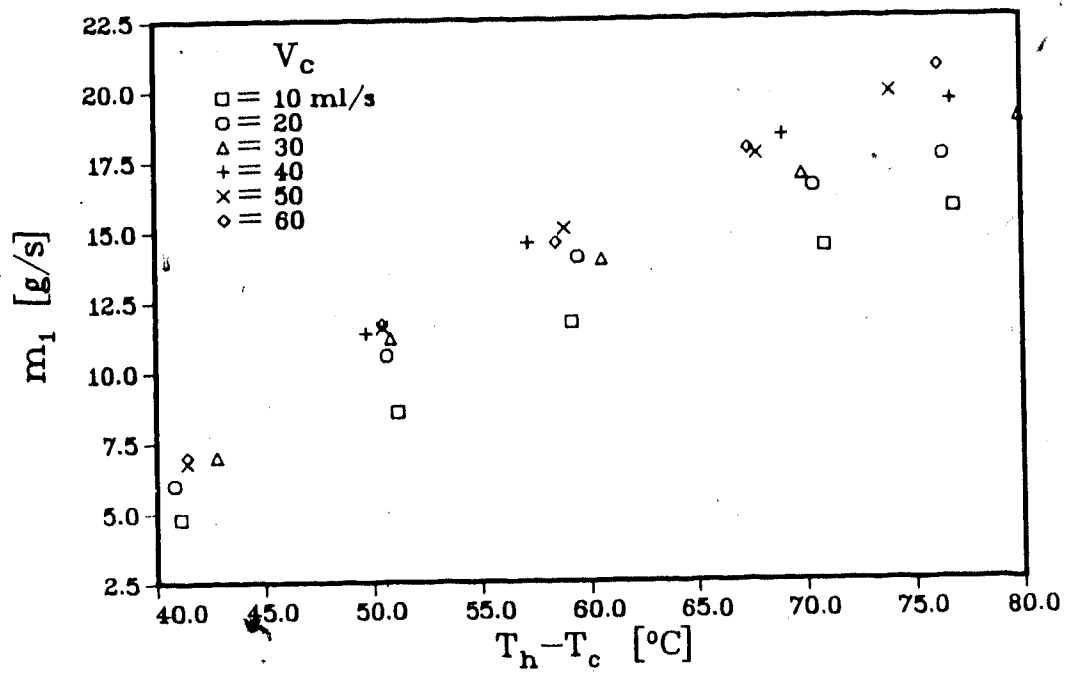


Fig. 2.6 Effect of system temperature difference on total thermosyphon mass flow rate

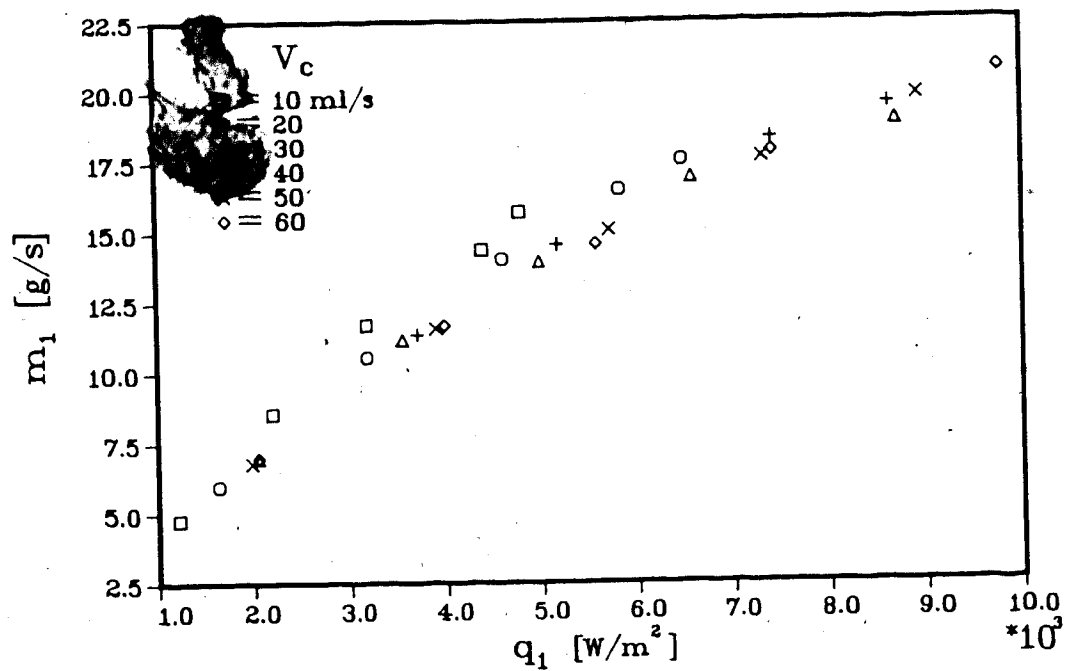


Fig. 2.7 Effect of average input heat flux on total thermosyphon mass flow rate

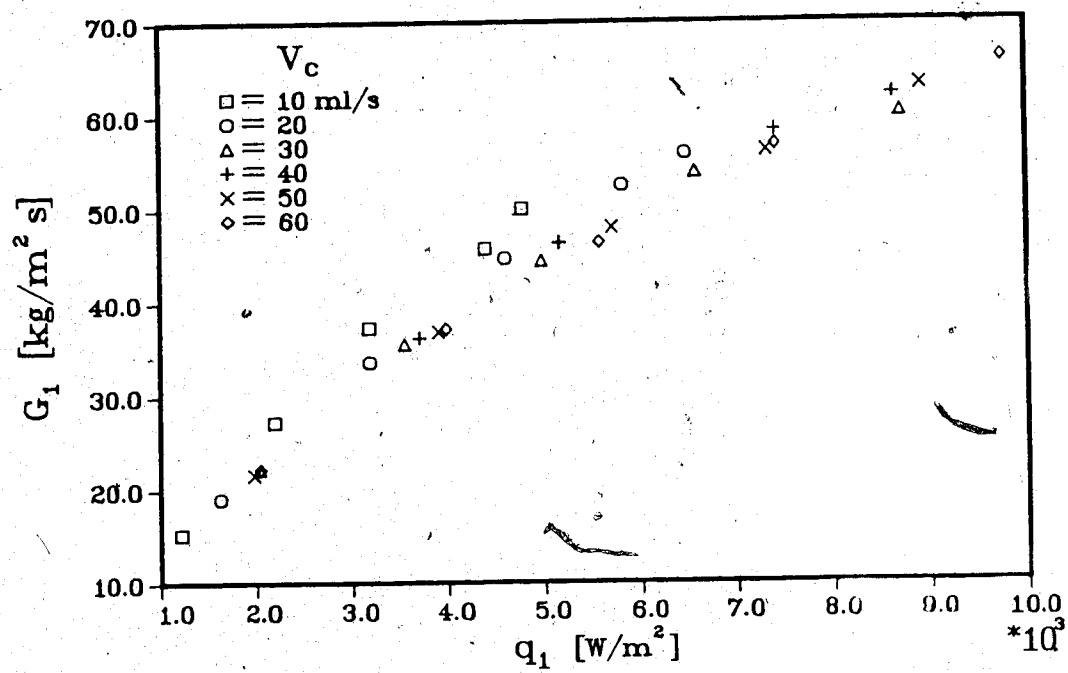


Fig. 2.8 Total thermosyphon mass flux at lower heat exchanger inlet

system temperature difference, similar to that shown by Eq.(2.23) for the lower heat exchanger. The system effectiveness is plotted as a function of the working fluid Reynolds number in Fig. 2.9. The effectiveness is greatest for the combination of lowest cooling water flow rate and highest primary loop flow rate, which also corresponds to the highest heat source temperature. Note that the range of Reynolds number encountered in the single phase tests indicates that the natural circulation flow lies in the laminar regime, although inherent disturbances in the system may affect this.

Unfortunately, the total heat extraction will not be a maximum when the effectiveness is greatest. Fig. 2.10 shows a comparison between total heat extracted and system effectiveness in order to show the envelope of operating conditions. The heat source temperature is increasing from bottom to top in the figure.

The thermodynamic efficiency of the system as a whole as calculated by Eq.(2.24) is plotted against the natural circulation Reynolds number in Fig. 2.11. As with effectiveness, the maximum efficiency is found for a combination of low cooling water flow rate, high heat source temperature, and high working fluid flow rate. A single heat exchanger may be expected to attain efficiencies near 80% as compared to the maximum of about 33% for the low temperature difference two heat exchanger system used here. The figure indicates that both higher heat source temperature and

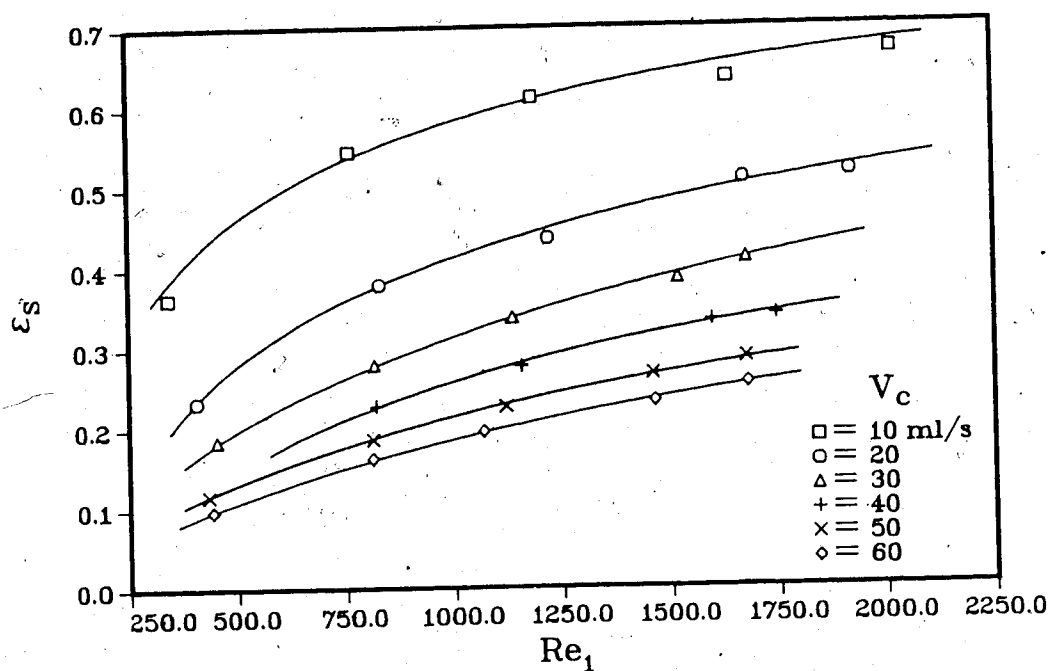


Fig. 2.9 Effect of working fluid Reynolds number at lower heat exchanger inlet on system effectiveness

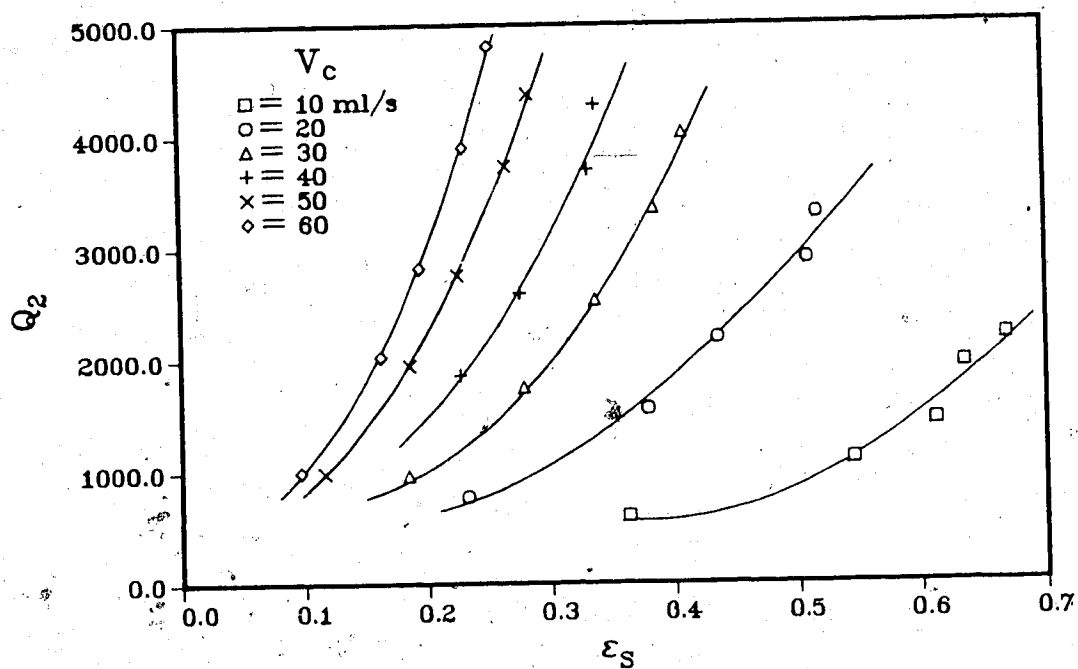


Fig. 2.10 Comparison of system heat recovery and effectiveness

primary loop flow rate contribute to better efficiency. The object of the study is to recover heat from a low grade energy source, so the increase of heat source temperature is not an available option. However, improvements could be made by eliminating the flow restrictions caused by the instrumentation and the use of relatively small tubes in the primary loop. This in turn would allow an increase in the natural circulation rate, and a higher system efficiency. Fig. 2.12 shows the effect of average input heat flux on the efficiency, with the results coinciding with those in Fig 2.11. For any given cooling water flow rate, an increase in heat flux will increase the overall efficiency.

Heat extraction, effectiveness, and thermodynamic efficiency of the liquid-phase water system are all positively affected by an increase in the total temperature difference across the system and by an increase in the natural circulation rate in the primary loop. Because the driving force for natural circulation is balanced by viscous friction, decreasing the friction losses in the primary loop is one method of improving performance. This could be done by eliminating unnecessary fittings, tubing size changes, and small diameter tubes, which are required in the experimental system to accommodate instrumentation. As well, unnecessary horizontal distance between the heat source and heat sink should be avoided to keep friction losses to a minimum. Of course, any improvement in the performance of the individual heat exchangers would also benefit the system

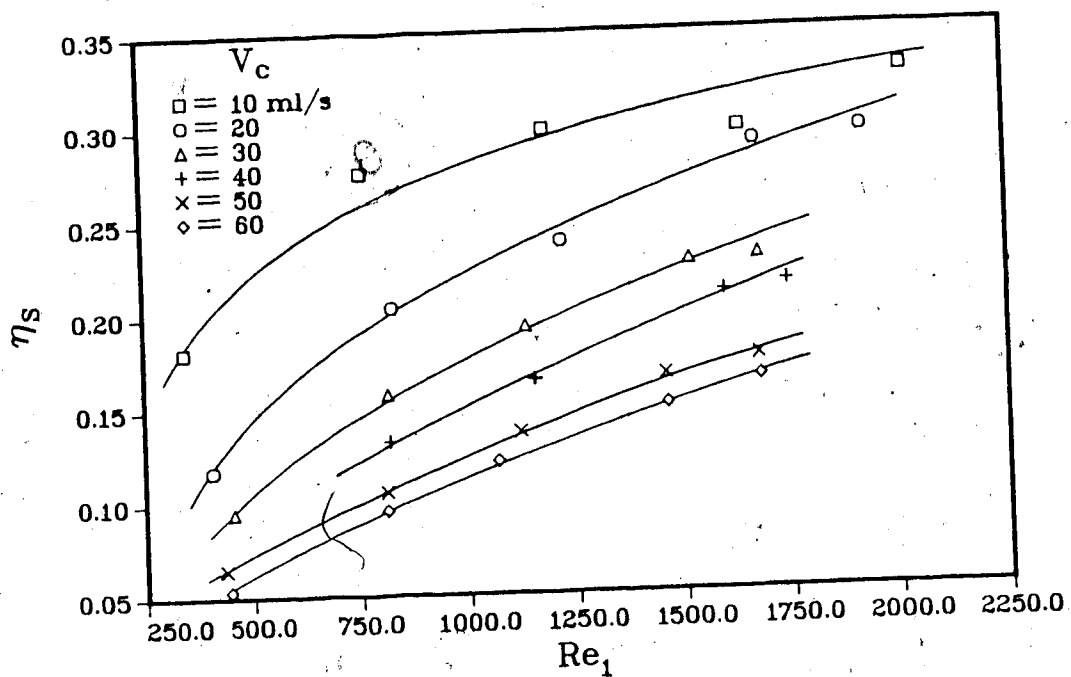


Fig. 2.11 System thermodynamic efficiency vs. working fluid Reynolds number

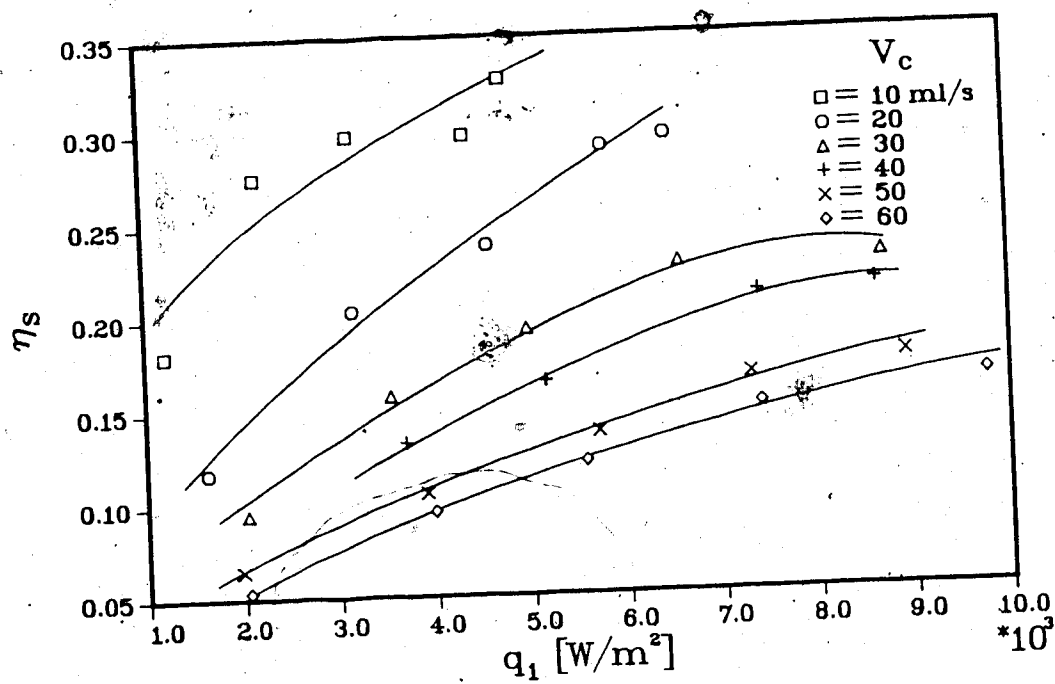


Fig. 2.12 Effect of input heat flux on thermodynamic efficiency

as a whole.

2.6.2 Lower Heat Exchanger

An analysis of the performance of the heat exchangers with single phase operating conditions is relatively simple, and it is of interest to examine the lower heat exchanger as it is a compact unit. It is approximately 25 centimeters (10 in.) in height, with a coil diameter of 34.8 cm (14 in.). The inside tube of the heat exchanger is of non-circular shape, so the hydraulic diameter is used as an equivalent dimension. The inner heat transfer area was calculated by enlarging a cross-sectional print of the inner tube, measuring the inside perimeter, and multiplying by the effective length. A planimeter was used to find the cross-sectional area, which is required for the calculation of hydraulic diameter.

Figures 2.13 and 2.14 show the arithmetic mean and logarithmic mean overall heat transfer coefficients calculated from Eqs. (2.8) and (2.10) plotted against the average input heat flux. Cooling water flow rate is an indirect parameter here as it affects the flow rate in the primary loop and causes changes in the input heat flux. The use of heat flux as the independent variable virtually eliminates the effect of change in the natural circulation flow rate caused by the alteration of the cooling water flow. However, this effect becomes apparent when comparing the overall coefficient to the Dean number of the natural

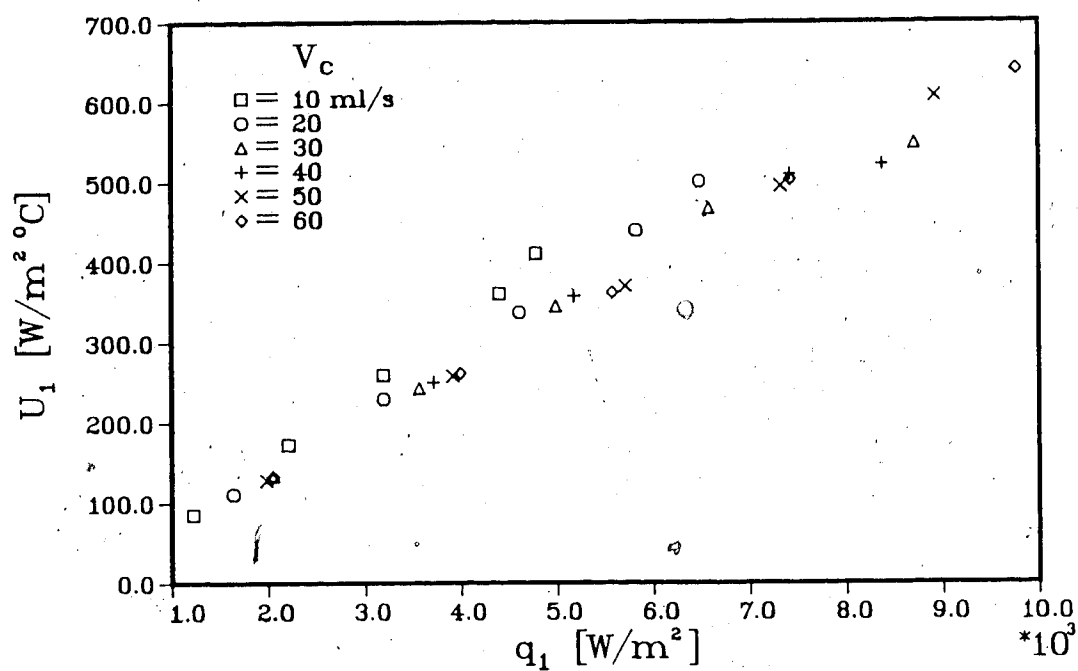


Fig. 2.13 Arithmetic mean overall heat transfer coefficient for lower heat exchanger

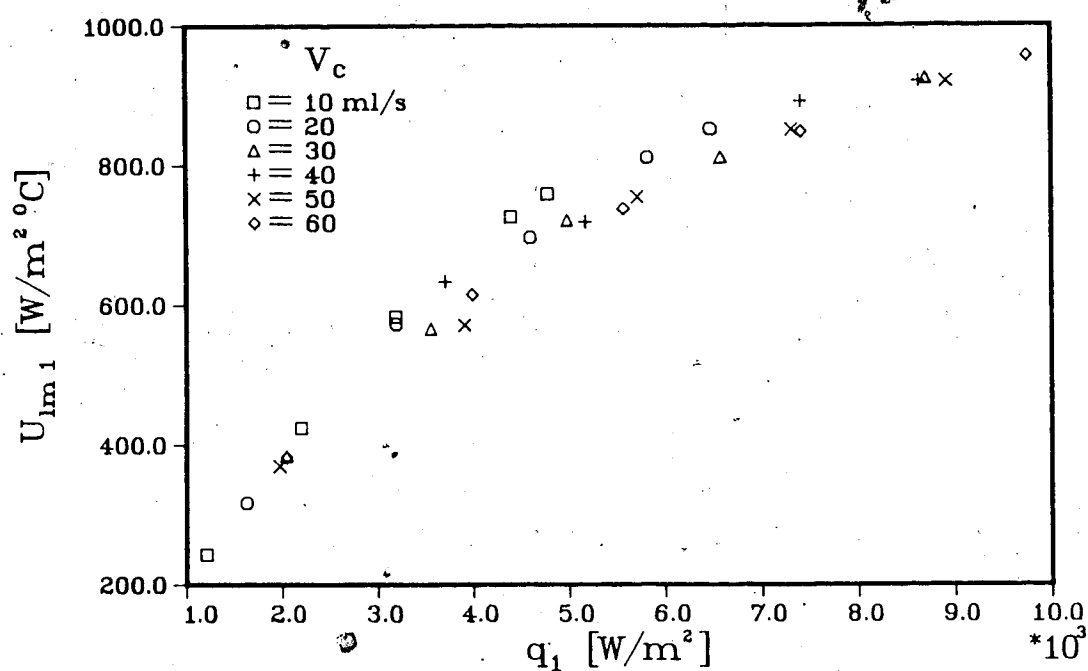


Fig. 2.14 Logarithmic mean overall heat transfer coefficient for lower heat exchanger

circulation flow in the coiled inner tube, shown in Figures 2.15 and 2.16. The increase in cooling water flow rate causes a rise in the flow rate of the natural circulation loop, lowers the inlet temperature of the working fluid at the lower heat exchanger, and thus provides for better performance of the unit. This illustrates that the characteristics of individual components may be linked to flow and heat transfer processes that are physically separated from each other. They are interrelated through the natural circulation flow in the primary connecting loop.

The effect of the natural circulation flow rate on the effectiveness of the heat exchanger calculated by Eq.(2.23) is shown in Fig. 2.17. Although the effectiveness falls rapidly with increasing mass flow rate, the minimum value encountered over the test range was about 0.965, which is relatively high.

The effect of Dean number for the inner curved, twisted pipe on the Nusselt number calculated from Eq.(2.16) is shown in Figure 2.18. The validity of the tube wall temperature assumption given by Eq.(2.12) may be examined by comparing the experimentally determined Nusselt number with the correlation for flow in a helically coiled tube given by Eq.(2.21). These are plotted against the Reynolds number for the natural circulation flow in the inner heated tube in Fig. 2.19. The indication from this is that the assumptions used to calculate the experimental Nusselt number are acceptable for indicating trends.

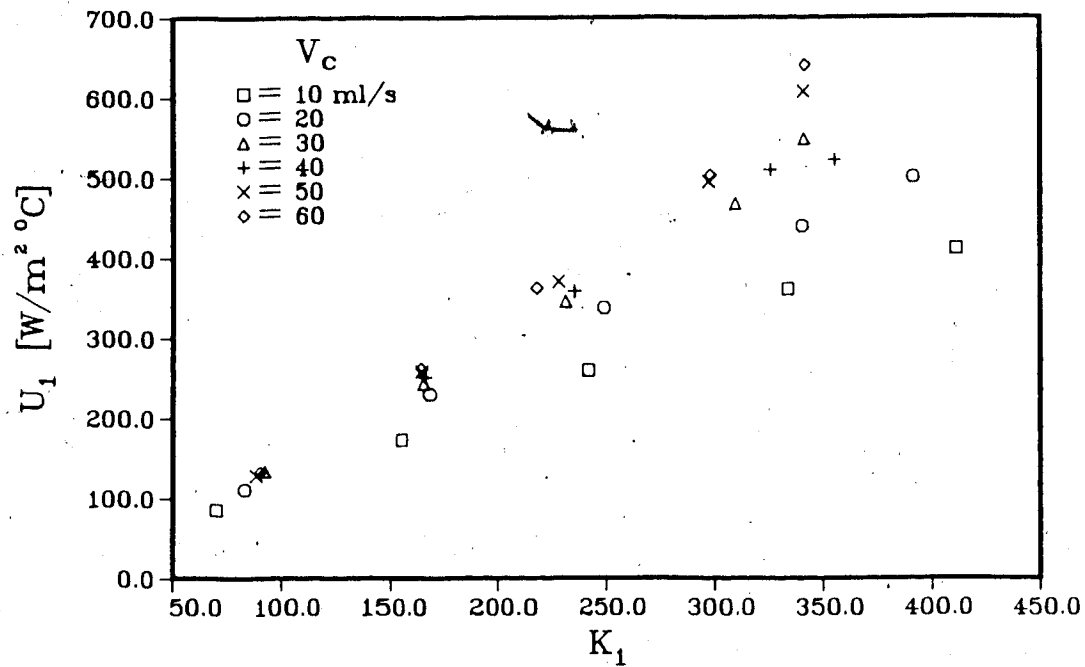


Fig. 2.15 Dean number effect on arithmetic mean overall heat transfer coefficient

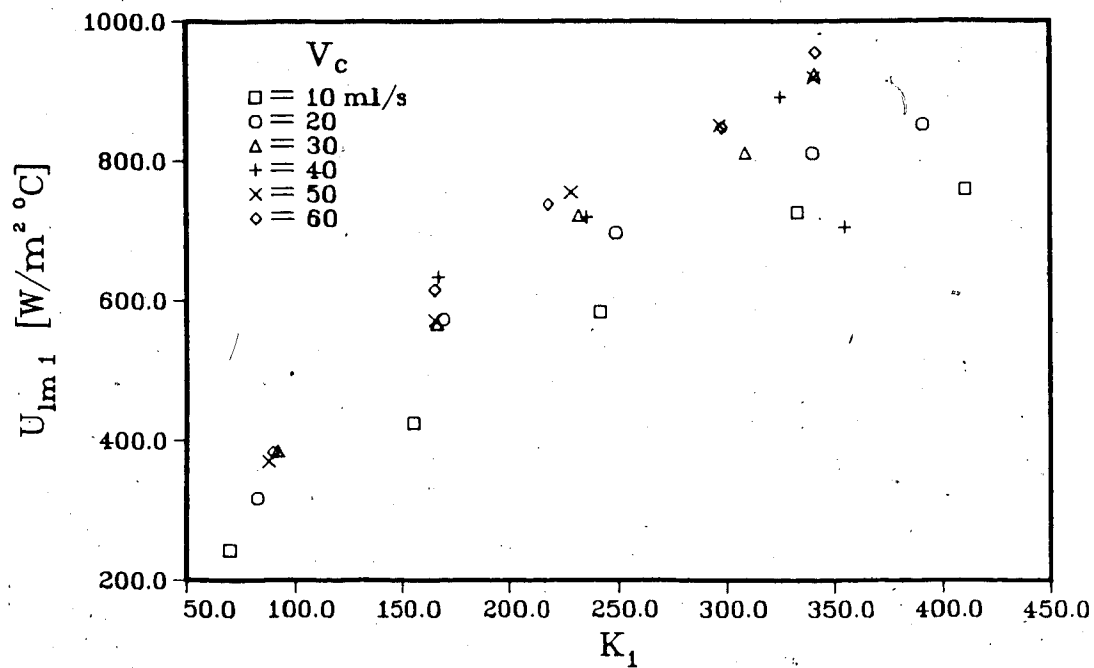


Fig. 2.16 Dean number effect on logarithmic mean overall heat transfer coefficient

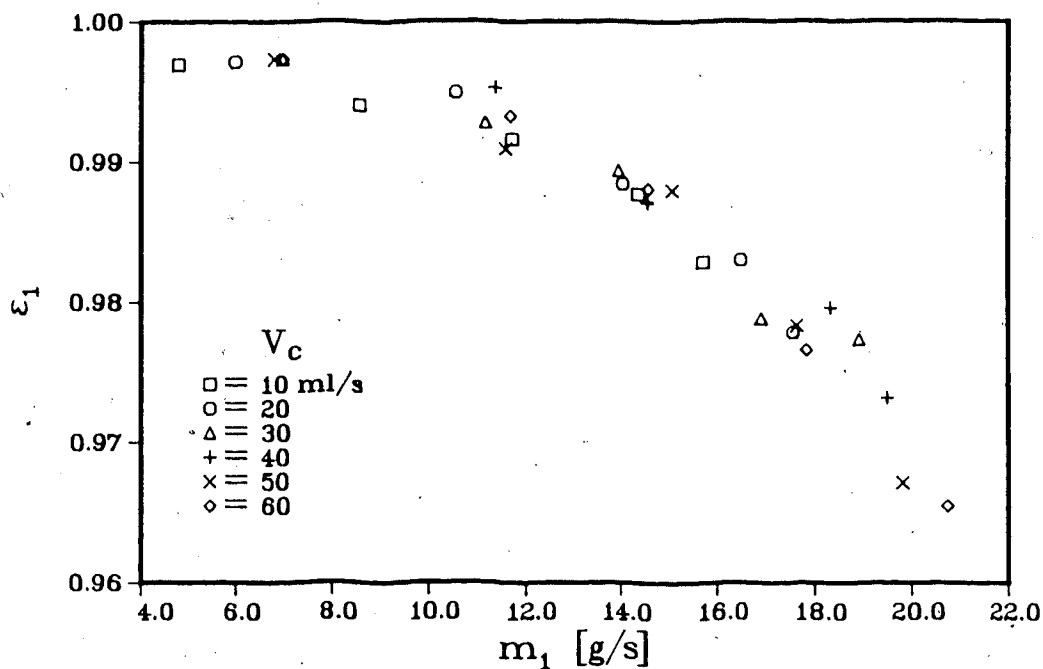


Fig. 2.17 Effect of thermosyphon flow rate on heat exchanger effectiveness

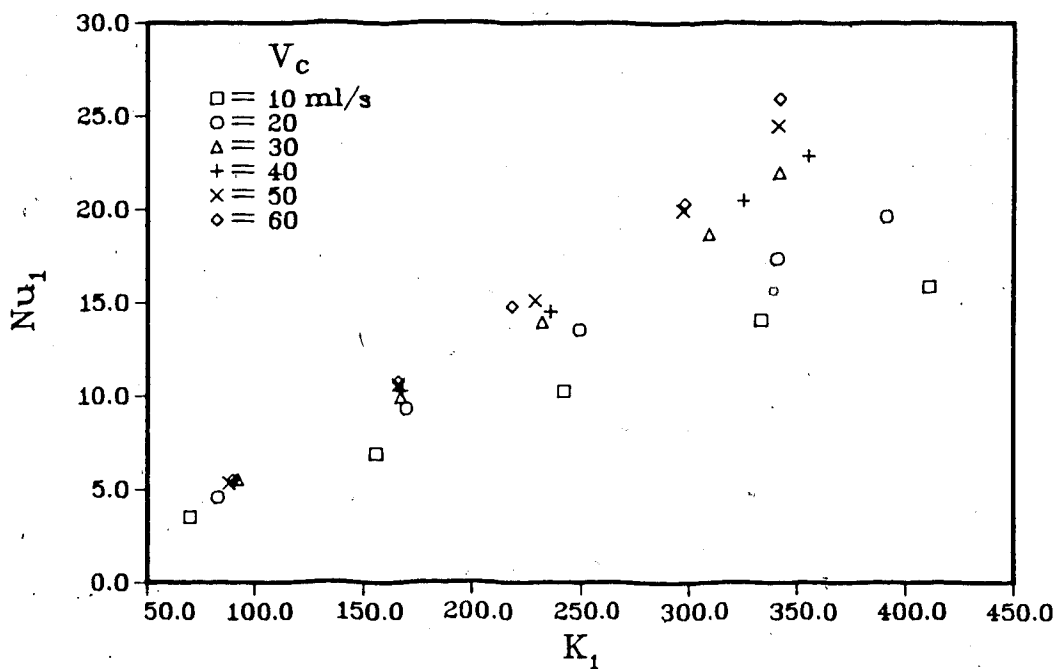


Fig. 2.18 Average Nusselt number vs. Dean number in lower heat exchanger coil

It is also possible to calculate the Nusselt number in terms of the Graetz number as per McAdams [27]. For small Graetz number, the asymptotic solution is given by

$$Nu = 0.5 Re Pr d/l \quad (2.25)$$

The equation is valid for a constant wall temperature condition and parabolic velocity profile, and represents the upper bound for the Nusselt number in a circular tube.

Fig. 2.20 shows the experimentally determined Nusselt number plotted against inverse Graetz number along with the solution from Eq.(2.25). The test data correlates well with a simple power relation as shown in the figure. The inverse Graetz number is modified in a non-dimensional manner to include curved tubes by replacing the Reynolds number with Dean number and the resulting correlation is shown in Fig. 2.21. The coefficients a and b described in Eq.(2.20) are 1.116 and -1.404, respectively.

In heated tubes there is a possibility that secondary flow caused by buoyancy effects along the tube wall is enhancing the heat transfer. A dimensionless parameter which represents the ratio of buoyancy forces to viscous forces is known as the Rayleigh number, defined here as

$$Ra = Gr Pr d/l \quad (2.26)$$

with the Grashof number given by

$$Gr = g \beta (\Delta T) d^3 / \nu^2 \quad (2.27)$$

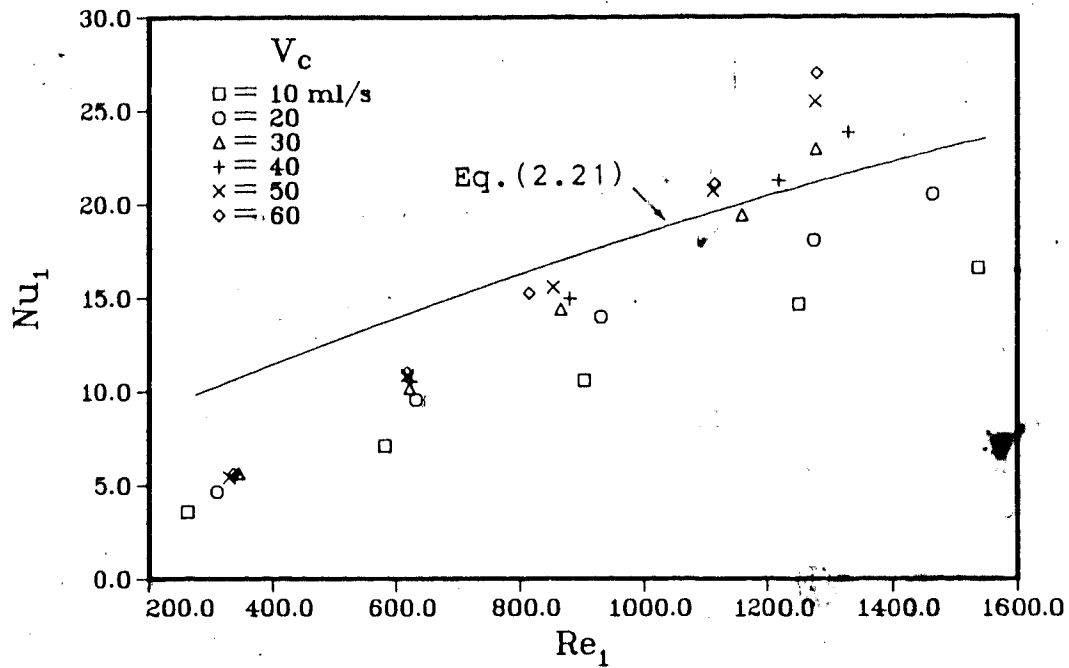


Fig. 2.19 Comparison of Nusselt number with coiled tube correlation

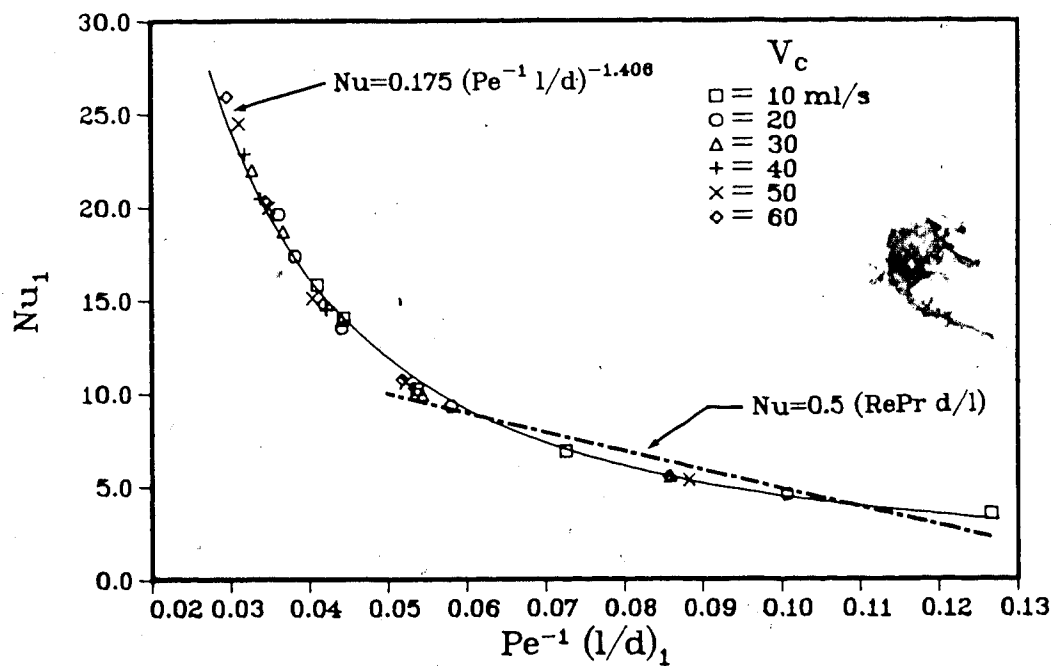


Fig. 2.20 Inverse Graetz number effect on average Nusselt number for thermosyphon flow in the lower heat exchanger

By comparing Fig. 2.22 with data compiled by Metais and Eckert [28], it is possible to determine the flow regime; be it forced, free, or mixed. Since the pitch of the coil is less than 3 degrees, the flow may be considered horizontal, and for comparison purposes the tube is assumed straight.

The operating range of the heat exchanger places the flow regime of the inner tube in the mixed convection region, indicating that local buoyancy effects may play a part in enhancing the heat transfer process. However, due to the presence of the spiral shaped flow boundary, it would be difficult to separate and quantify the buoyancy effects for flow in the inner tube. As well, the curvature of the tube induces secondary flow due to centrifugal forces, which becomes important over the range of Dean numbers encountered [29]. The combination of spiral geometry, curved tube and heated wall no doubt creates a condition of strong secondary flow and good mixing, which enhances heat transfer to the flowing fluid and is partly responsible for the high effectiveness values found for the heat exchanger.

2.6.3 Upper Heat Exchanger

The upper heat exchanger is a commercially available shell and coil unit designed for use as a condenser in phase change solar collectors, with a total capacity of 10-12 kilowatts. The cooling water passes through the coil, while

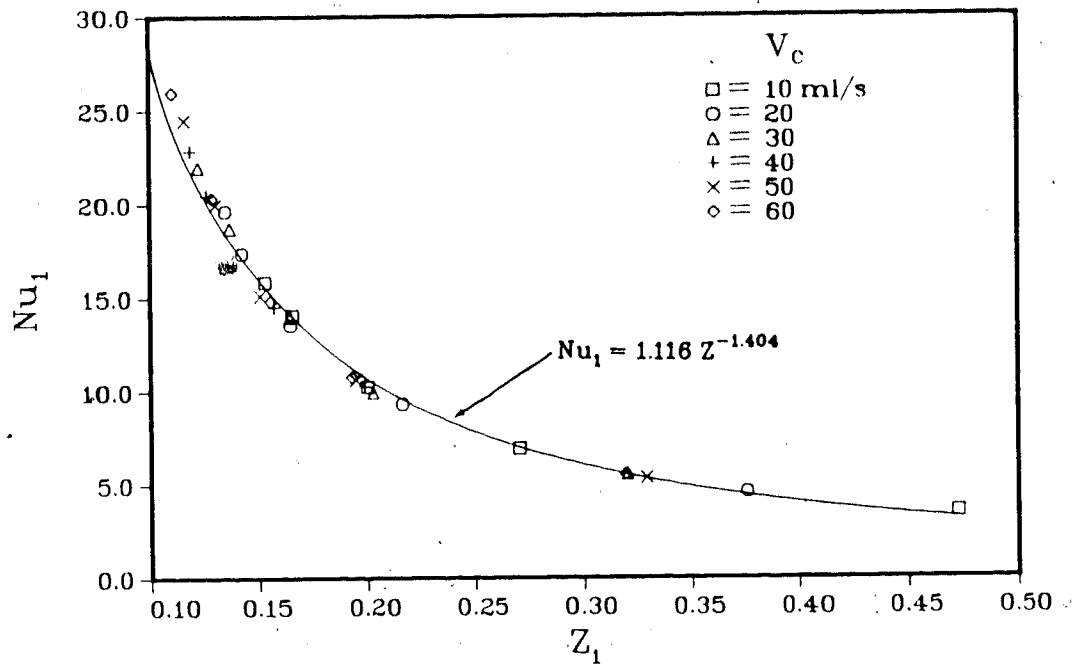


Fig. 2.21 Correlation of Nusselt number with modified inverse Graetz parameter

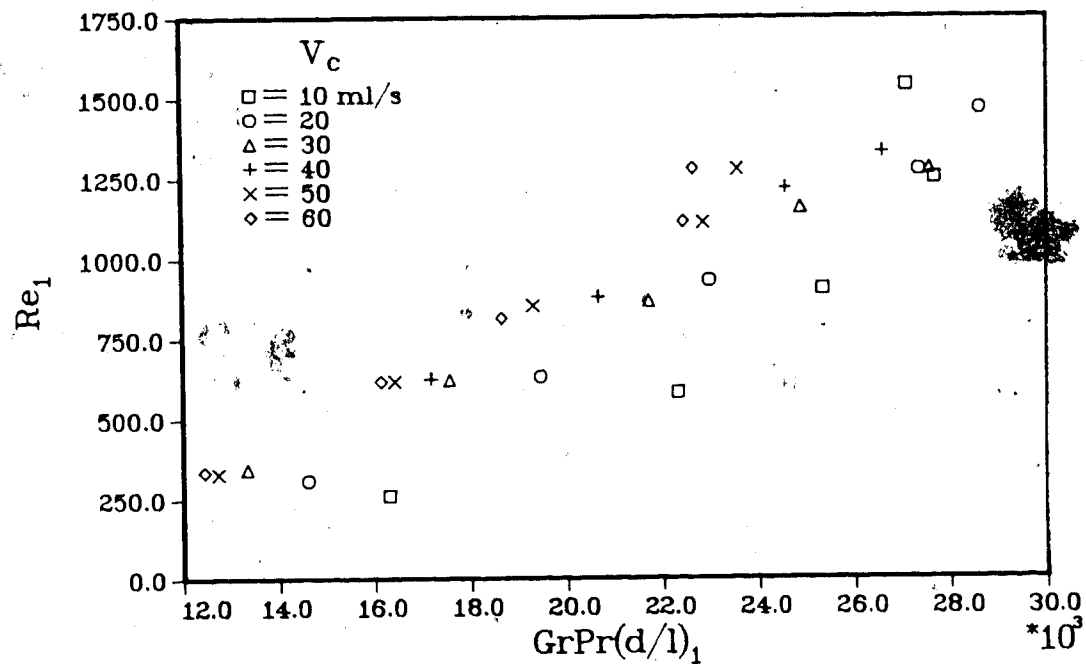


Fig. 2.22 Reynolds number vs Rayleigh number for flow regime determination

the hot water (working fluid) flows through the shell in counterflow. As with the lower heat exchanger, heat transfer calculations are based on the inner stream, so that cooling water flow rate now becomes a direct parameter.

Figures 2.23 and 2.24 show the arithmetic mean and logarithmic mean overall heat transfer coefficients plotted against the average wall heat flux through the inner surface of the tube. The magnitudes of the heat transfer coefficients are nearly the same for both the arithmetic and logarithmic mean temperature differences.

The coefficients are also plotted against Dean number in Figs. 2.25 and 2.26. The magnitude of the Dean number is a direct result of cooling water flow rate and is thus approximately constant for a given series of tests. The heat source temperature is now an indirect parameter and is increasing from the bottom to the top of the figure. A higher source temperature increases the natural circulation rate and temperature of the working fluid as mentioned earlier, and raises the overall heat transfer coefficient of the upper heat exchanger. This also has an effect on the Nusselt number for flow in the tube, as shown in Fig. 2.27, with the heat source temperature increasing vertically. Again the interaction of the separate loops caused by the primary natural circulation loop is observed.

Attempting to correlate Nusselt number with inverse Graetz number for the coiled tube is unsuccessful as shown in Fig. 2.28. This occurs because the value of the Graetz

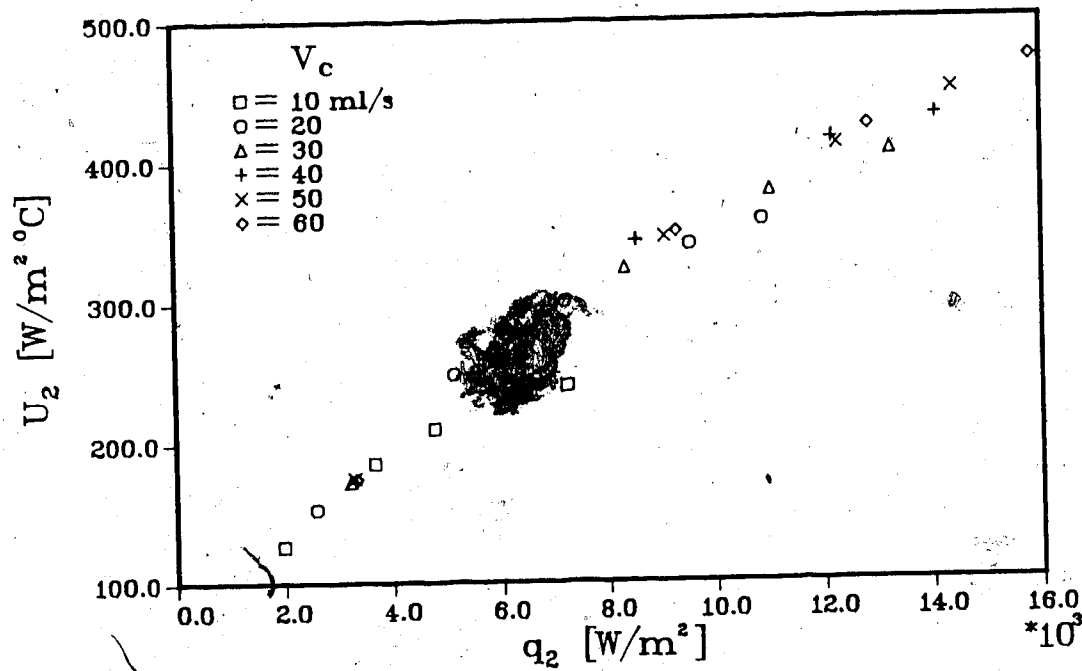


Fig. 2.23 Arithmetic mean overall heat transfer coefficient for the upper heat exchanger

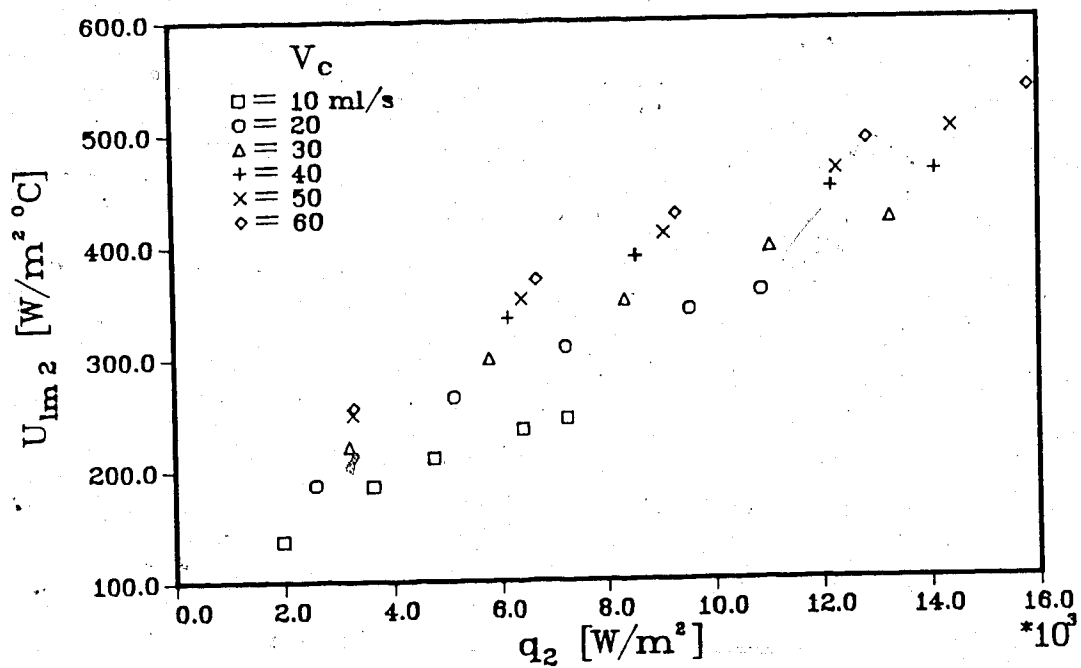


Fig. 2.24 Logarithmic mean heat transfer coefficient for the upper heat exchanger

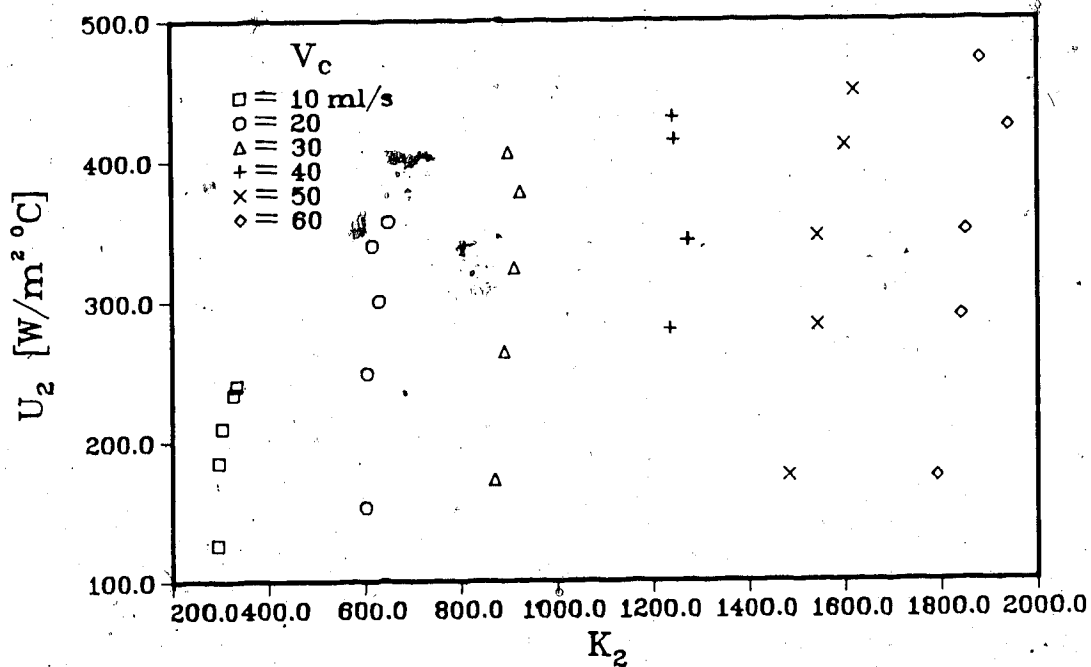


Fig. 2.25 Dean number effect on arithmetic mean overall heat transfer coefficient

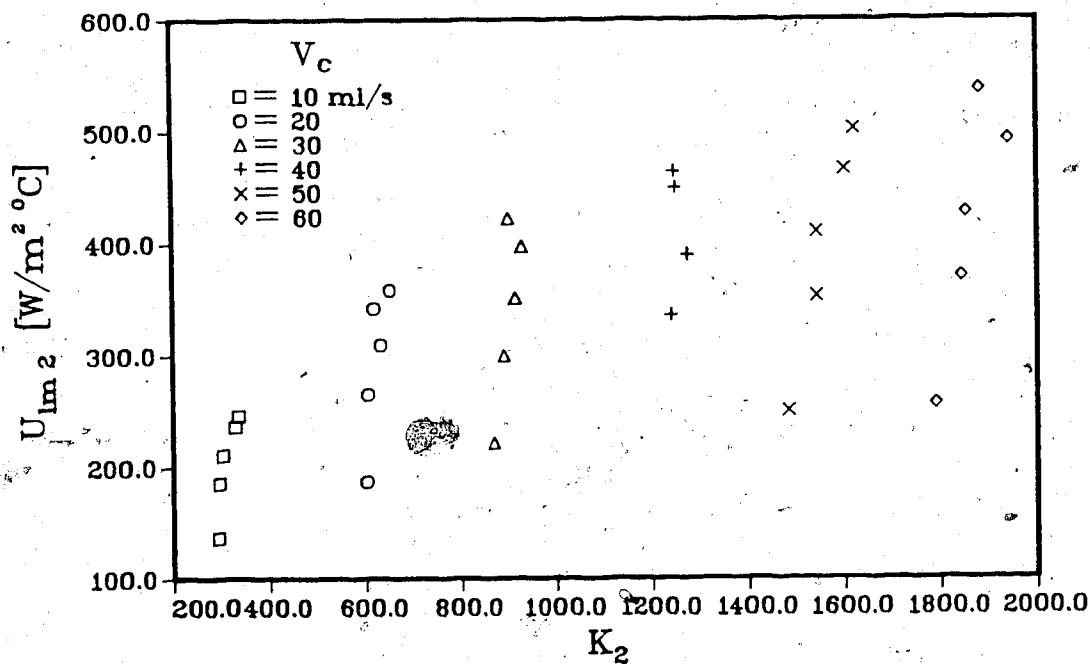


Fig. 2.26 Dean number effect on logarithmic mean overall heat transfer coefficient

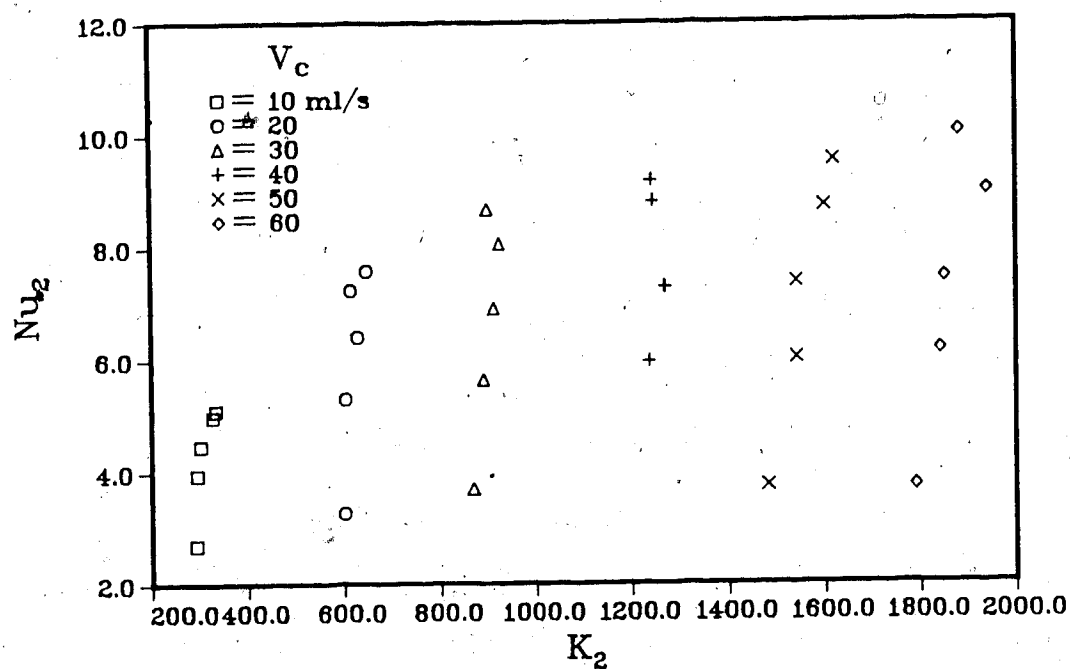


Fig. 2.27 Effect of Dean number on tube side Nusselt number in the upper heat exchanger

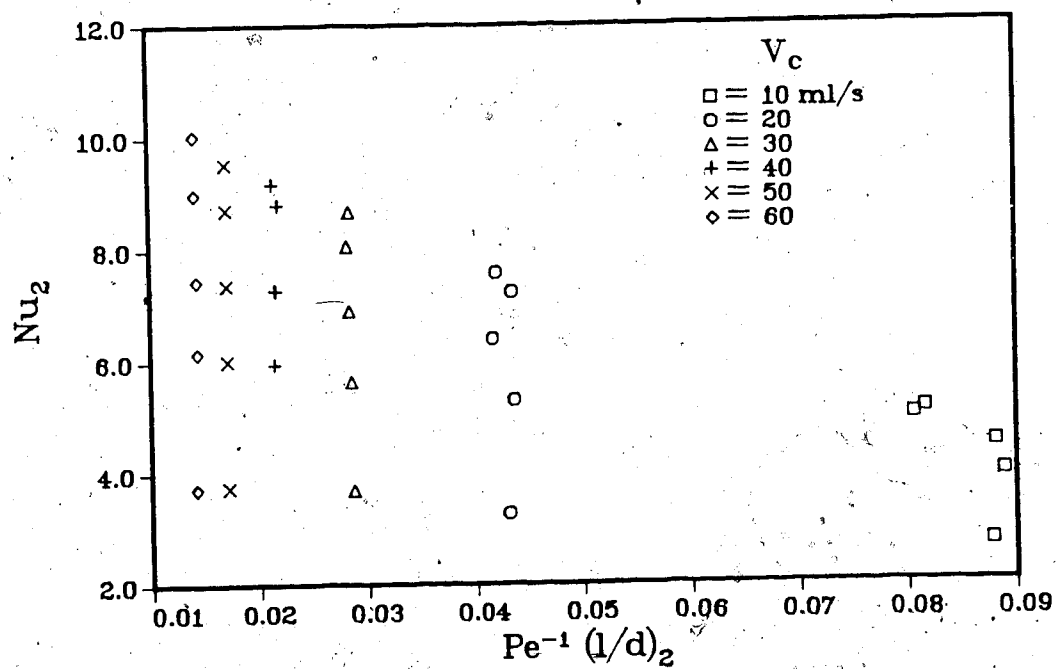


Fig. 2.28 Effect of inverse Graetz parameter on Nusselt number for tube side flow

parameter is dependent on the forced convection in the tube, while the Nusselt number is more dependent on the indirect parameters of heat source temperature and the flow rate in the primary loop, as illustrated by the previous plots of overall heat transfer coefficient and Dean number.

The fin side heat transfer coefficient is of interest for later comparison to two-phase results. This is calculated from Eq.(2.22), and is plotted in Fig. 2.29 showing the strong influence of the natural circulation mass flow rate.

The range of operation causes the effectiveness of this heat exchanger to be considerably lower than that calculated for the lower unit with a maximum of 0.93 and a minimum of 0.48. This is plotted against the fin side mass flow rate in Fig. 2.30.

The coils of the upper heat exchanger lie in vertical planes so that buoyancy effects due to heating which occur in the first 180 degrees of travel (upward direction) will be partially negated in the next 180 degrees of a coil (downward flow). No assumption of vertical or horizontal direction is useful here as the directional components of possible buoyancy forces oscillate in a sinusoidal manner as the flow proceeds through the coils. For reference, the plot of Reynolds number and Rayleigh number is shown in Fig. 2.31.

The contribution to secondary flow due to the curvature effect may be significant as the Dean numbers in the coil

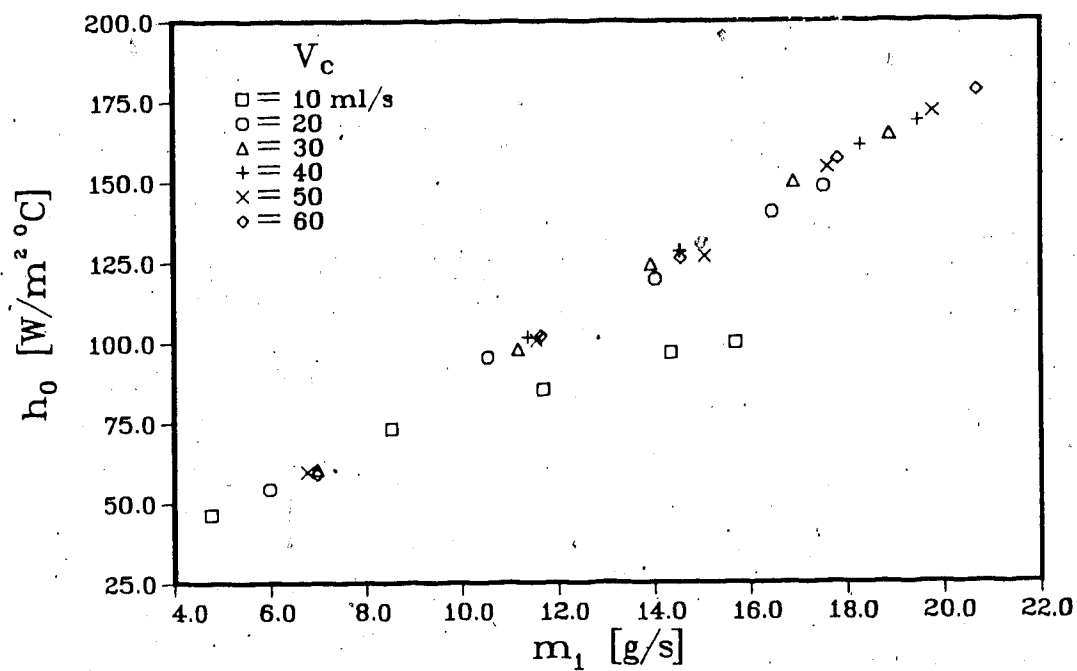


Fig. 2.29 Fin side heat transfer coefficient vs. thermosyphon mass flow rate for upper heat exchanger

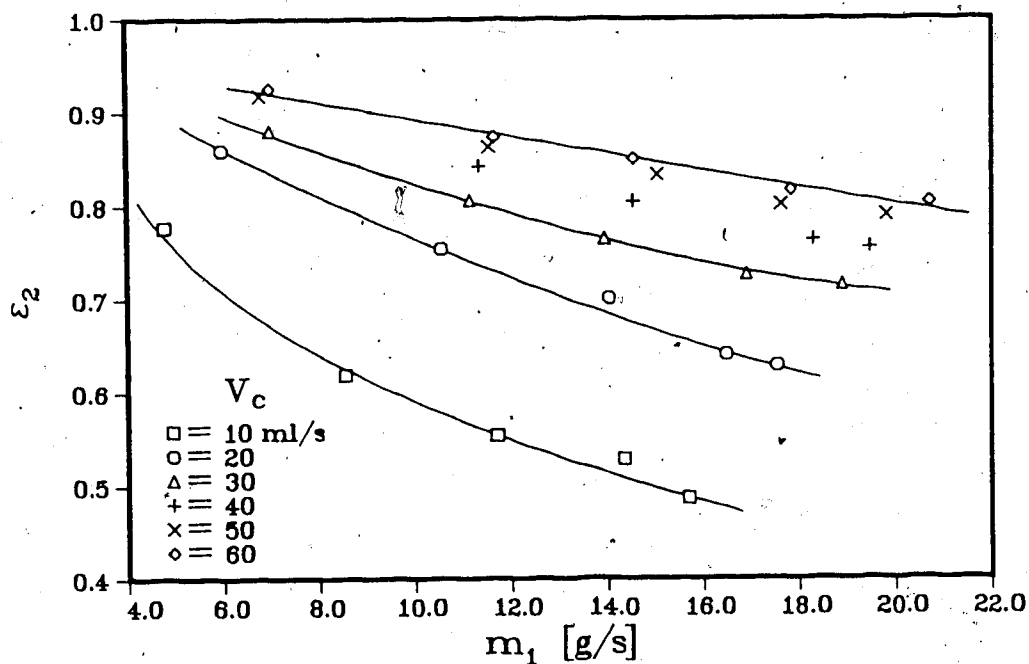


Fig. 2.30 Upper heat exchanger effectiveness vs. thermosyphon mass flow rate

are relatively large ($K=200-2000$). The flow is still laminar, as the critical Reynolds number for this coil geometry is over 10,000 according to Ito [30], and the maximum value encountered here is about 5600. The curvature effect is most easily examined by comparing the pressure drop in the coil to that in a straight smooth tube of the same length. Induced secondary flows should create better momentum transfer between the wall and core flow, thus increasing the pressure drop. The ratio of the two is plotted against Dean number in Fig. 2.32, along with a correlation for the pressure drop in curved tubes given by Ito [30]. The discrepancy at high Dean number could be due to entrance region effects or local buoyancy force induced flows which are difficult to describe due to the orientation of the coil. The curved tube pressure drop is a maximum of 8.5 times greater than that for a smooth straight tube with the same flow rate, indicating heat transfer augmentation due to the presence of secondary flow.

2.7 Forced Flow Results and Discussion

The conventional approach to transporting energy over a distance is to couple the heat source and heat sink with a working fluid loop and force the flow with a pump. A centrifugal pump was installed in the primary loop to study the system performance under forced flow conditions, and its location is shown in Fig. 2.1. The unit is designed for use in hydronic solar collector systems and thus has a small

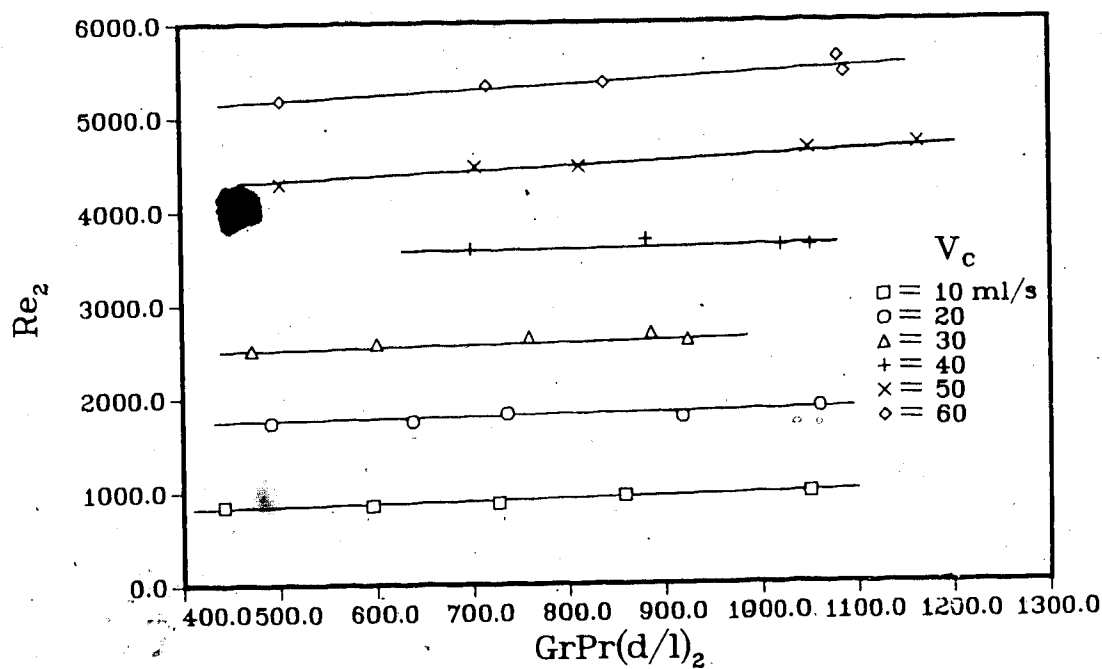


Fig. 2.31 Reynolds number vs. Rayleigh number for flow regime comparison

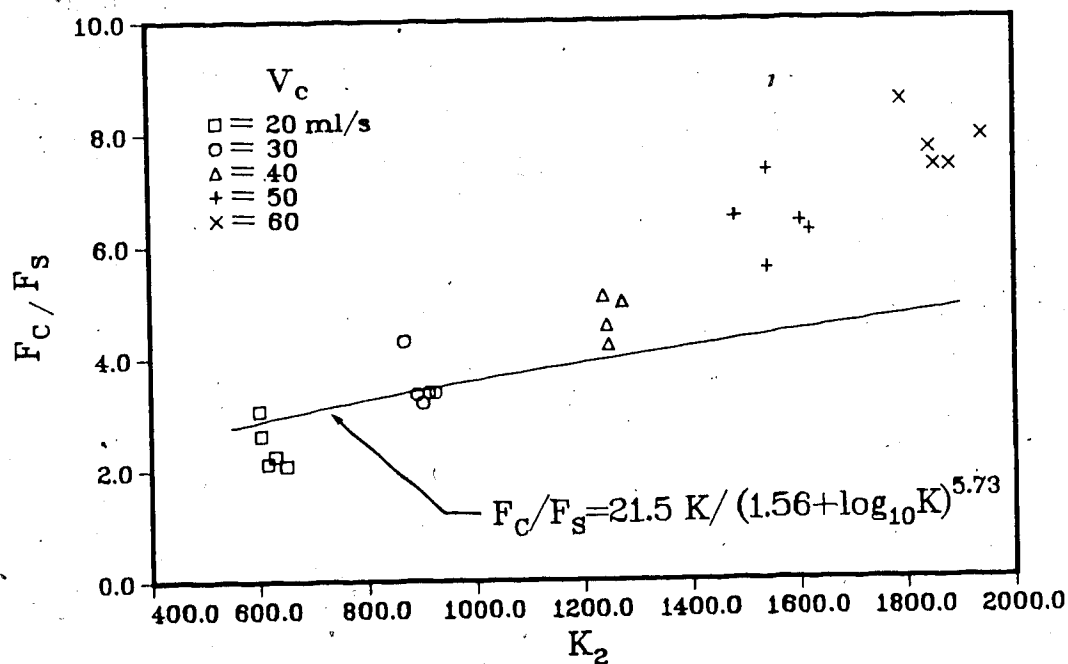


Fig. 2.32 Ratio of curved to straight tube pressure drop for upper heat exchanger coil

power requirement (14.9 Watts, 3000 rpm). The results presented here are primarily for comparison to the performance of the thermosyphon system.

The varied operating parameters used in these tests are heat source temperature; 55-95°C in increments of 10°C, and working fluid flow rate; 15-30 ml/s in increments of 5 ml/s. Cooling water temperature is held approximately constant as with the natural circulation tests, and the flow rate is fixed at 40 ml/s. Heating fluid flow is also constant at 40 ml/s.

The experimental procedure is similar to that described earlier, except that the flow rate in the primary loop is now controlled by operating a by-pass setup around the pump. The range of forced circulation flow rate was chosen so as to intersect that obtained in natural circulation tests.

As with the thermosyphon system, total heat input is equal to extraction except for heat losses to the surroundings and this is illustrated in Fig. 2.33. The maximum heat extraction has increased from 4200 Watts for the natural circulation system with a cooling water flow of 40 ml/s to 4800 Watts for the forced flow condition.

The effect of the difference in heat source and sink temperature on heat extraction is shown in Fig 2.34 for various working fluid flow rates. As indicated by the natural circulation tests, the higher primary loop flow rates yield better performance.

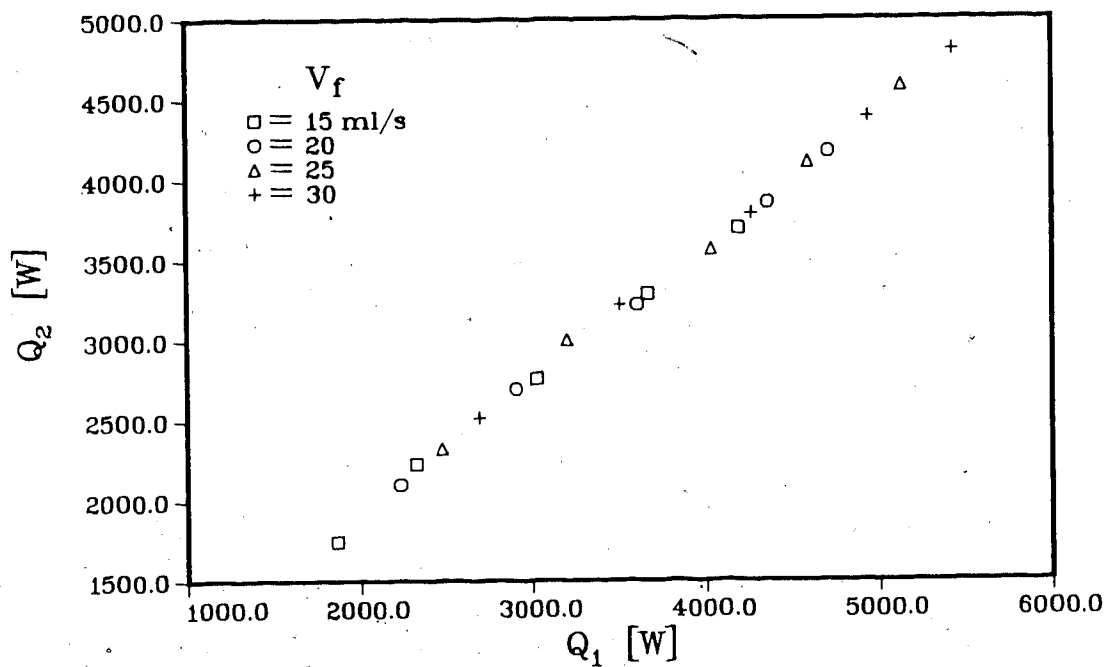


Fig. 2.33 Relationship between heat recovery and heat input for forced flow conditions

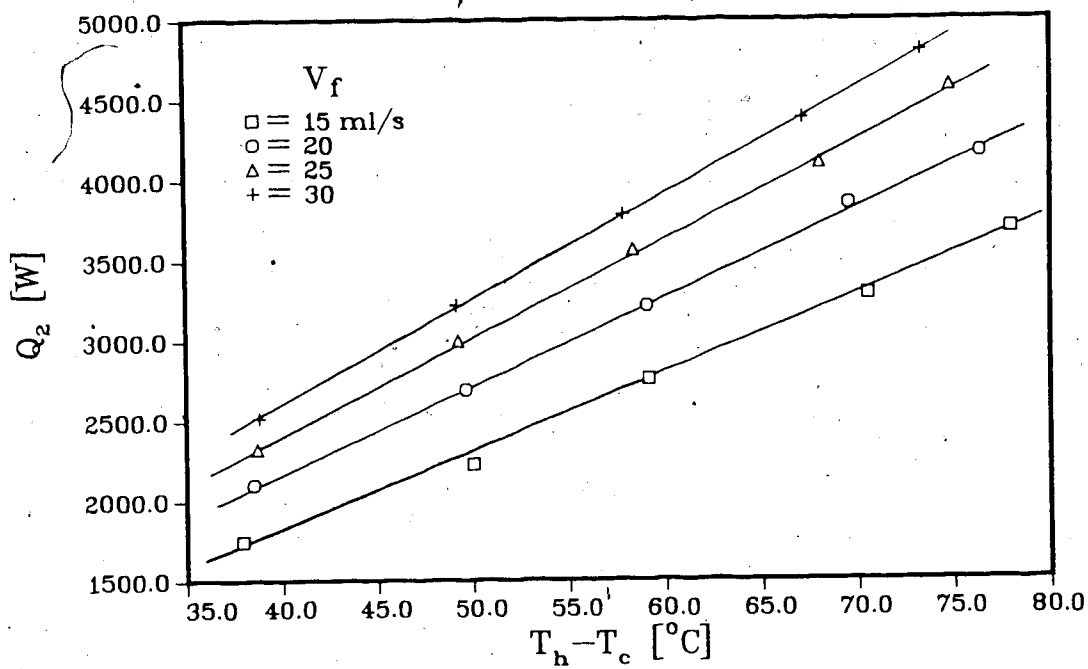


Fig. 2.34 Effect of system temperature difference on overall heat recovery

The overall effectiveness of the system is also enhanced by this increase in flow rate, as shown in Fig. 2.35. The effectiveness was increased from 0.32 to 0.39 by the inclusion of the pump for the same external operating parameters.

The thermodynamic efficiency is less dependent on the input heat flux as was the case for the natural circulation system, as shown in Fig. 2.36. This occurs because the primary loop flow rate is no longer a function of the heat input. This is further illustrated by Fig. 2.37 which shows the effect of the Reynolds number at the inlet tube of the lower heat exchanger on the efficiency. The various heat source temperatures are grouped together for a specific Reynolds number. For the same external parameters, the total thermodynamic efficiency of the system including the power consumed by the pump has increased only marginally from 0.2 for natural circulation to 0.24 for forced flow.

The behaviour of the lower heat exchanger under the forced flow condition is shown in Fig. 2.38, with the overall heat transfer coefficient plotted against the average wall heat flux. The strong effect of the primary loop flow is seen here and in Fig. 2.39 where the effect of the Dean number on the average Nusselt number is shown. Note the linearity of the results.

The correlation between the average Nusselt number and modified inverse Graetz parameter for the inner tube of the lower heat exchanger is shown in Fig. 2.40 and fairly good

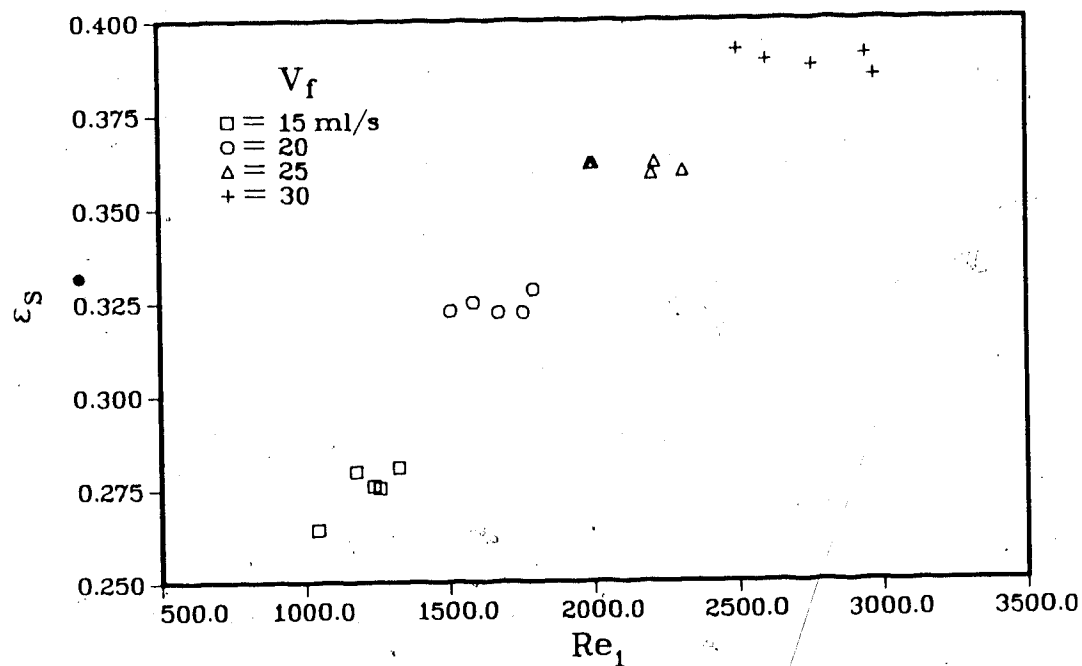


Fig. 2.35 Effect of forced flow Reynolds, number on system effectiveness

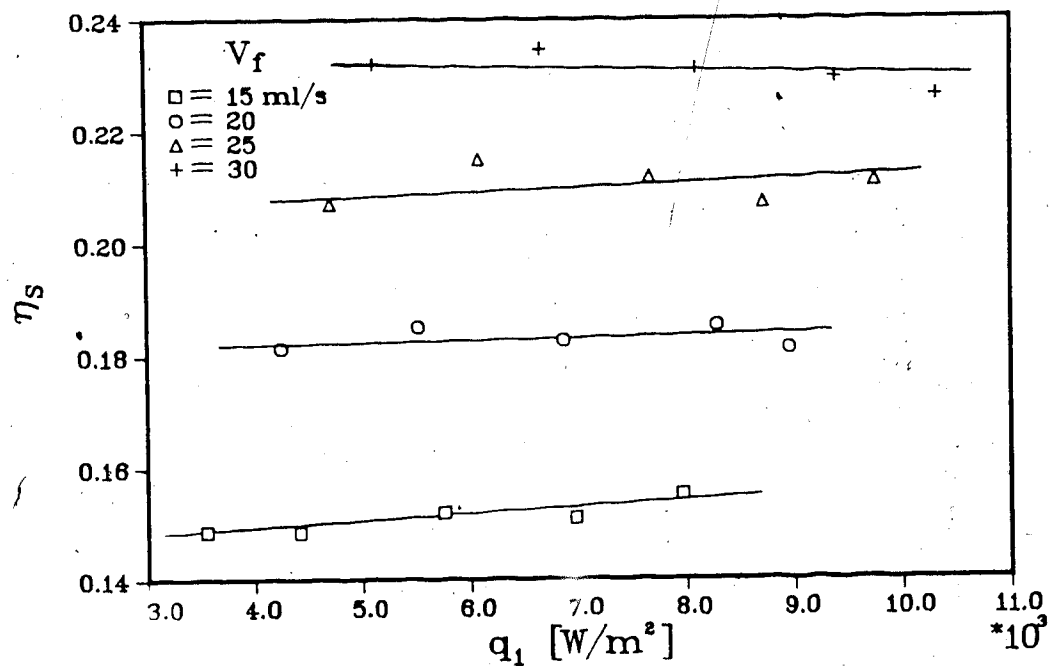


Fig. 2.36 Effect of input heat flux on thermodynamic efficiency

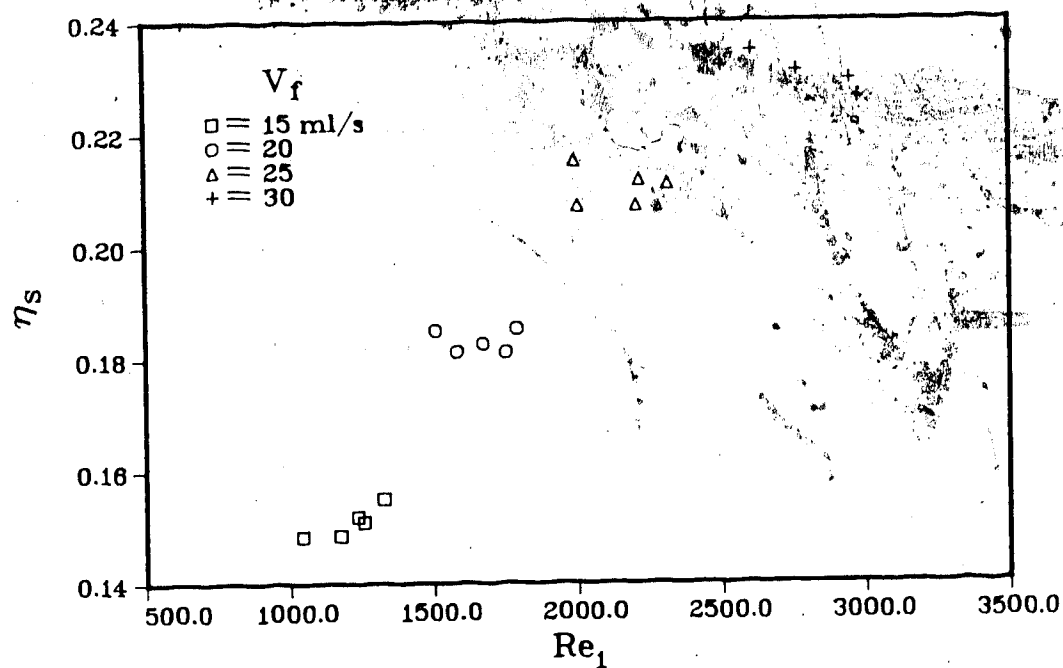


Fig. 2.37 System thermodynamic efficiency vs. forced flow Reynolds number

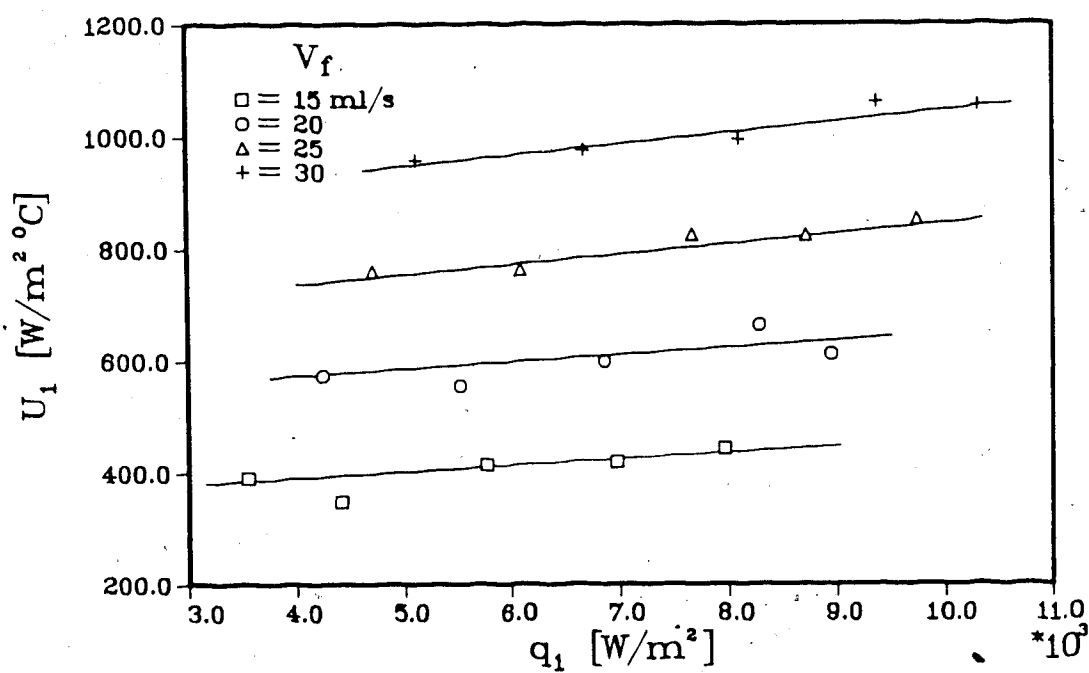


Fig. 2.38 Arithmetic mean overall heat transfer coefficient for lower heat exchanger with forced flow conditions

agreement is found.

The upper heat exchanger behaves similarly to the lower unit when examining the effect of the average wall heat flux on the overall heat transfer coefficient, as in Fig. 2.41. The forced flow effect is large as expected, and this is also the case for the fin side heat transfer coefficient, seen in Fig. 2.42. The effects of indirect parameters such as heat source temperature on the performance are virtually eliminated for the forced flow condition as compared with the natural circulation system. This is a direct result of holding the primary flow rate fixed, as opposed to the natural circulation system where the flow is a function of the external parameters.

2.8 Conclusion

The closed loop liquid phase thermosyphon charged with distilled water was found to successfully transport heat from the low grade liquid heat source loop to the liquid heat sink loop at a maximum rate of 4200 Watts under steady state conditions. This occurred for the highest heat source temperature (95°C) and highest cooling water flow rate (60 ml/s). Due to the short height of the heating and cooling sections as compared to the overall vertical separation, the system was not self starting.

The rate of heat recovery, overall effectiveness, and system thermodynamic efficiency were all found to be favourably affected by higher system temperature differences

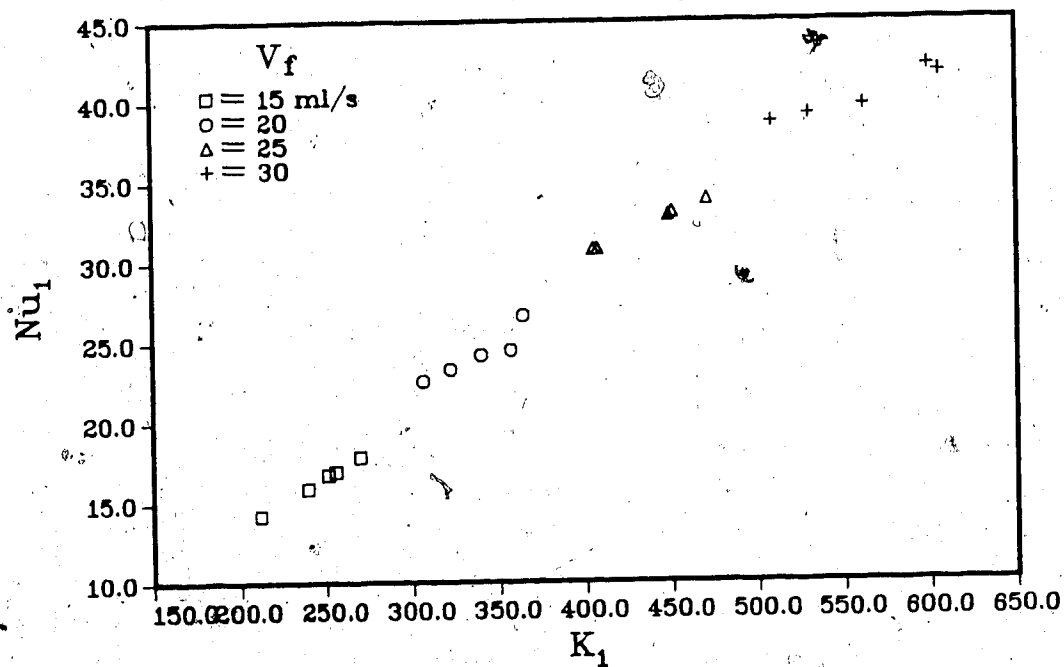


Fig. 2.39 Effect of forced flow Dean number on Nusselt number for inner coiled tube

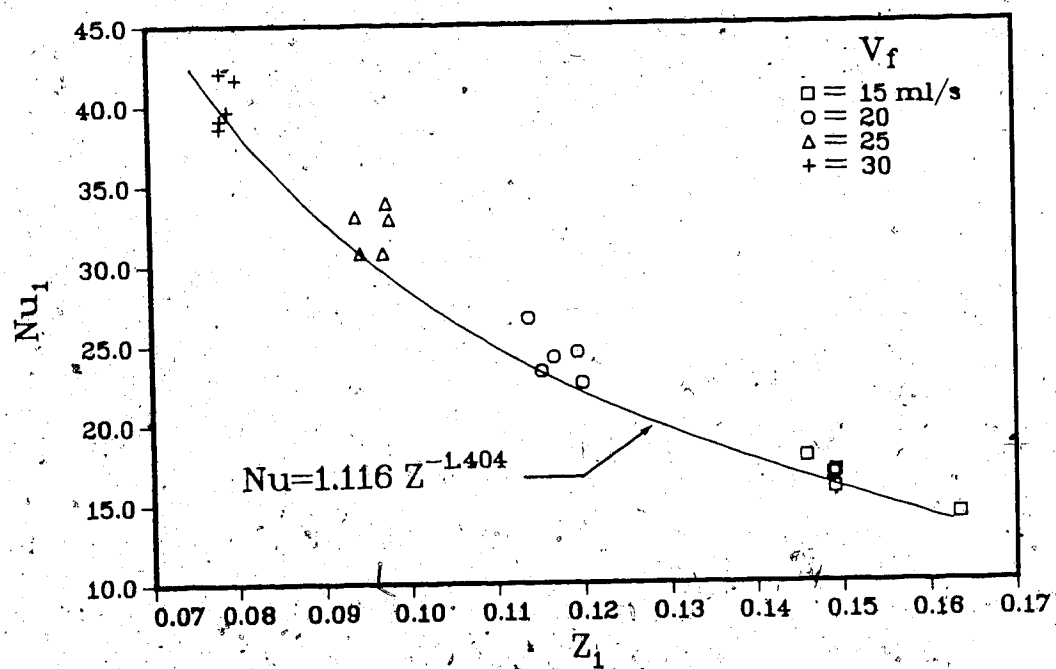


Fig. 2.40 Lower heat exchanger Nusselt number vs. modified inverse Graetz parameter for forced flow

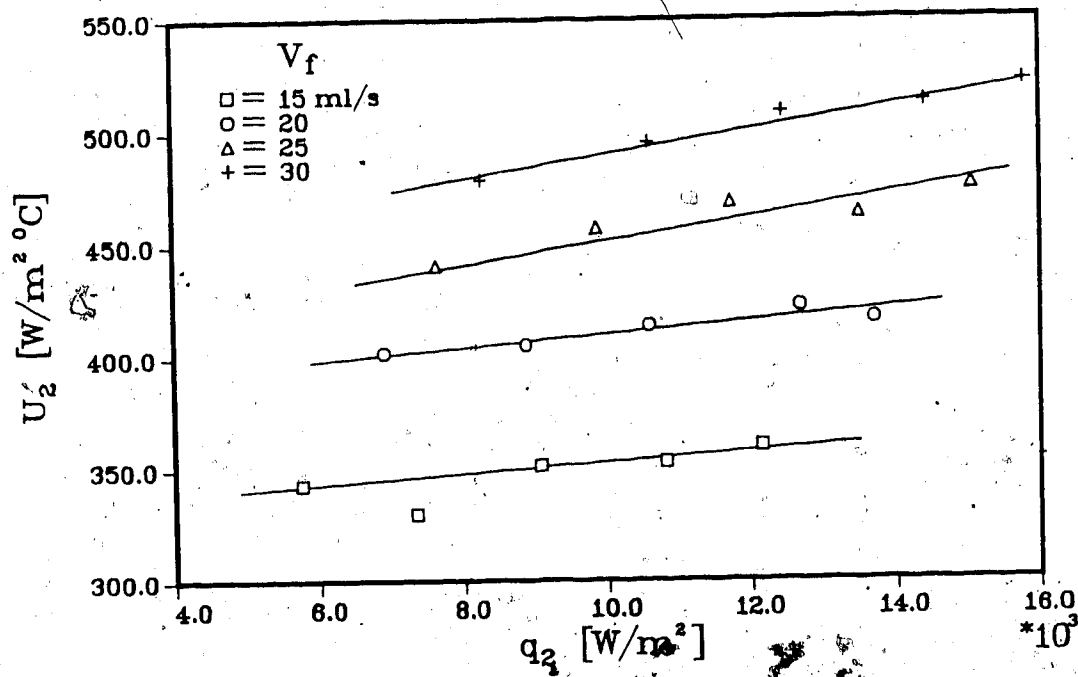


Fig. 2.41 Arithmetic mean heat transfer coefficient for upper heat exchanger

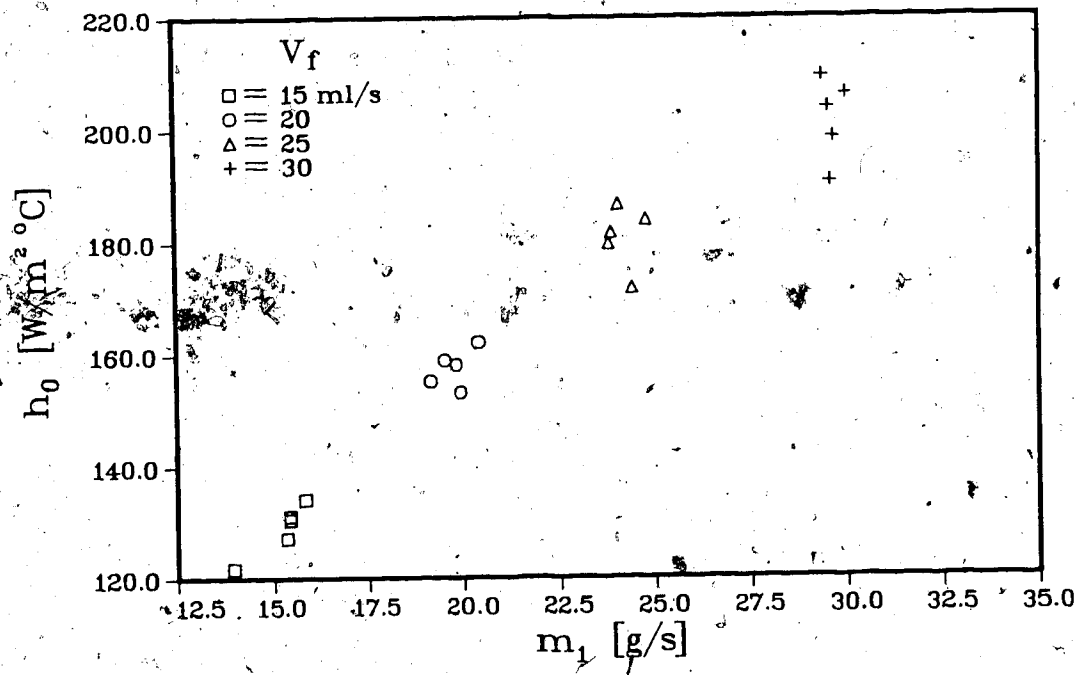


Fig. 2.42 Fin side heat transfer coefficient vs. forced primary loop mass flow rate

and increased working fluid natural circulation rate. The maximum effectiveness and efficiency were found to be 0.32 and 0.33, respectively.

The natural thermosyphon flow increased with higher coolant flows and increasing heat source temperature due to their effects on the density of the fluid in the different legs of the primary loop. The major contributor was found to be heating fluid temperature, and the maximum mass flow rate obtained was 21 g/s, corresponding to a lower heat exchanger inlet tube Reynolds number of 2050.

It was found that the effect of both the coolant flow and system temperature difference on the thermosyphon mass transport could be represented singularly by the input heat flux. Over the range of tests conducted, increases in input heat flux corresponded to higher primary loop flow rates. It is desirable to increase the thermosyphon flow, and one possibility is to eliminate flow restrictions caused by small tube sizing, instrumentation, or the bulk temperature measurement meshes.

The primary natural circulation loop was found to form a sympathetic link between the secondary loops, so that the performance of the heat exchangers became functions of far removed parameters. The lower heat exchanger was very effective, and the Nusselt number for flow in the inner tube correlated well with an inverse Graetz parameter using a simple power relation. The operating ranges of both units indicates augmented heat transfer due to secondary flows,

and a significant increase in the pressure drop of the upper helical coil over the straight tube case was found.

Extensive information is provided on the operating characteristics of these compact units for future reference.

Forcing the flow in the primary loop with a centrifugal pump did increase heat recovery, but caused only marginal changes in the overall effectiveness and efficiency of the system. The linking effect between the behaviour of physically separated components of the system as observed for thermosyphon conditions was eliminated.

3. Closed Loop Two-Phase Water Thermosyphon Tests¹

3.1 Introduction

Present phase change solar collector systems require working fluids which boil at relatively low temperatures at atmospheric pressure, such as refrigerants R-113 (45°C) or R-11 (23°C). Another possible arrangement for phase change low grade energy recovery is to use a normally high boiling temperature liquid such as water subjected to a vacuum in order to lower the boiling point. This simple but novel idea has been employed in some closed tube thermosyphon work, but a lack of literature exists for its use in a low grade energy recovery closed loop thermosyphon. Thus, the steady state operating and heat transfer characteristics of the experimental system are studied with water at an initial evaporator pressure of 34 kPa absolute (20 in. of mercury vacuum). This lowers the saturation temperature of water from 100°C at atmospheric pressure to approximately 55°C in the primary loop evaporator tube, so that low grade tests may still be conducted. Water was selected for this investigation in order to easily obtain single phase data as a reference and to study two-phase system performance with low vapor quality flow. In addition, water has other

¹ an ASME paper based on the contents of this chapter has been accepted for publication and will be presented at the 23rd ASME/AICHE/ANS National Heat Transfer Conf., Denver Colorado, Aug 4-7, 1985

² the lower heat exchanger and upper heat exchanger will be henceforth referred to as the evaporator and condenser, respectively

advantages over refrigerants such as low cost, availability, and ease of handling.

The operating principle of the two-phase system is essentially the same as that for the liquid-phase case, except that the driving force for natural circulation is increased. This is due to lower density liquid-vapor flow in the riser line from the evaporator, and the increased pressure in the evaporator due to vapor generation. The return lines to the evaporator inlet still contain the higher density liquid. The higher two-phase convective boiling and condensation heat transfer coefficients are expected to improve performance of the heat exchangers, thus benefitting the overall system.

3.2 Experimental Apparatus and Instrumentation

The experimental apparatus is essentially the same as that for single phase tests except that the effects of a liquid-vapor separator located in the riser line will be investigated (see Fig. 2.1). The separator (accumulator) is located at the entrance to the condenser, where it separates off the liquid component of the flow and returns it to the inlet of the evaporator through a line referred to as the downcomer. The cold condensate tube and the downcomer tube are joined by a tee upstream of the evaporator.

The benefits of such a device are two-fold. First, the hot liquid returned to the evaporator brings the working fluid closer to its saturation temperature, allowing for

V

more latent heat transfer. The drier vapor component of the flow which enters the upper heat exchanger allows for less liquid flooding of the finned surface. Flooding is undesirable because the layer of liquid increases the heat transfer resistance.

Additional heaters were installed in the hot water tank to bring the total power input to 5.7 kilowatts. This was done because the tank temperature tended to decline somewhat in the high heat extraction single-phase tests, and the heat transfer was expected to be even higher for the two-phase system.

A more accurate rotameter was installed in the secondary heating loop, as the heat input to the boiling working fluid in the evaporator must now be calculated from the heat given up by the heating water. The range and accuracy of the rotameter are 2.8-36.6 ml/s, and ± 0.2 ml/s, respectively.

In a two-phase natural circulation system such as this, the fluctuations of the pressure and flow rates in the primary loop may be of the same magnitude as their respective mean values. A static pressure tap, Validyne differential pressure transducer, and reference pressure tank were installed in the condensate line to monitor the system pressure fluctuations. The downcomer and condensate flow rates were measured with turbine flow meters, and the system pressure and flow rate fluctuations were recorded on Hewlett Packard chart recorders. The condensate flow meter

and downcomer flow meter ranges and accuracies are 5-80 ml/s ± 0.3 ml/s and 3-60 ml/s ± 0.2 ml/s

The measuring instruments were recalibrated as before, and the treated distilled water in the working fluid loop was flushed out and replaced.

3.3 Experimental Procedure

The operating parameters studied with the two-phase water system are heat source temperature (55-95°C), cooling water flow rate rate (10-70 ml/s), open or closed downcomer line, and the initial amount of liquid in the system. The different liquid levels used in the primary loop are referred to as charge levels, which are measured as a fraction of the vertical distance between the evaporator inlet tube and the horizontal axis of the condenser (100, 70, and 20%). The evaporator pressure was initially set at 20 inches mercury vacuum or about 34 kPa absolute evaporator pressure using a simple venturi and domestic water supply arrangement.

Due to the change in the time of year that the tests were conducted, the cooling water tank temperature ranged from 14-19°C as opposed to 13-17°C for the single-phase tests. The heating water circulation rate was held approximately constant at 30-35 ml/s for all tests.

The startup sequence was similar to that used for the single-phase tests, except that the natural circulation process was for the most part self starting (the centrifugal

pump was not used to initiate the flow). The time between the initiation of the secondary loop flows and primary loop natural circulation was never more than two minutes for a successful self-starting test, and more than 30 minutes with no flow was considered a failed test. Such failures occurred for a combination of low initial liquid charge level and low heat source temperature. Natural circulation starts more readily at higher charge levels due to the syphoning effect in the tubes.

A steady state was assumed to exist when the bulk temperatures and flow rates were judged to be constant at all locations in the system. The computer acquired data were read consecutively 20 times and then averaged. The total acquisition time was of the order of one minute.

3.4 Data Analysis

The analysis of the experimental data is similar to that used for the single phase tests, and additional equations required for the two-phase flow and heat transfer processes will be given here. The properties of the liquid components of fluid streams in the heat exchanger were evaluated at the entrance bulk temperature, and steam properties at the saturation temperature. The heat transferred to the working fluid stream in the evaporator may be broken into three components: the sensible heating of the subcooled liquid, latent heat gain of the two-phase liquid-vapor mixture, and superheating of the vapor phase.

This total heat gain is represented by

$$Q = \dot{m} [C_{pl}(T_s - T_i) + xh_{fg} + C_{pv}(T_o - T_s)] \quad (3.1)$$

Because the heat exchangers are well insulated, the total heat gained by the working fluid is equal to that amount released by the heating fluid, and a similar situation exists at the condenser. This enables the important flow property of vapor mass quality at the evaporator exit and condenser inlet to be calculated by the following equations for the case of no superheating. The vapor mass quality (often referred to in short as quality) may be simply defined as the ratio of the mass of vapor present to the total mass of the flow.

$$x_1 = [Q_1/\dot{m}_1 - C_{pl}(T_s - T_i)]/h_{fg} \quad (3.2)$$

$$x_2 = [Q_2/\dot{m}_2 - C_{pl}(T_s - T_o)]/h_{fg} \quad (3.3)$$

In this study the values of x_1 and x_2 are less than 20% and 30%, respectively. The increase in vapor quality from the evaporator exit to the condenser inlet is due to the presence of the liquid-vapor separator for the open downcomer series of tests.

The overall heat transfer coefficients for the heat exchangers are based on an arithmetic mean temperature difference. The coefficients were also computed with the log mean temperature difference, but only a slight discrepancy

between the two definitions was found.

The two-phase heat transfer process for natural convection boiling inside a coiled spiral tube is very complicated and it is useful to study the experimental results using two-phase flow and heat transfer parameters such as the Martinelli parameter X_{tt} and boiling number Bo which are defined as

$$X_{tt} = (1/x - 1)^{0.9} (\rho_g/\rho_f)^{0.5} (\mu_f/\mu_g)^{0.1} \quad (3.4)$$

$$Bo = q_{fg} / (G h_{fg}) \quad (3.5)$$

The experimental heat transfer coefficients for convective boiling in the evaporator will be compared to the predictions of Shah [31], and Shrock and Grossman [32] which can be calculated from

$$Nu_t = 230 Bo^{0.5} \quad (3.6)$$

$$Nu_t / Nu_s = 7.39 \times 10^3 (Bo + 1.5 \times 10^{-4} X_{tt}^{-0.66}) \quad (3.7)$$

with

$$Nu_s = h_s d / K_f \quad (3.8)$$

The modified Dittus-Boelter expression for the turbulent single phase heat transfer coefficient is required for these

correlations in the form

$$h_s = 0.023 [R_e(1 - x)]^{0.8} Pr^{0.4} k_f/d \quad (3.9)$$

The Shah correlation has been shown to be valid for very low quality saturated boiling [31], and the Shrock-Grossman prediction is meant to apply for a quality range from 0-50% [32] for vertical flow boiling.

Beatty and Katz [33] presented a modified Nusselt theory correlation equation for the condensation heat transfer coefficient of vapor on low finned horizontal tubes. This correlation provides a reference only for the present experimental results where the fin geometry is distorted and the fins are subject to liquid flooding. The properties of liquid water required in the analysis of the experimental data are computed from the equations given in [20] (Appendix II). Cubic spline interpolation from steam tables is used for the properties of steam.

3.5 Results and Discussion

3.5.1 Overall System Characteristics

Due to the large set of experimental parameters varied during the course of the tests, not all data will be shown on each graphical representation of the results. Rather, one parameter such as charge level will be fixed, and the effect of varying the coolant flow will be examined. Another possibility is to fix both the charge level and cooling

water flow rate and illustrate the effect of the downcomer flow. In this manner, a typical cross section of the entire data set may be presented without densely cluttered graphics.

The effects of the operating parameters on the overall thermal performance of the two-phase thermosyphon system are examined first. The heat recovered by the cooling water Q_2 is plotted against the difference between heat source and heat sink temperatures ($T_h - T_c$), in Figs. 3.1 and 3.3 where the effects of the operating parameters can be clearly seen. As expected, the effect of increasing the heat source temperature and cooling water flow rate is to increase the rate of heat recovery. Higher charge levels and open downcomer from the liquid-vapor separator also improve performance. The maximum value of heat recovery rate of 4600 Watts represents a 15% improvement over that obtained in single phase tests.

The improved performance at higher charge levels is puzzling at first because the condenser coil may be partially immersed in liquid, and condensation area reduced. However, this enhanced performance with the low vapor quality and high liquid entrainment flow may be attributed to improved mixing and higher working fluid flow rates, which provides a large amount of sensible heat transfer, as well as the additional latent heat release.

This is substantiated by examining the mass flux at the evaporator inlet as a function of average wall heat flux q ,

as plotted in Figs. 3.4, 3.5, and 3.6. The effect of charge level is seen in Fig. 3.5, and a 100% charge level indicates that the working fluid initially fills the primary loop to the horizontal axis of the condenser. The greater mass flow rates for higher charge levels along with the low vapor quality flow help to explain the rise in heat recovery with increasing charge level noted in Fig. 3.2. Fig. 3.6 shows that with the downcomer from the accumulator open, the mass flux is considerably higher than for the case of closed downcomer. The total mass flux for the two-phase case is approximately double that obtained in single phase tests over the same range of input heat flux, with a maximum value of $G_1 = 137 \text{ kg/m}^2\text{s}$.

Figs. 3.7 and 3.8 show the effect of wall heat flux q_1 on the evaporator tube exit quality x_1 , and the effect of condenser inlet quality x_2 on heat recovery rate Q_2 for 70% charge level. The vapor quality depends on charge level for a given heat source temperature, and it represents the contribution of the latent heat component in heat transport as opposed to sensible heating or cooling. The effect of input wall heat flux q_1 on the system thermodynamic efficiency defined by Eq. (2.24) is shown in Figs. 3.9 and 3.10 with the lowest cooling water flow rate and highest charge level producing the best results. The maximum efficiency of 40% is a 7% improvement over that obtained with the single phase water system under the same operating conditions. Again this low value can be attributed to the

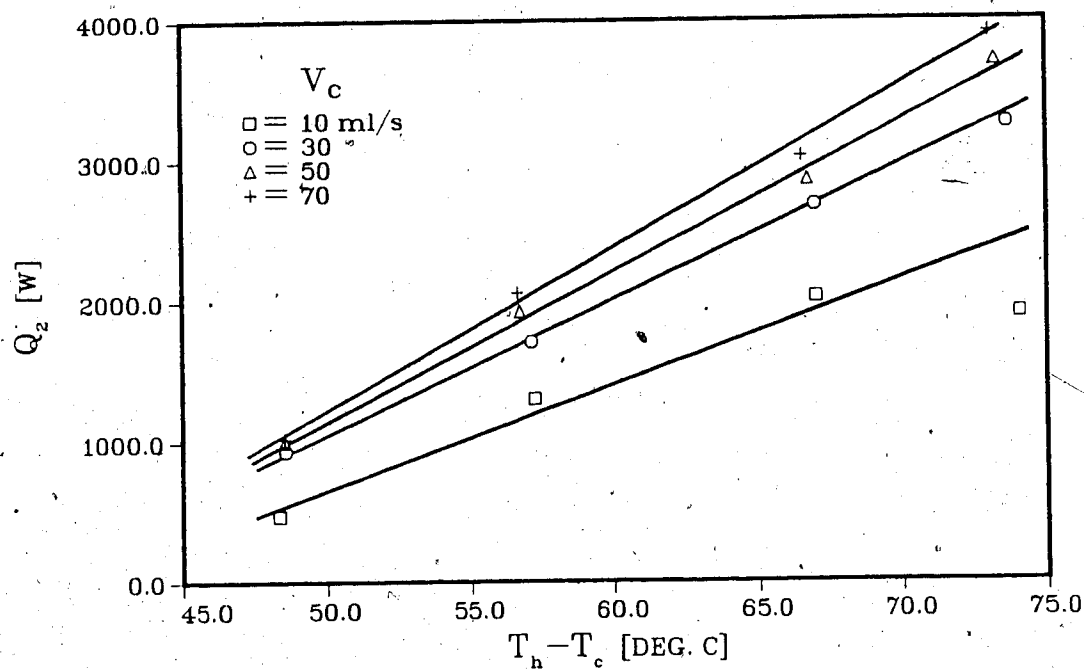


Fig. 3.1 Effect of cooling water flow rate on Q_2 vs. $T_h - T_c$ with 70% charge level and downcomer closed

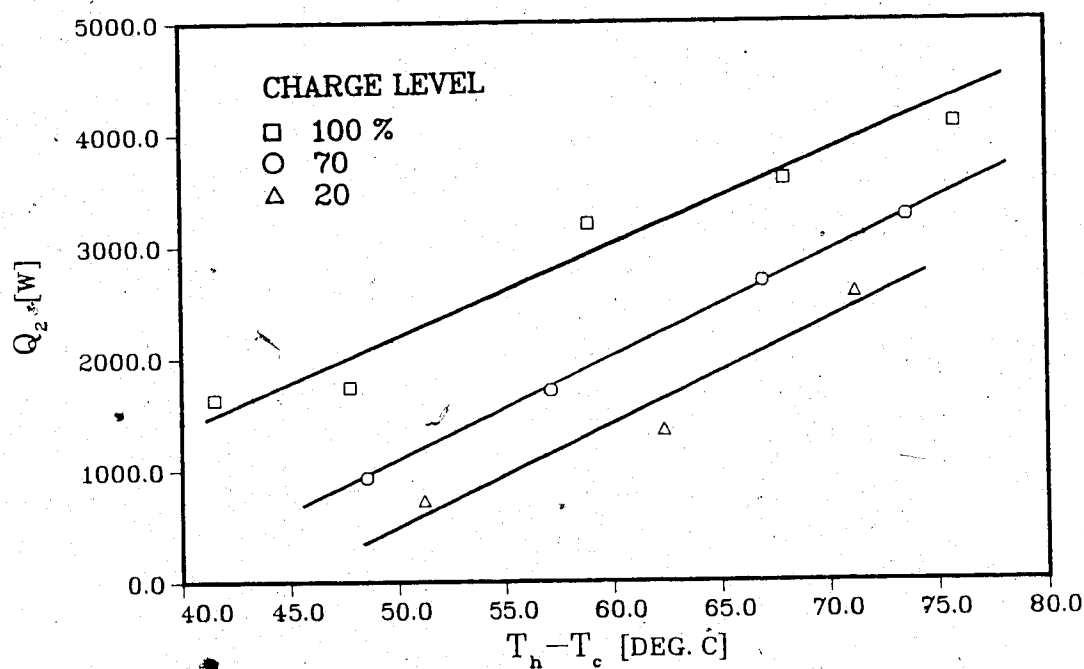


Fig. 3.2 Effect of charge level on Q_2 vs. $T_h - T_c$ with $V_c = 30$ ml/s and downcomer closed

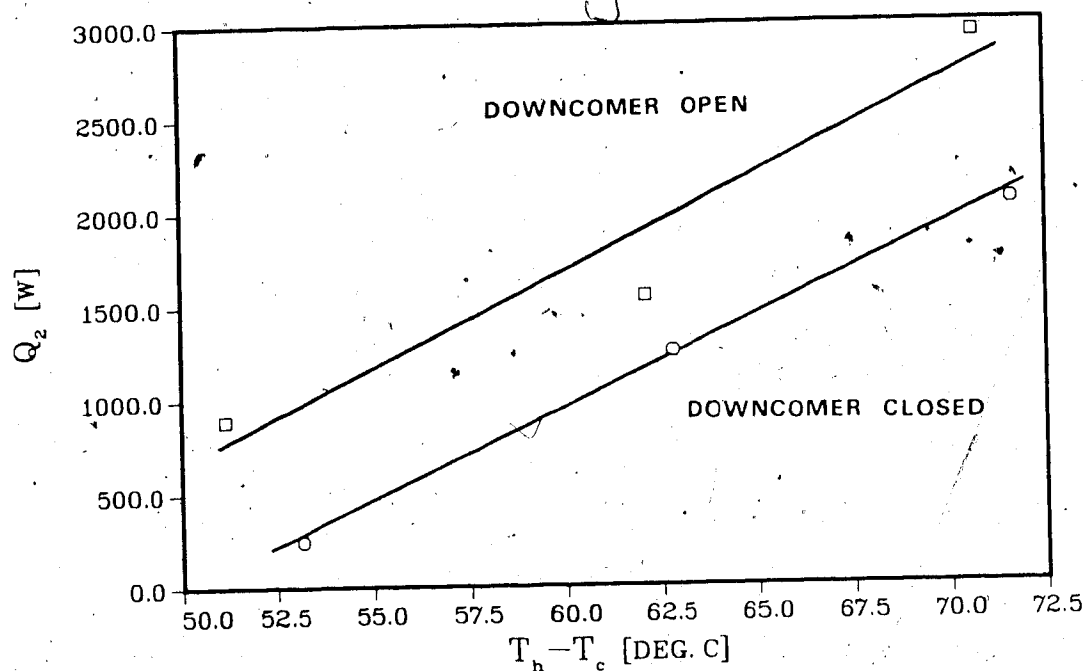


Fig. 3.3 Effect of downcomer on Q_2 vs. $T_h - T_c$ with 20% charge level and $V_c = 70$ ml/s

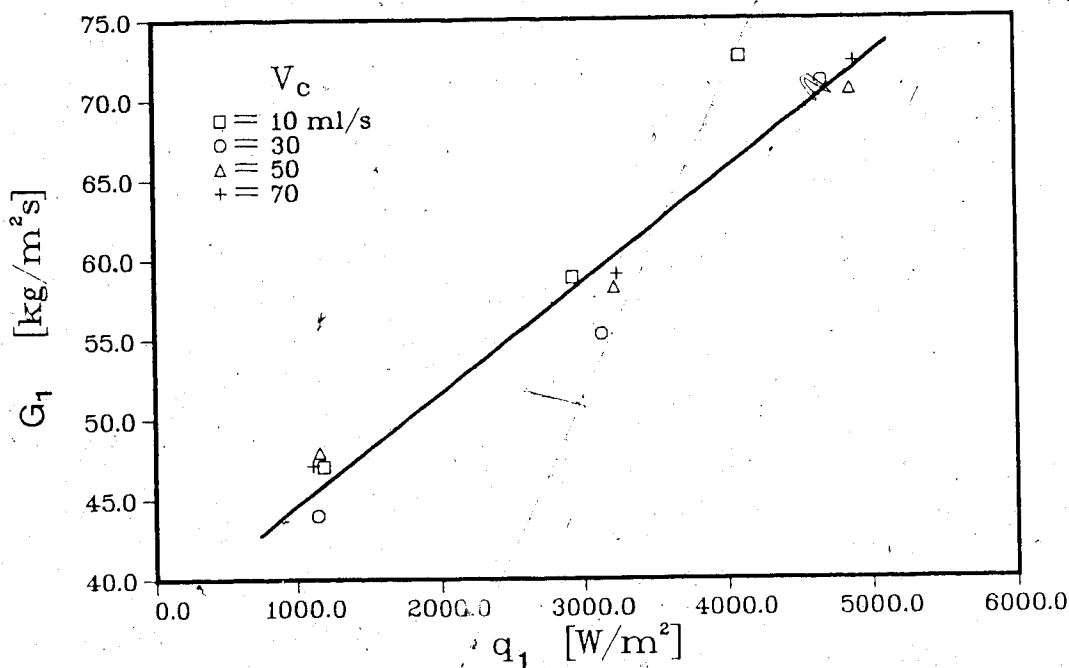


Fig. 3.4 Evaporator tube inlet mass flux vs. wall heat flux with 20% charge level and open downcomer

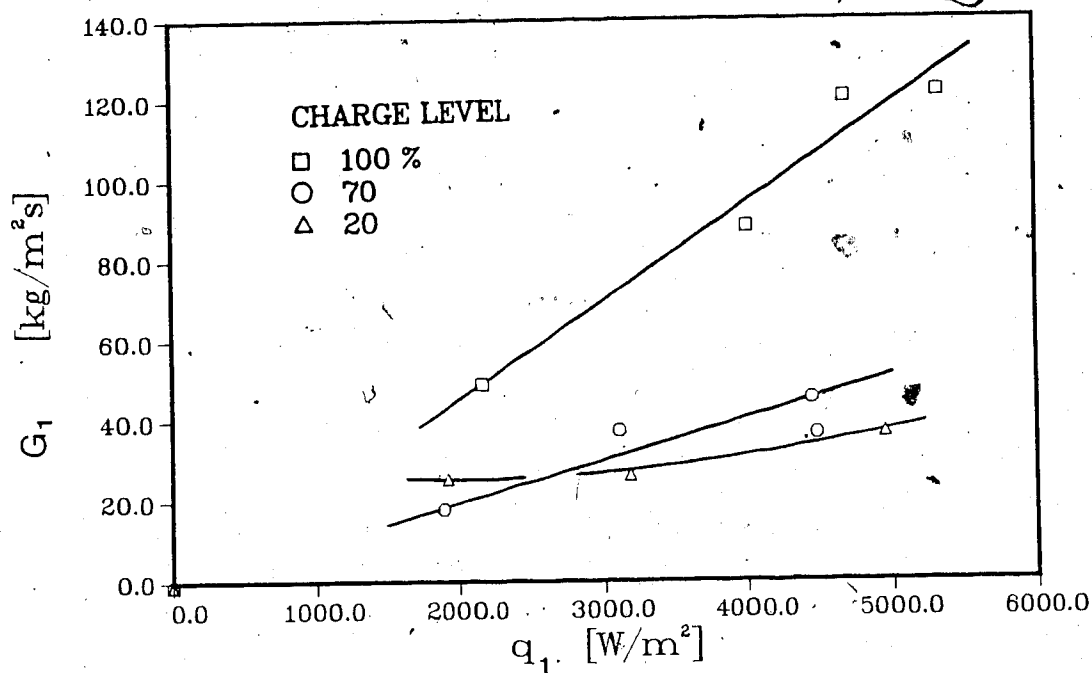


Fig. 3.5 Effect of charge level on G_1 vs. q_1 with $V_c=10$ ml/s and closed downcomer

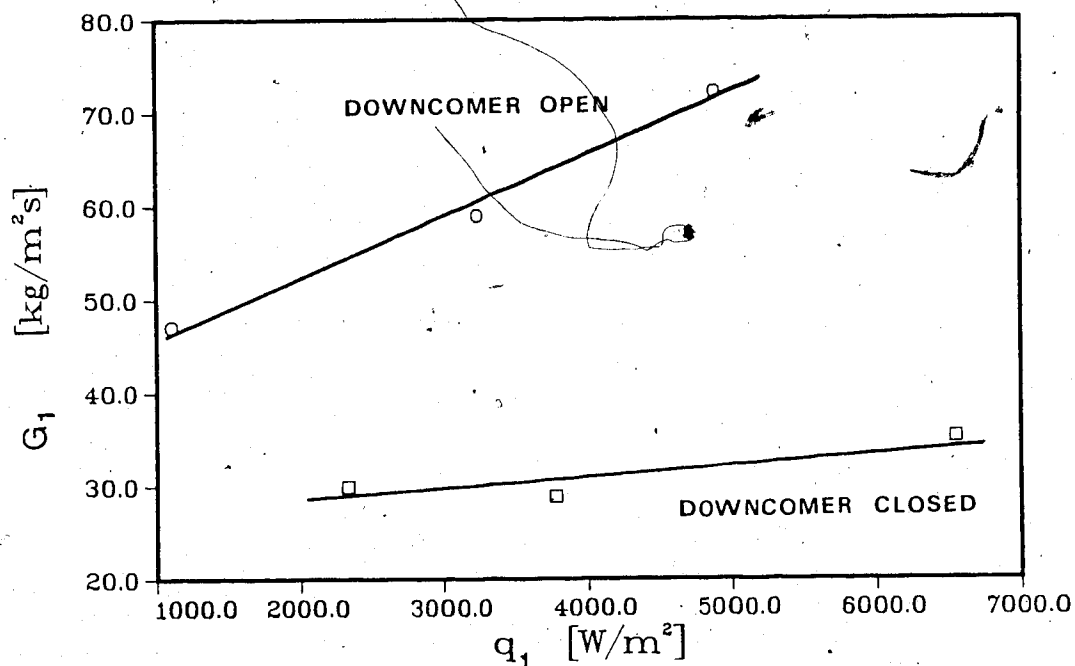


Fig. 3.6 Effect of downcomer on G_1 vs. q_1 with 20% charge level and $V_c=70$ ml/s

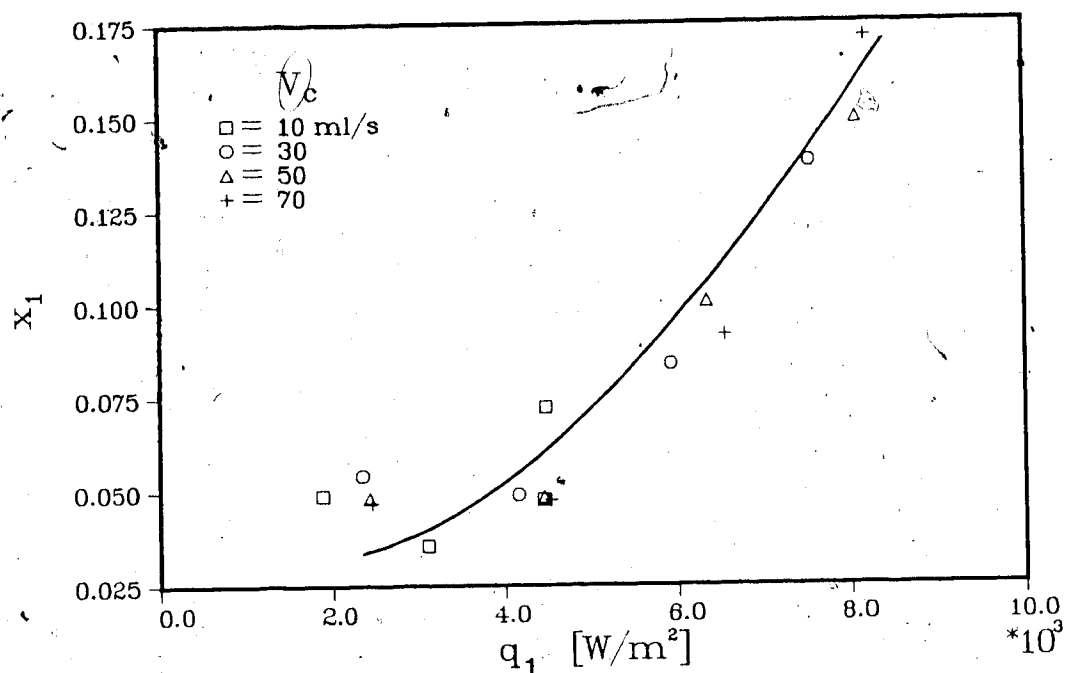


Fig. 3.7 Evaporator exit vapor quality vs. heat flux with 70% charge level and closed downcomer

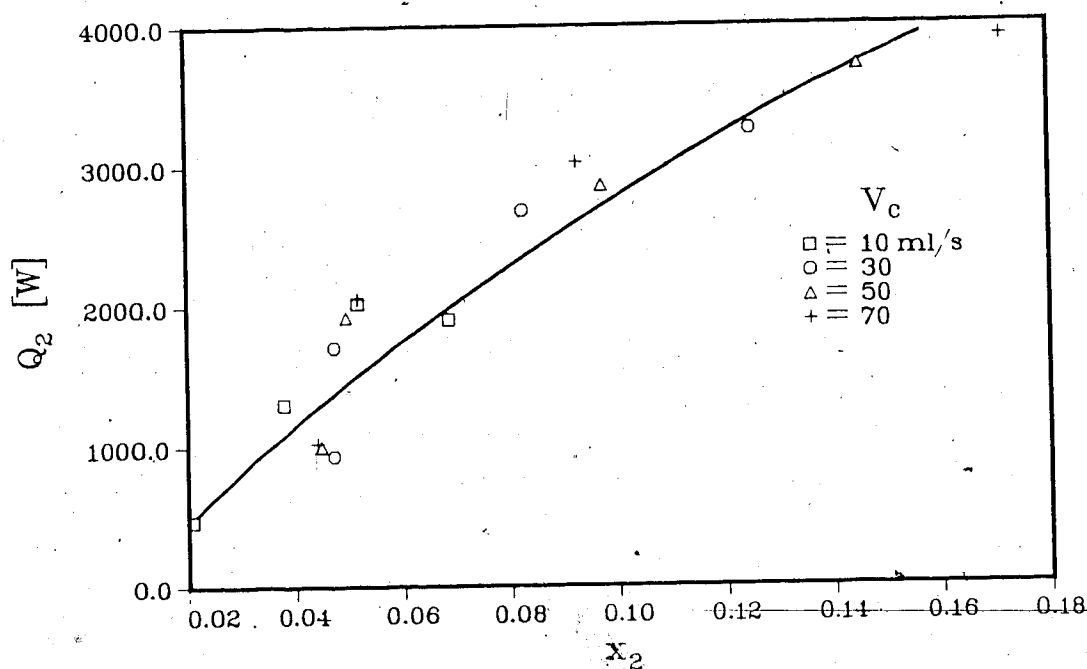


Fig. 3.8 Heat recovered vs. condenser shell side vapor quality with 70% charge level and closed downcomer

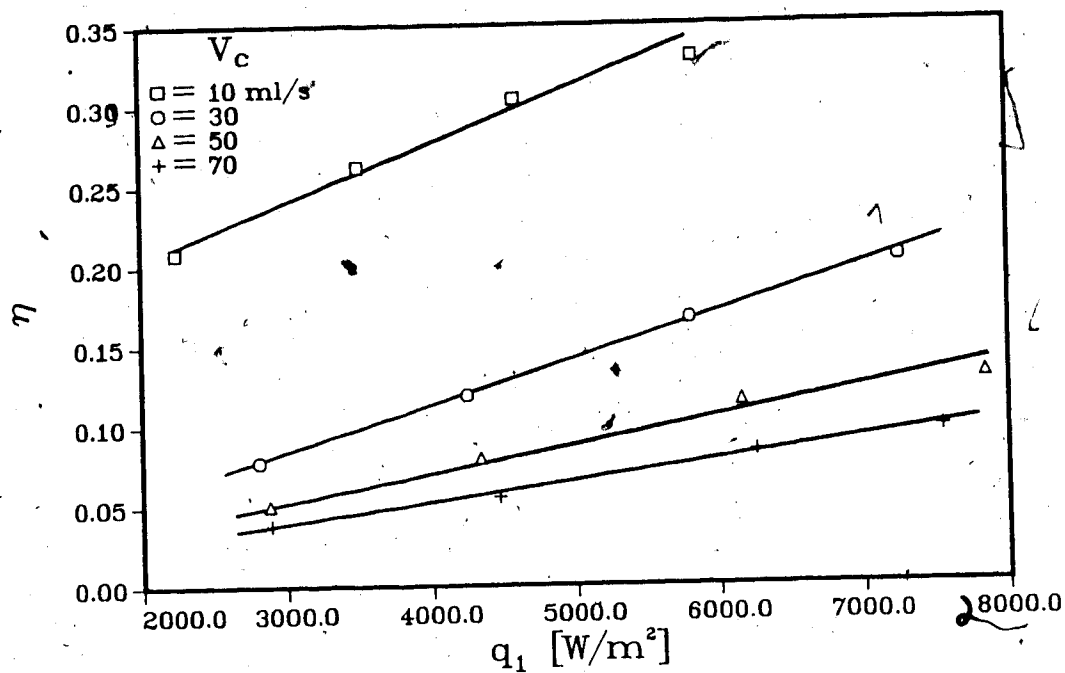


Fig. 3.9 System efficiency vs. input heat flux with 70% charge level and open downcomer

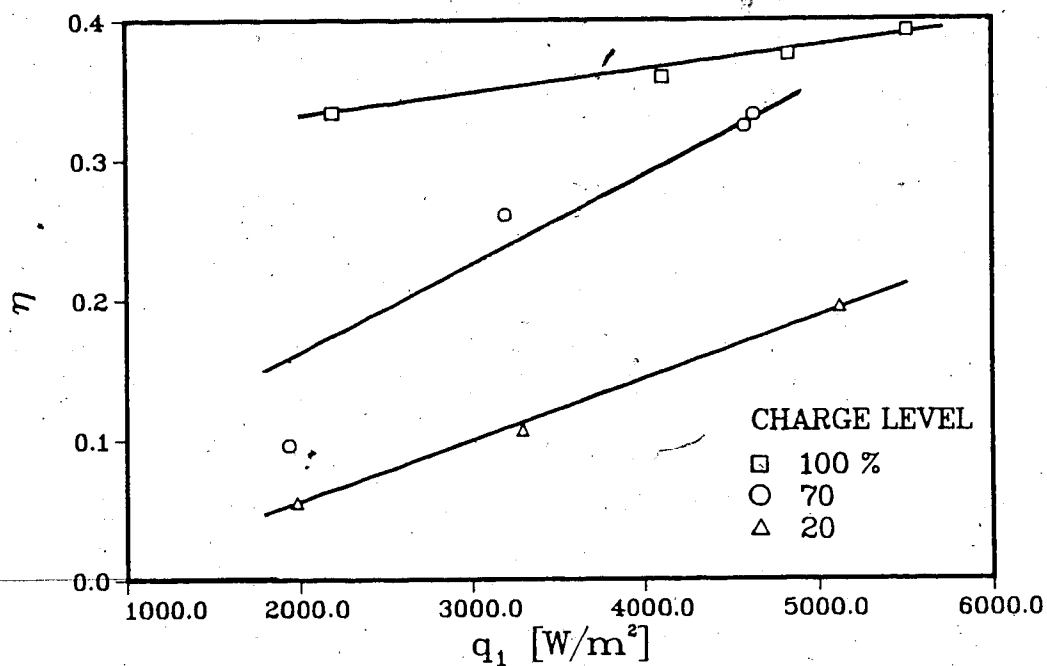


Fig. 3.10 Effect of charge level on η vs. q_1 with $V_c=10$ ml/s and closed downcomer

flow restrictions in the working fluid loop caused by the measuring instruments, with the primary losses due to the small orifices in the turbine flow meters and the wire meshes.

The fluctuating phenomena of thermosyphon flow rates, system pressure, and evaporator exit temperature are inherent to a two phase thermosyphon system and typical chart records are shown in Fig. 3.11. The analog records provide a good visual indication of the type of oscillations involved, but beyond that are not particularly useful. Of interest are the frequency of the oscillations and the variance of the amplitudes which are difficult to accurately extract from a record of this nature. For this reason, digital methods of processing these signals is pursued in, the next chapter for the two-phase refrigerant R-113 tests.

3.5.2 Upper and Lower Heat Exchangers

The effects of wall heat flux q_1 , charge level and liquid-vapor separator on the overall heat transfer coefficient U_1 of the evaporator can be seen in Figs. 3.12 and 3.13. The performance of the evaporator improved considerably over the single phase case with the maximum value of $U_1 = 1370 \text{ W/m}^2\text{°C}$ being approximately double that previously obtained.

The performance of the condenser under the conditions of low quality flow and high liquid entrainment and flooding is of interest. The effects of inlet quality x_2 , cooling

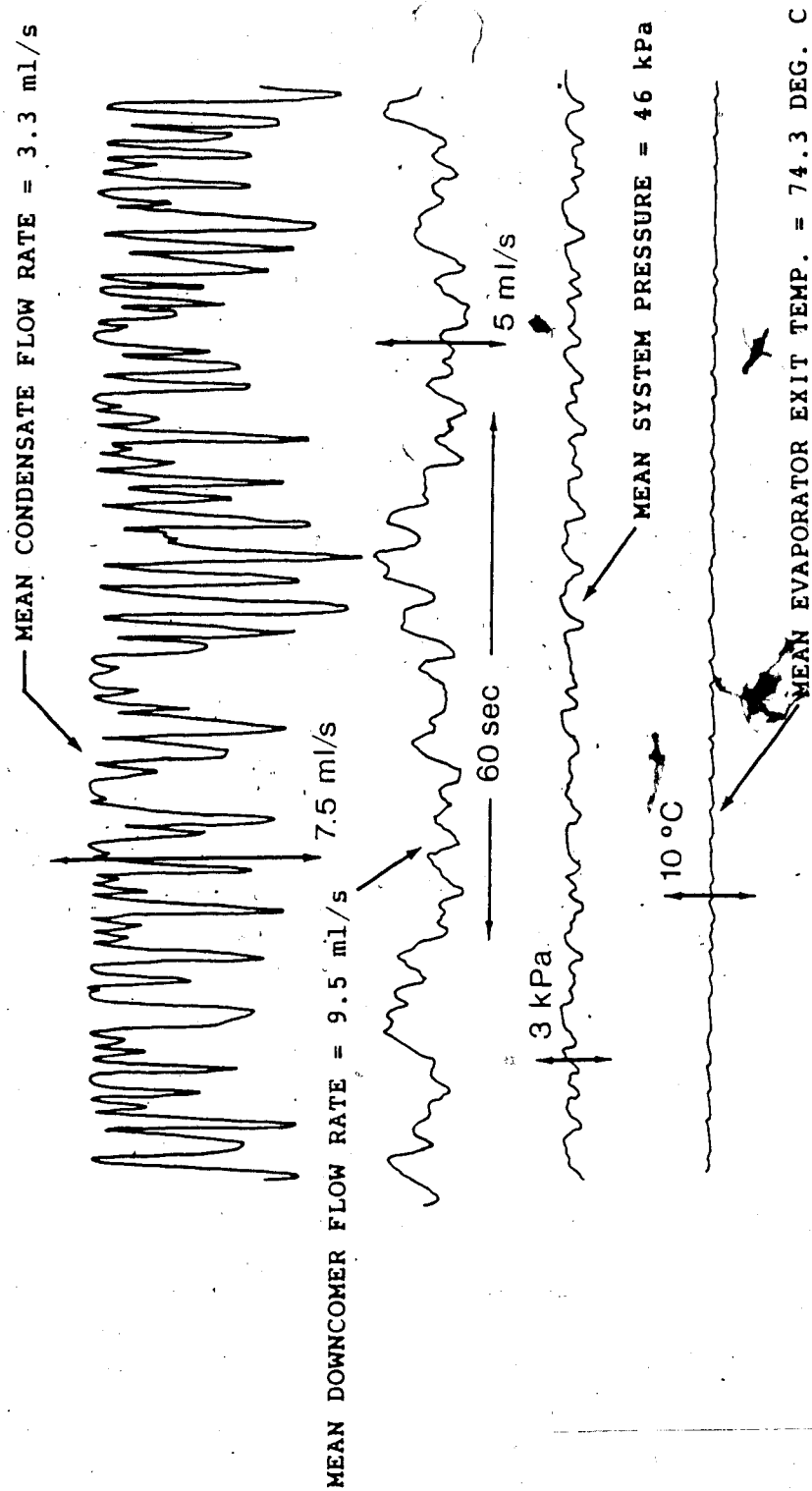


Fig. 3.11 Examples of fluctuating phenomena for 20% charge level, $T_h = 75^\circ\text{C}$, $V_c = 30\text{ ml/s}$, and downcomer open

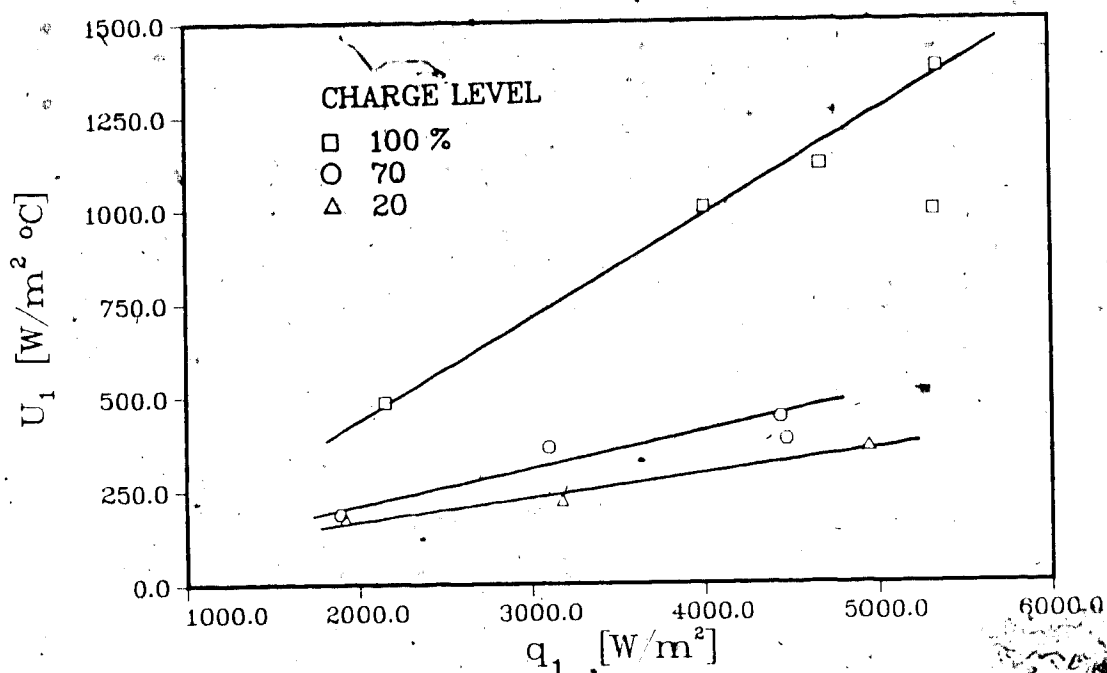


Fig. 3.12 Effect of charge level on U_1 vs. q_1 with closed downcomer and $V_c = 10$ ml/s

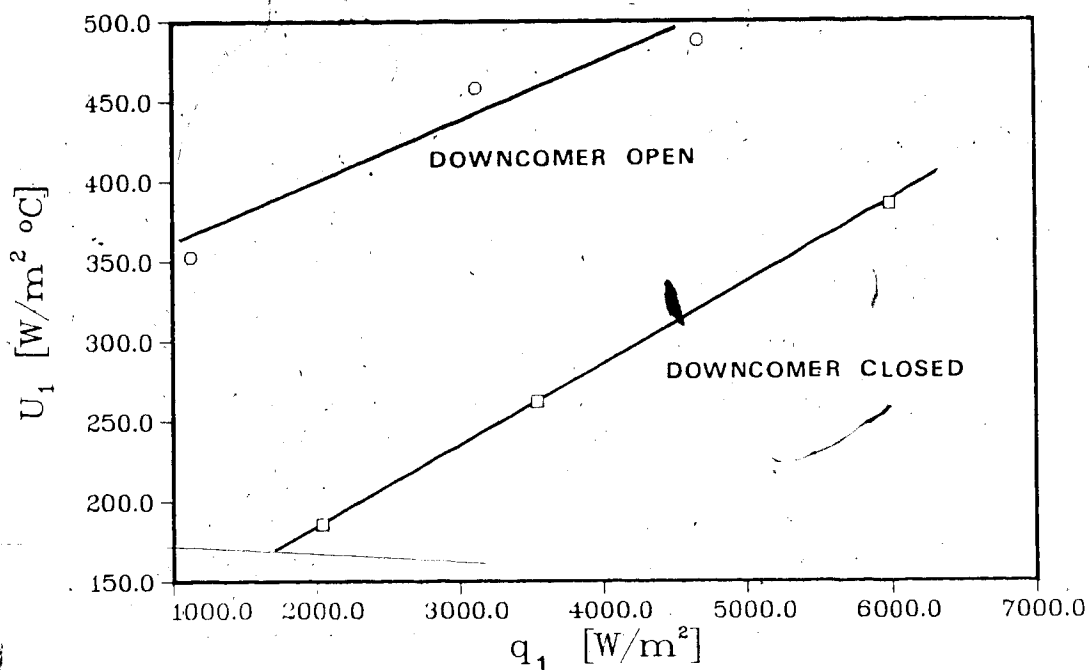


Fig. 3.13 Effect of downcomer on U_1 vs. q_1 with 20% charge level and $V_c = 30$ ml/s

water flow rate, charge level and downcomer on the overall heat transfer coefficient U_2 are shown in Figs. 3.14, 3.15, and 3.16. As is expected, increasing the cooling water flow rate causes a significant rise in the value of heat transfer coefficient. Higher charge levels result in increased working fluid flow rates and again help to improve performance. The effect of opening the downcomer is to raise the vapor quality in the condenser, which increases the latent component of the heat transfer. The condenser overall heat transfer coefficients for low quality two-phase flow are about 3 times those obtained in single phase for similar operating parameters.

3.5.3 Evaporator Convective Boiling

It is useful to compare the experimental values for the two-phase water heat transfer coefficient h_{exp} with those of the modified Dittus-Boelter equation h_s for single phase turbulent heat transfer, Eq.(3.9), and the results are shown in Fig. 3.17 using the inverse Martinelli parameter for flow in the evaporator tube. The ratio h_{exp}/h_s is lower than would be expected for a high vapor quality situation, however the trend to increase with higher flow quality and larger $1/X_{tt}$ does exist. The high data points near the origin of the horizontal coordinate on the plot are no doubt caused by low quality high speed flow at high charge levels yielding a large amount of sensible heat transfer.

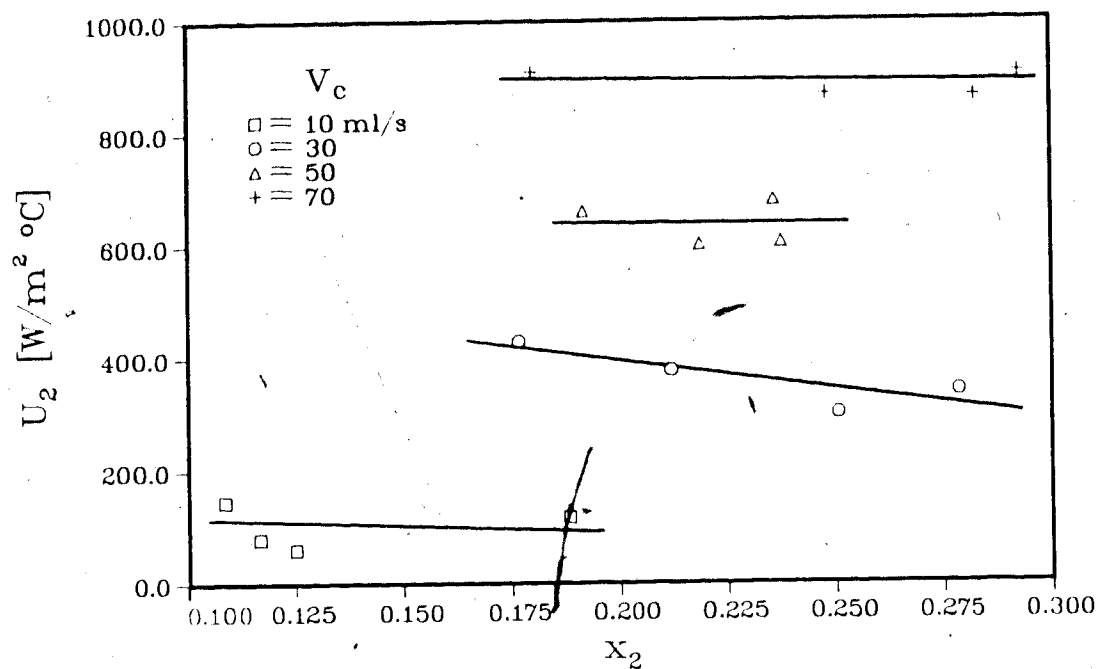


Fig. 3.14 Effect of cooling water flow rate on U_2 vs. x_2 with 70% charge level and open downcomer

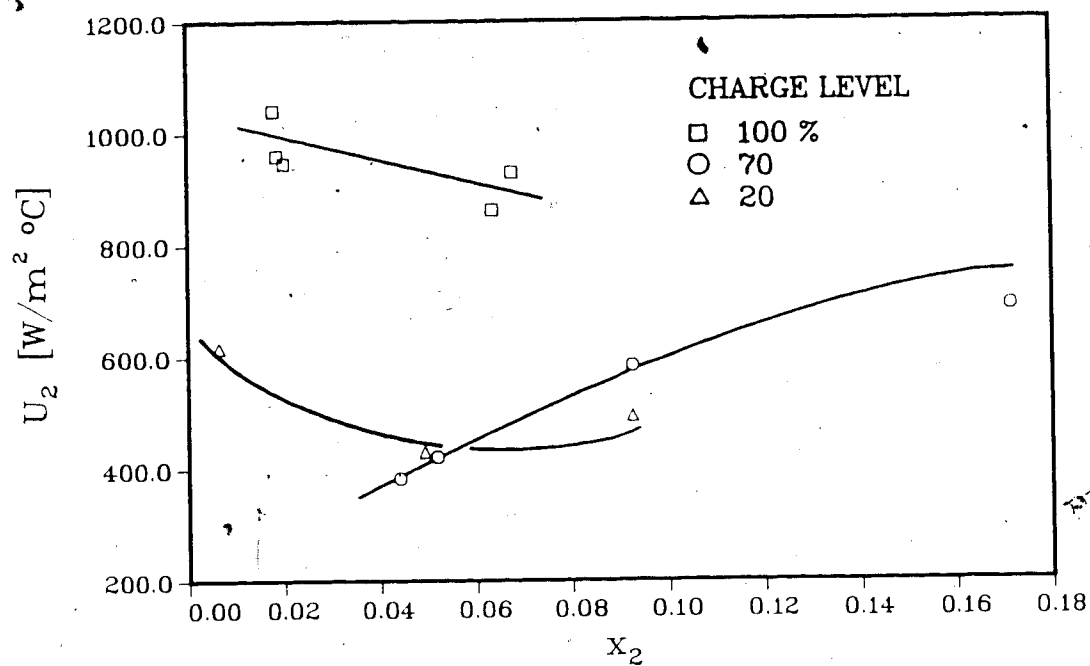


Fig. 3.15 Effect of charge level on U_2 vs. x_2 with closed downcomer and $V_c = 70$ ml/s

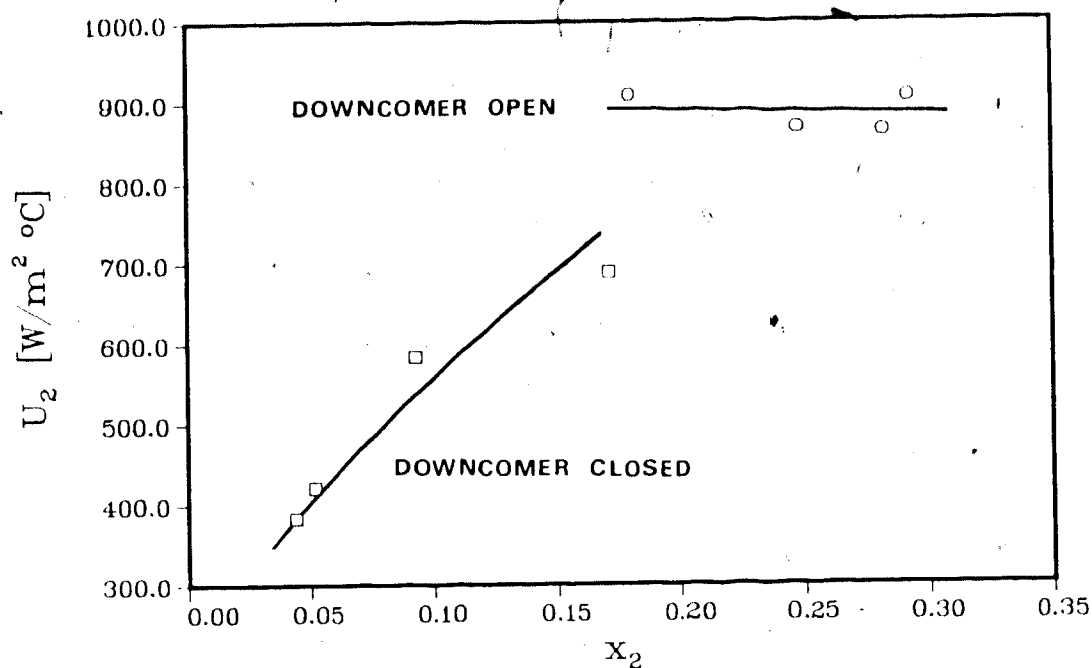


Fig. 3.16 Effect of downcomer on U_2 vs. x_2 with 70% charge level and $V_c = 70$ ml/s

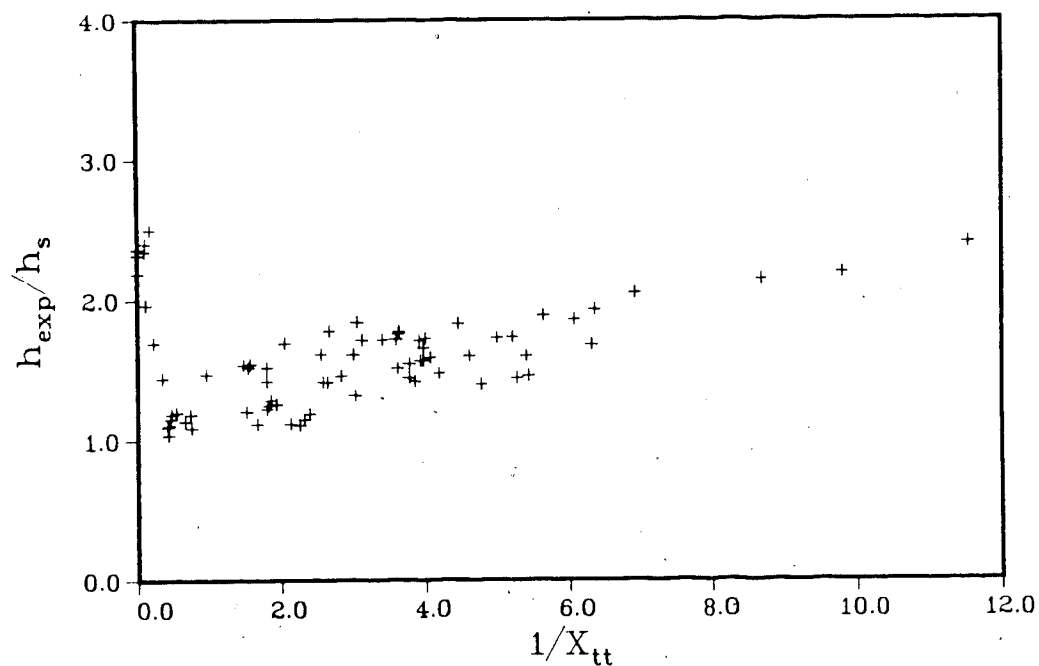


Fig. 3.17 Comparison of experimental evaporator heat transfer coefficient with single phase component correlation

The experimental results are also compared with the predictions of Shah, and Shrock and Grossman, and are shown in Figs. 3.18 and 3.19 using the parameter Boiling number. The trend in the experimental data is to agree with the simple Shah correlation when $Bo > 3 \times 10^{-3}$. As can be seen in Fig. 3.19, the Shrock-Grossman correlation seems to overpredict in the range of boiling number greater than 1.0×10^{-3} .

The single phase tests indicated that the Nusselt number for flow in the inner tube of the lower heat exchanger correlated well with the Graetz parameter. Because the flow quality is low, the same correlation equation is shown in Fig. 3.20 with the two-phase data and the dotted line indicates an extrapolation. In view of the different flow regimes involved, this simple correlation does provide a reasonable estimate of the value of the Nusselt number for the low quality two-phase flow in the evaporator tube. This may be geometry dependent however, and further work must be done to determine the effect of other flow conditions and tube geometries on this simple correlation.

The condensation heat transfer outside the low integral fins of the coiled circular condenser tube is rather complicated. The values of the fin side heat transfer coefficients calculated using Eq.(2.22) are shown in Fig. 3.21 with shell side vapor quality as the major parameter. Comparison with the ideal case predicted by the Beatty-Katz correlation reveals that the experimental heat

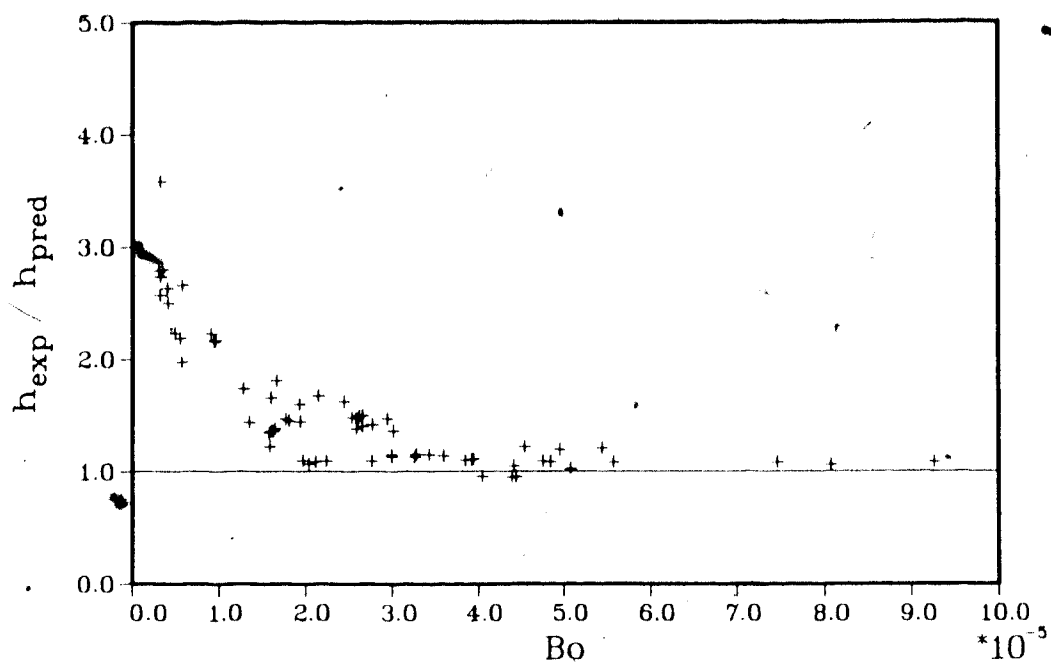


Fig. 3.18 Comparison of experimental evaporator heat transfer coefficient with Shah correlation

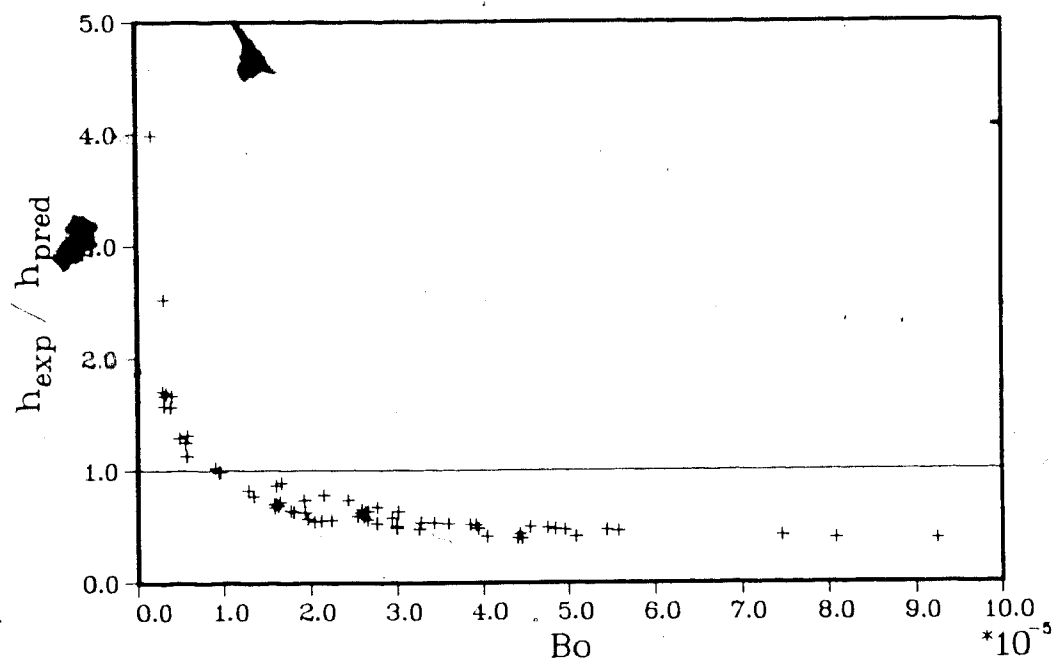


Fig. 3.19 Comparison of experimental evaporator heat transfer coefficient with Shrock-Grossman correlation

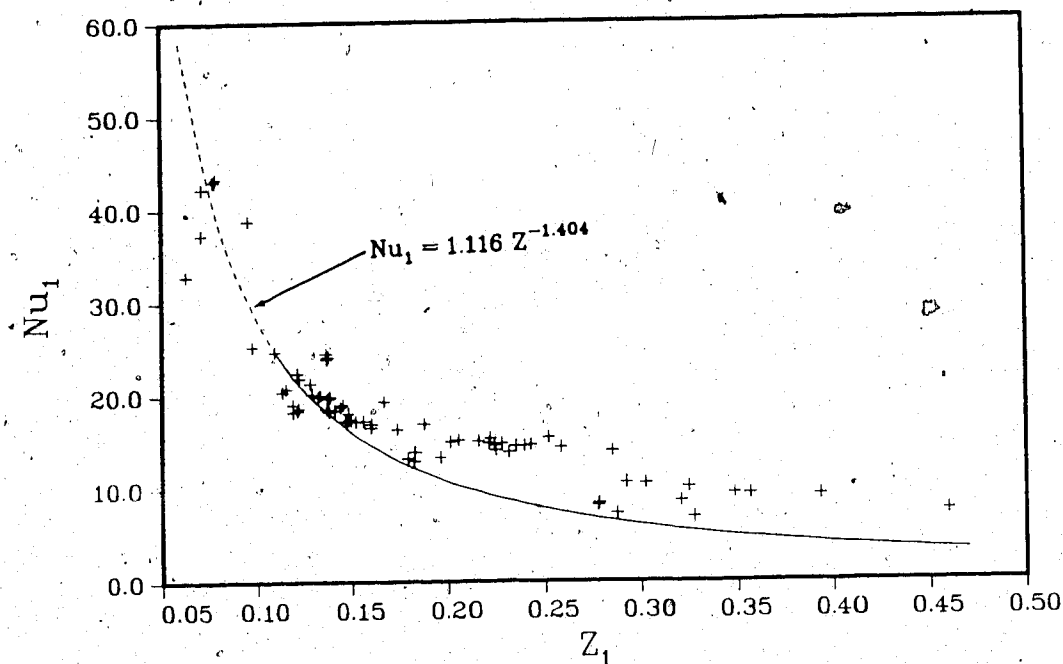


Fig. 3.20 Two-phase water Nu_1 vs. Z_1 with all data and comparison with single phase results

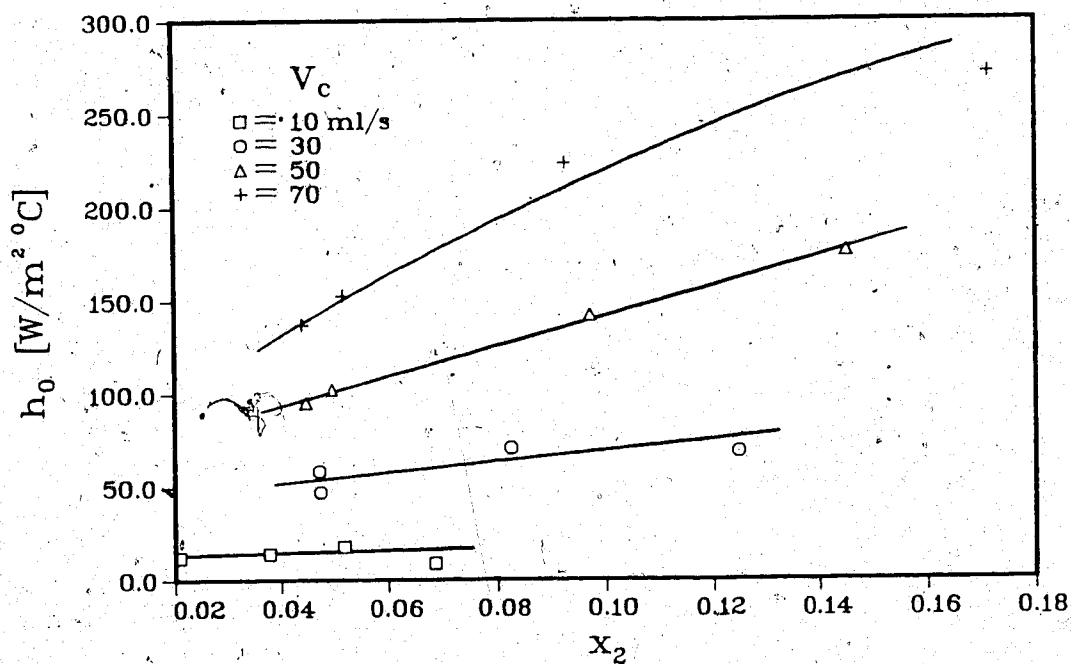


Fig. 3.21 Effect of cooling water flow rate on condenser shell side heat transfer coefficient vs. quality with 70% charge level and closed downcomer

transfer was several orders of magnitude lower than expected. In subsequent Freon tests, the steel shell of the condenser was replaced with a Pyrex glass tube for flow visualization purposes. It was revealed that even for low initial liquid charge levels in the system, vapor generation in the evaporator displaces liquid into the condenser shell and floods the coil, thus reducing condensation area. Liquid entrainment into an empty condenser shell is also serious for high surface tension liquids such as water, where the normally vacant space between the fins may be constantly occupied by stagnant liquid. Thus the tube condensation area takes on a modified cylindrical shape with only small rings of copper exposed for direct condensation.

3.6 Conclusion

The low quality flow closed loop two-phase thermosyphon system tested performed well and increased the level of heat extraction by 15% over its single phase counterpart. Natural circulation was for the most part self initiating, and occurred within minutes after heating and cooling was applied to the primary loop.

The greatest advantage over the single phase system is the large increase in working fluid flow rate under similar operating conditions, which has positive effects on performance in other areas. No doubt agitation caused by the phase change process in both the evaporator and condenser were additional factors in improving performance through

better heat transfer coefficients.

The primary loop mass flow rate was found to increase for higher values of input heat flux, as increased vapor generation caused higher flow velocities with liquid entrainment. This is also reflected in better performance with higher vapor quality flow. The open downcomer and 100% charge level parameters also contributed to greater mass transport, and thus enhanced the overall performance.

The simple Shah correlation valid for low quality flow agreed with the experimental determination of the evaporator tube heat transfer coefficient for Boiling numbers greater than 3, although limited data is available in this region. A simple power correlation between Nusselt number and inverse Graetz number obtained for the evaporator with single phase flow was compared to the low quality convective boiling data encountered here, and the favourable results indicate that further study is warranted.

The condenser fin side heat transfer coefficients were considerably lower than predicted by Nusselt theory, and it is most likely that condenser flooding and liquid entrainment have reduced the heat transfer to an enhanced sensible form.

4. Closed Loop Two-Phase Refrigerant R-113 Thermosyphon Tests

4.1 Introduction

Many flouorocarbon refrigerants are ideal for low temperature energy recovery because they have low saturation pressures at low temperatures, and low liquid phase heat capacitance. This enables two phase flow to be achieved easily, and allows for better efficiency due to higher heat transfer coefficients and flow rates. Additionally, they have low freezing points and do not cause scaling and fouling, which makes for long maintenance free life of the thermosyphon loop. Such refrigerants normally have low toxicity, and have been used in the food industry for years.

A condensed pamphlet is available from Dupont [34] which contains a summary of common refrigerants and their properties. Refrigerant R-113 was chosen for these tests as it has a suitable saturation temperature for the range of test parameters desired. Some important physical properties of R-113 [34,35,36] are shown in Table 4.1.

The present experimental closed loop thermosyphon was charged with this refrigerant to determine the optimum operating parameters for the low grade energy recovery situation. The range of operation is from mid vapor quality flow to superheated vapor in the riser line. In addition to the heat transfer analysis of the system, flow visualization photographs are presented in this chapter to give a better

Table 4.1 Properties of Refrigerant R-113

Chemical Name	TRICHLOROTRIFLUOROETHANE
Chemical Formula	$\text{CCl}_2\text{F}-\text{CClF}_2$
Molecular Weight	187.39 g/mol
Boiling Point at 1 atm	47.47°C
Freezing Point	-35°C
Critical Pressure	33.7 atm
Critical Temperature	214.1°C
Saturated Liquid Density	1569 kg/m ³
Latent Heat of Vaporization	152 kJ/kg
Saturated Liquid Specific Heat	0.953 kJ/kg K

understanding of the flow regimes encountered. As well, the pressure and flow rate fluctuations in the primary loop are examined more closely, and the two-phase pressure drop results for flow in the evaporator tube are included.

4.2 Experimental Apparatus and Instrumentation

The fluid in the primary loop was drained down and the tubes flushed with distilled water to remove any debris left over from previous tests. The steel condenser shell was then replaced with a transparent Pyrex glass tube. This was done to enable flow visualization photographs of the condensation process to be taken, as results from the two-phase water tests indicate that the heat transfer mechanism in the heat exchanger is not properly represented by Nusselt theory. An axial dispersal tube was installed in the condenser so that Freon vapor would be better distributed on the finned coil. This was constructed simply of a half inch copper tube with many radial holes located so as to direct the spray onto the coil. The system was then dried by continuously passing

compressed air through the primary loop for 72 hours. Before the loop was charged with Freon, the system was evacuated with a vacuum pump for 48 hours to ensure that no air or moisture remained.

Photographs of the flow were also taken at the evaporator exit through the lowermost sight glass, the location of which may be seen in Fig. 2.1. A tripod mounted Nikon FM2 35 mm camera with a 50 mm micro-lens was used with Kodak Tri-X ASA-400 black and white film. The liquid R-113 was dyed red with Trace internal leak detector. As Freon vaporizes, the dye is rejected and remains with the liquid component of the two-phase mixture. When illuminated from behind the sight glass or condenser shell, and photographed with black and white film, the vapor is light in appearance, and the liquid dark.

The analog signals for the fluctuating primary loop flow rates and pressure which were recorded on chart recorders for the two-phase water tests were found to be extremely difficult to quantitatively analyze. For the Freon series of tests, these signals were additionally processed with a fast Fourier transform spectrum analyzer (Nicolet Scientific Corporation 444A Mini-Ubiquitous FFT)⁵ to determine their frequency contents. The frequency spectrums were hard copied from the FFT with a Watanabe X-Y recorder. The analog signals were still recorded on Hewlett Packard chart recorders for visual interpretation.

⁵ henceforth referred to as FFT

When the flow at the evaporator exit is in the two-phase region, the working fluid exit temperature will be the saturation temperature at that point, and this quantity is required in the calculation of the vapor mass quality. However, it was anticipated that the flow at the evaporator exit would enter the superheated vapor region, thus making it difficult to determine the local saturation temperature. For this reason additional static pressure taps and pressure transducers were installed in the working fluid loop at the evaporator exit and condenser inlet to measure the local pressures. With this information, it is possible to compute the saturation temperature from the thermodynamic relationships between pressure and temperature in the saturation region of the refrigerant.

As before, all the instruments were recalibrated before the new series of tests were begun.

4.3 Experimental Procedure

The operating parameters studied with the two-phase refrigerant charged system are heat source temperature (45-85°C), cooling water flow rate (25, 35, 55, and 75 ml/s), and initial liquid Freon charge level (100, 65, and 20%). The downcomer line from the liquid-vapor separator to the evaporator inlet was always open. The heating water flow rate was held between 32 and 36 ml/s, and the cooling water temperature was constant in the range of 10-12°C. The lower limit of the cooling water flow rate range was raised from

10 ml/s to 25 ml/s because wear in the bearings of that particular flow meter were causing some inaccuracies at very low flow rates.

The initial system pressure for all tests was the vapor pressure of R-113 at room temperature (about 40 kPa absolute). This was obtained by drawing a vacuum on the system until boiling was achieved, then allowing the system to settle for one hour before a test was begun.

The startup sequence is the same as that for the previous tests, and self-starting two-phase natural flow was always achieved within 20 seconds of the circulation of the secondary loop fluids. Photographs of the transition between flow regimes at the evaporator exit were also taken.

A steady state was judged to exist when the short term time averaged temperatures and system pressure (averaged over about a one minute period) were constant over about a 30 minute time interval. The final computer acquired data were read consecutively 30 times and then averaged. Additionally, the fluctuating flow rates and system pressure voltage signals were sampled consecutively 100 times each at a rate of 10 readings per second. This data was then analyzed to determine the statistical variance of the signals for various operating conditions.

The data was stored in hard copy form on paper, and on Hewlett Packard magnetic tape cassettes, and later transferred to the University computer system for final analysis.

4.4 Data Analysis

The analysis of the experimental data is similar to that done in the previous chapters except that the properties of the working fluid are that of refrigerant R-113. Correlation equations developed for refrigerants by Fujii, Noshu, and Honda [37] are used and the FORTRAN library of R-113 properties may be found in Appendix III. The properties of the cooling and heating water streams are given by the correlations mentioned in Chapter 2, and may be found in Appendix II.

A statistical analysis of the fluctuating signals from the primary loop instrumentation was done to gain further insight into the mechanisms of the instabilities involved in a closed loop two-phase system. The frequency spectrum was obtained by processing the data with an FFT spectrum analyzer. It is also useful to examine the variance of an output signal, which is calculated by [38]

$$s^2 = \frac{\sum_{i=1}^n (e_i - E)^2}{n-1} \quad (4.1)$$

where E is the mean voltage output of the sampled data and e_i is the amplitude of the i th sample. The raw variance of the voltage output may be converted to the true variance in units of flow rate (ml/s) or pressure (kPa) by multiplying by the square of the slope of the linear calibration curve:

$$v = m^2 s^2 \quad (4.2)$$

The experimental heat transfer results for convective boiling in the evaporator were compared with the correlations of Shah, and Shrock and Grossman in Chapter 3. For the Freon tests, a correlation developed by Kandlikar (1982) will also be applied. This empirical equation is an extension of Chen's proposal [39] that the two-phase heat transfer be treated as a result of two separate processes, with a convective component and nucleate boiling component. The total heat transfer is given by

$$h_t = h_{\text{pool}} + h_{\text{conv}} \quad (4.3)$$

For R-113 in horizontal convective boiling Kandlikar's correlation [40] gives

$$h_t = [D1 Co^{D2} (25Fr)^{D5} + D3 Bo^{D4} (25Fr)^{D6} (1.35)] h_s \quad (4.4)$$

with the dimensionless parameters Froude number Fr and Convection number Co given by

$$Fr = G^2 / (\rho_f^2 g d) \quad (4.5)$$

$$Co = \left(\frac{1-x}{x} \right)^{0.8} (\rho_g / \rho_f)^{0.5} \quad (4.6)$$

The constants required for the correlation are given in

Table 4.2.

The degree of superheating of the vapor at the evaporator exit is of interest and this is simply the difference between the measured temperature and the saturation temperature calculated from the local pressure. In order to check the accuracy of the predicted saturation temperature, the measured and calculated temperatures can be compared while the flow is still in the two-phase regime. When this is done, the degree of superheating is zero, as both values should yield the saturation temperature. The maximum error between the two was found to be 0.9°C over the range of tests conducted in the saturation region, which is considered to be excellent agreement.

4.5 Results and Discussion

4.5.1 Overall System Characteristics

The overall thermal performance of the system, convective boiling heat transfer and pressure drop results, and analysis of the fluctuating phenomena caused by flow instabilities in the refrigerant charged thermosyphon are examined graphically in this chapter. Due to the voluminous amount of data gathered during the course of the tests, only representative portions of the results can be shown here, as was indicated in Chapter 3 for the two-phase water tests. Data points which occur for different heat source temperatures will be included in all figures. In this way

Table 4.2 Kandlikar Correlation Coefficients

	<u>Co<0.65</u>	<u>Co>0.65</u>
D1	1.091	0.809
D2	-0.948	-0.891
D3	887.46	387.53
D4	0.726	0.587
D5	0.333	0.096
D6	0.182	0.203

the individual effects of different external operating parameters can be more clearly seen. In cases where these effects are not individually important, all data points will be shown.

The cooling water heat extraction is plotted against the temperature difference between the heat source and heat sink in Figs. 4.1 and 4.2 where the effects of cooling water flow rate and charge level are seen. An interesting phenomenon occurs for a condition of high cooling water flow rate or low liquid charge level. As the temperature difference increases for these situations, the curves begin to flatten out, indicating that the system overall heat transfer coefficient is falling. This was not the case for the liquid-phase or low quality two-phase water thermosyphons, as any increase in overall temperature difference produced higher heat extraction. This will be later shown to be the result of superheated vapor production in the evaporator. Up until the point that the curves begin to flatten, higher cooling water flow rates and a lower charge level result in improved performance.

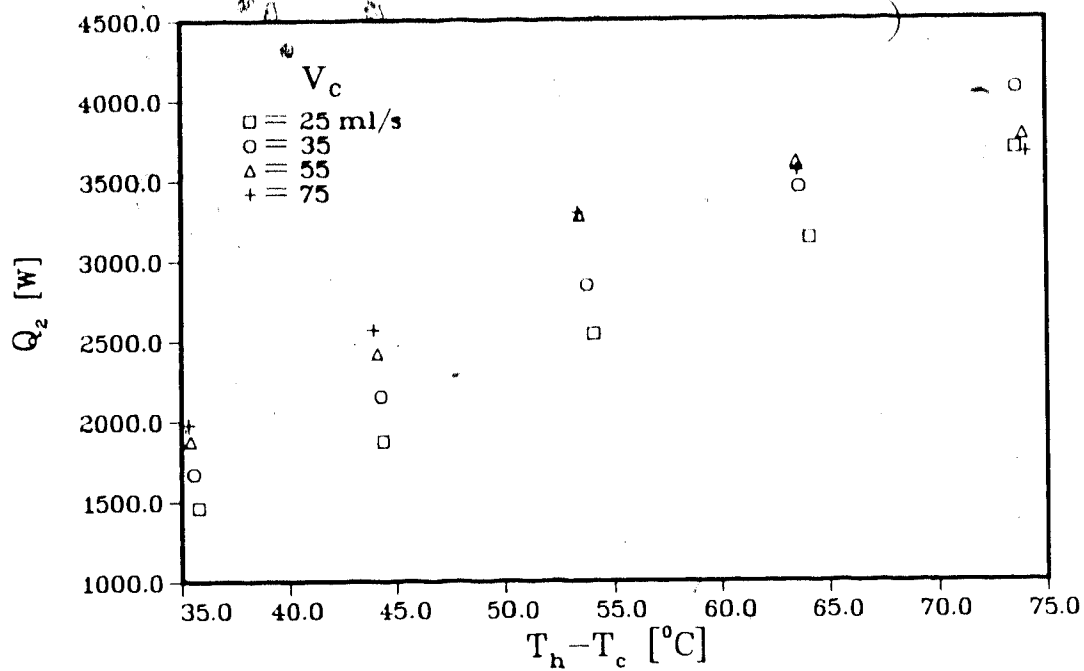


Fig. 4.1 Heat recovery vs. system temperature difference with 20% charge level

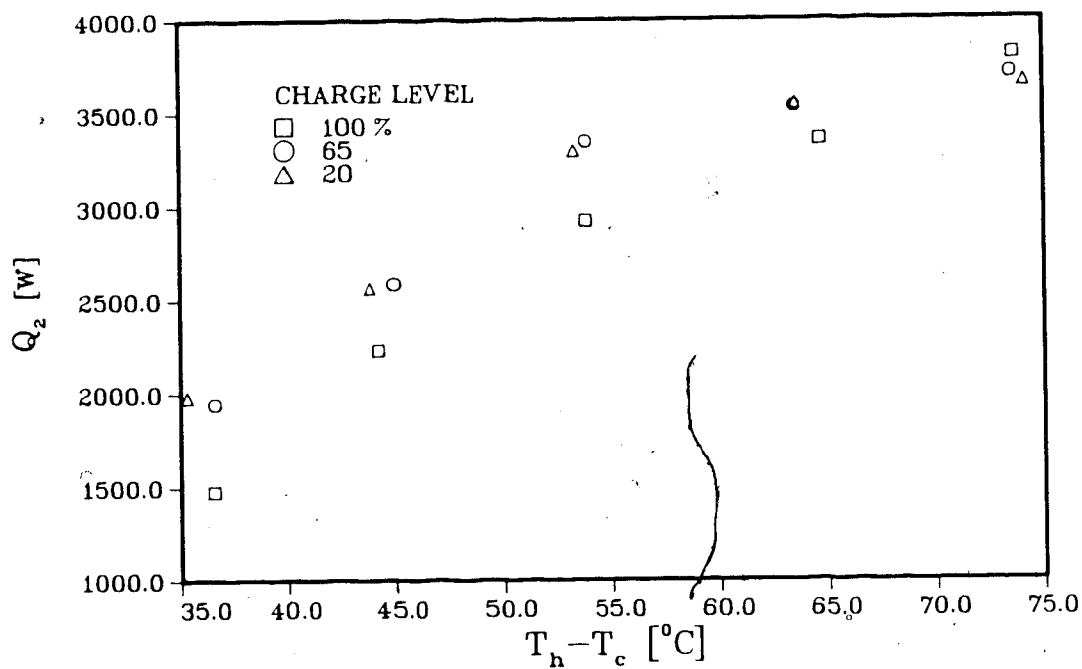


Fig. 4.2 Heat recovery vs. system temperature difference with $V_c = 75$ ml/s

It was noted in previous chapters that the mass flow rate of the working fluid in the primary loop increased for a higher input heat flux, which in turn resulted in increased heat extraction. This is not the case for the high quality flow Freon system as is shown in Fig. 4.3. Note that the total mass flux through the evaporator reaches a somewhat constant level, even though the heat flux is increasing. As the heat input goes up, so does the rate of vapor generation and the vapor mass quality. The final result is that although the mass transport has reached a steady value, the heat input and thus heat extraction is increasing as shown in Fig. 4.4, due to the latent energy content of the flow. Thus a distinguishing feature of this system is that energy transfer occurs through higher latent heat content and lower flow rate, as opposed to the low quality water system which was characterized by high mass flow rates and large sensible heat transfer.

In order to better understand the overall process of heat transport in the system, it is necessary to further examine the properties of the flow in the primary loop at the evaporator, riser line, and condenser. The low saturation temperature, liquid specific heat, and latent heat of vaporization of R-113 allows much greater vapor qualities to be achieved than were possible for the water system. The evaporator exit vapor mass quality is plotted against the average input heat flux in the evaporator tube in Figs. 4.5 and 4.6. A vapor quality of 1.0 indicates that

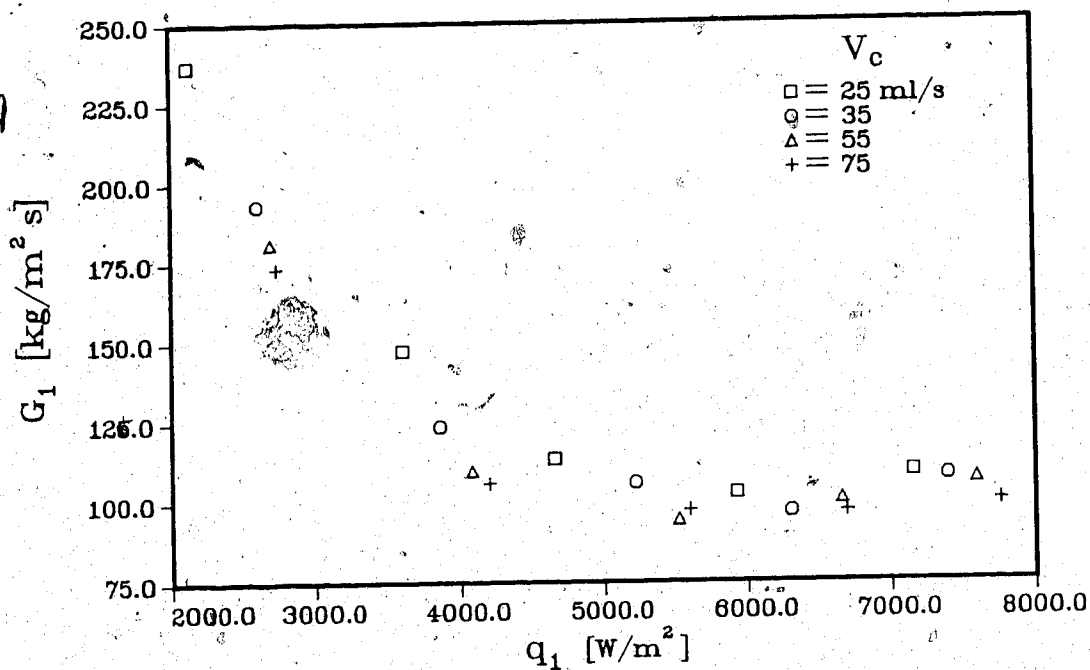


Fig. 4.3 Total working fluid mass flux at evaporator inlet for 100% charge level

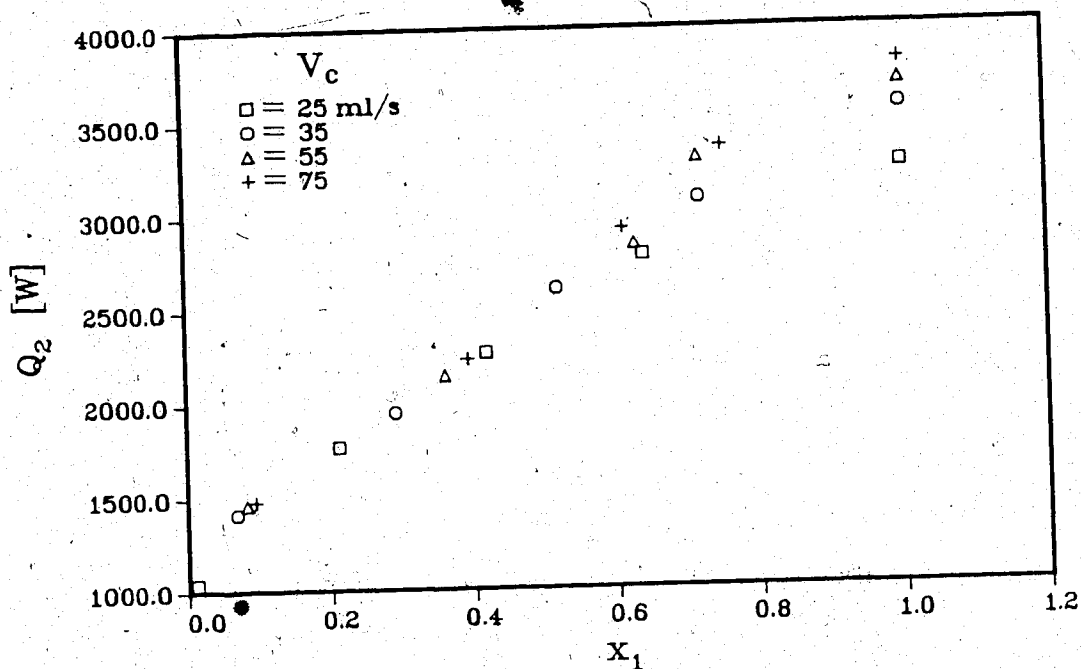


Fig. 4.4 Effect of evaporator exit quality on total heat recovery for 100% charge level

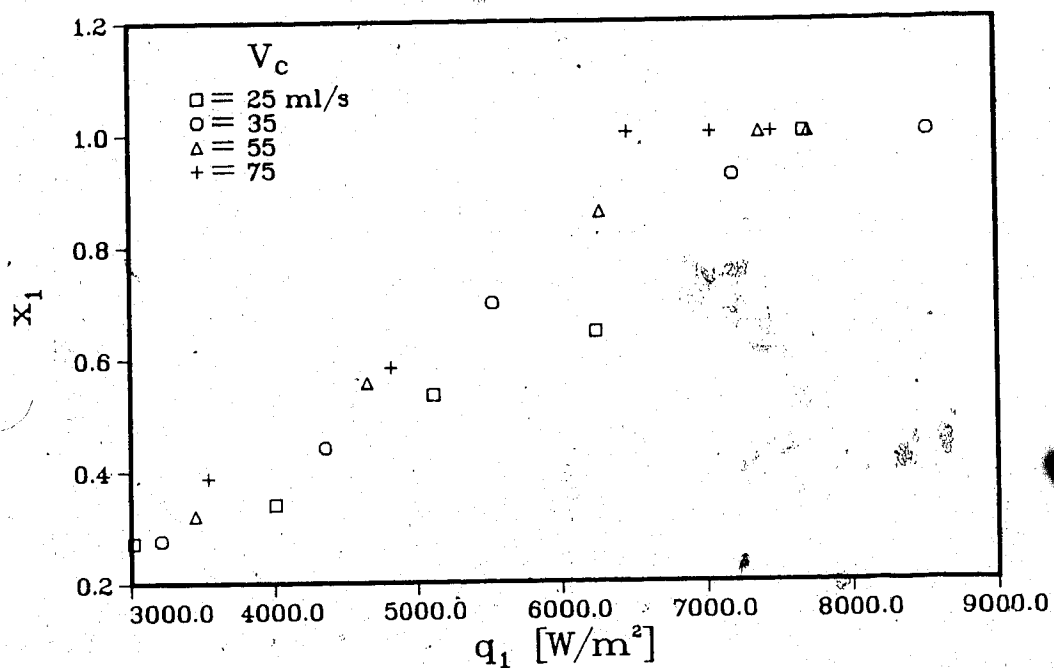


Fig. 4.5 Evaporator exit quality vs. wall heat flux with 65% charge level

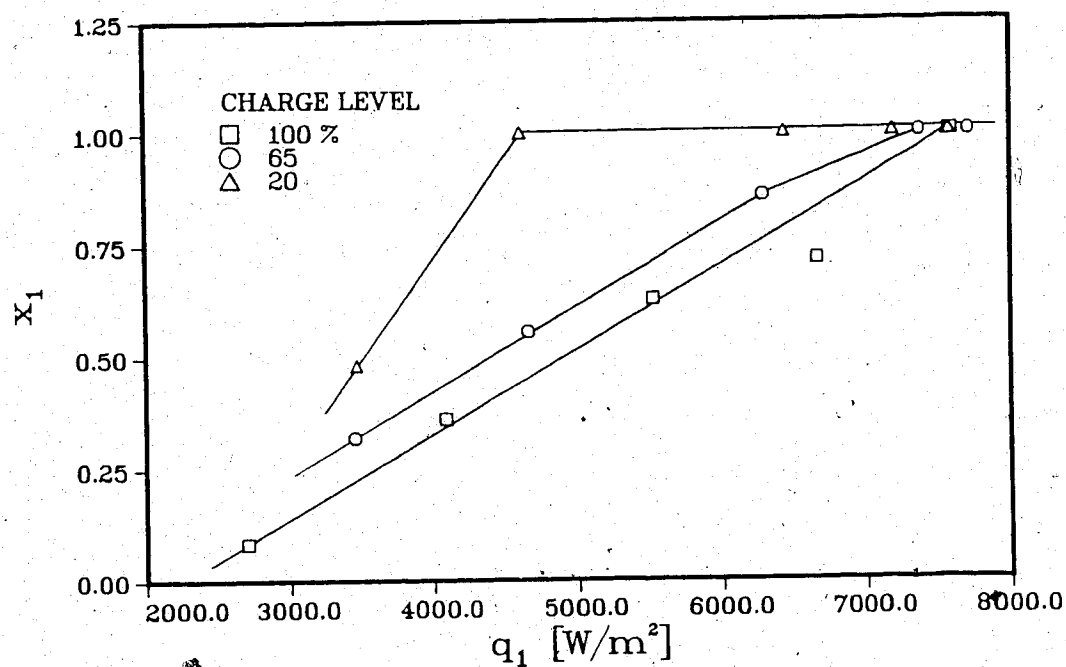


Fig. 4.6 Evaporator exit quality vs. wall heat flux with $V_c = 55$ ml/s

the flow is either saturated or superheated vapor, thus the input heat flux which is required to generate superheated vapor for a particular operating condition may be identified. Note that higher cooling water flow rates produce somewhat higher quality flow, and lower charge levels drastically increase the vapor quality for the same heat flux.

A quality of 1.0 indicates only that superheating is occurring, and it is also useful to have a quantitative indication of superheating. For this reason the degree of superheat (DSH) of the fluid at the evaporator exit is plotted against the input heat flux in Figs. 4.7 and 4.8. DSH is the amount above saturation that the vapor is heated, and is given by the difference between the exit temperature and the saturation temperature at that point. As indicated by Figs. 4.7 and 4.8, higher cooling water flow rates and lower charge levels allow superheating to occur earlier and in larger amounts.

It was found that increasing the cooling water flow rate lowered the pressure in the primary loop, thus lowering the saturation temperature in the evaporator. This enhances vapor generation giving higher quality flow, and a greater possibility of superheating. The lower charge levels promote superheating because there is less liquid in the system, which results in a smaller static head at the evaporator. The absolute pressure is then lower, and this also decreases the saturation temperature. The effect of cooling water flow

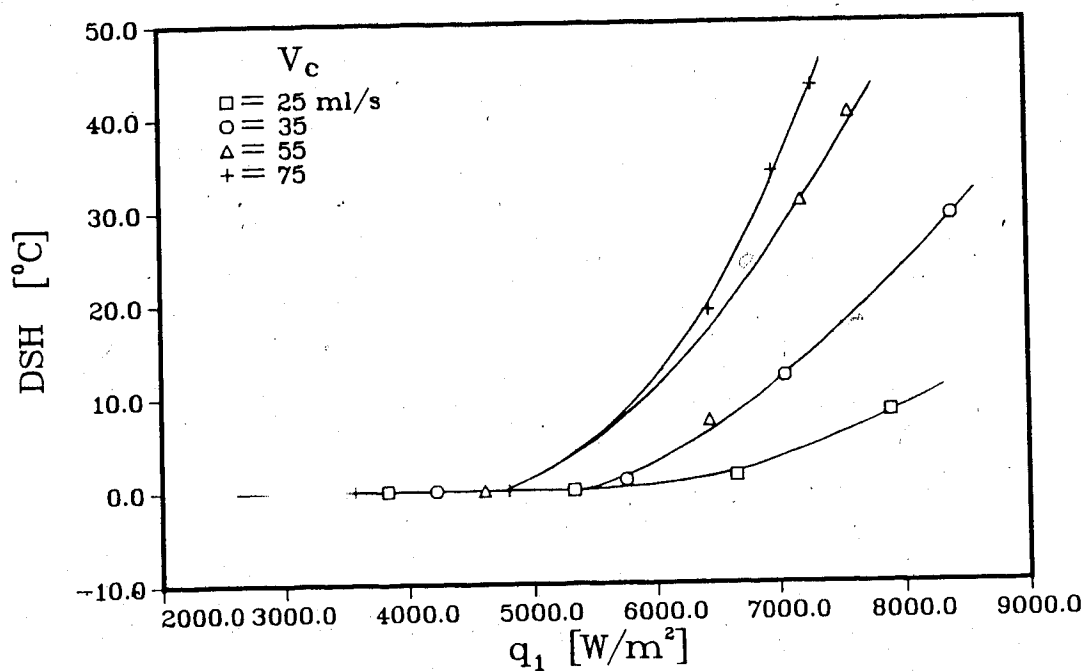


Fig. 4.7 Effect of cooling water flow rate on vapor superheating at evaporator exit with 20% charge level

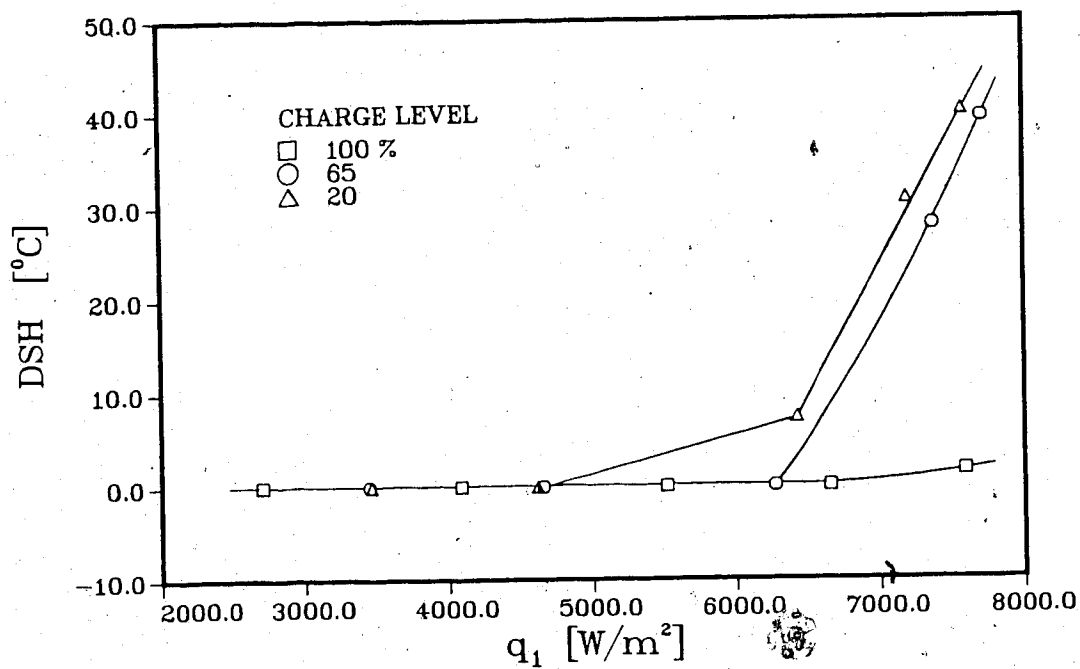


Fig. 4.8 Effect of charge level on vapor superheating at evaporator exit with $V_c = 55$ ml/s

rate is felt strongly at the evaporator, as was found to be the case for the liquid-phase and two-phase water thermosyphons. The indication from these figures is that the vapor enters the superheated regime for an input heat flux around 6000-7000 W/m².

Figs. 4.9 and 4.10 show the effect of the difference between the wall temperature and the evaporator saturation temperature on the exit quality and average wall heat flux for the same conditions. The temperature difference required to increase the flow quality to the superheated state is about 15°C. At this point the heat flux flattens off immediately, even though the temperature difference is increasing. This indicates that the internal heat transfer coefficient is dropping, as more of the inner surface area of the evaporator tube becomes dry. This has detrimental effects on the overall performance as is discussed later in this chapter.

The effects of external parameters on the flow in the evaporator tube have been examined, and it is also of interest to see the changes that occur due to the presence of the riser tube and liquid-vapor separator. Figs. 4.11 and 4.12 show the condenser shell side vapor quality as a function of the evaporator exit quality. Fig. 4.11 illustrates the effect of the liquid-vapor separator on the flow as the condenser quality is roughly 1.5 times that at the evaporator exit. The two-phase mixture has been dried somewhat with a portion of the liquid component separated

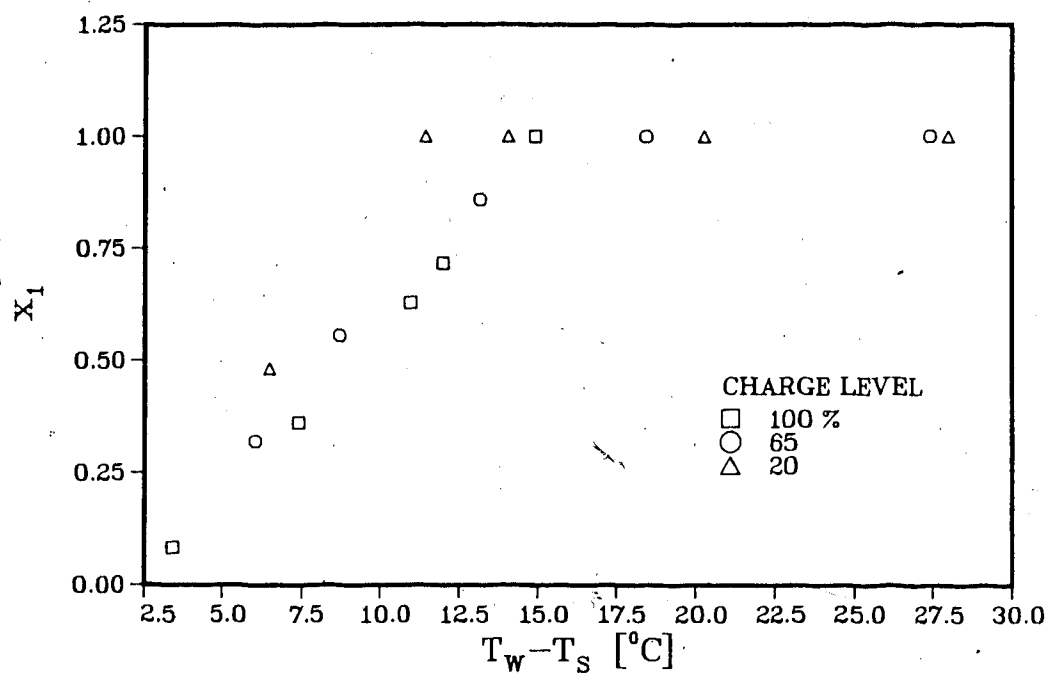


Fig. 4.9 Evaporator exit quality vs. ($T_w - T_s$) for $V_c = 55$ ml/s

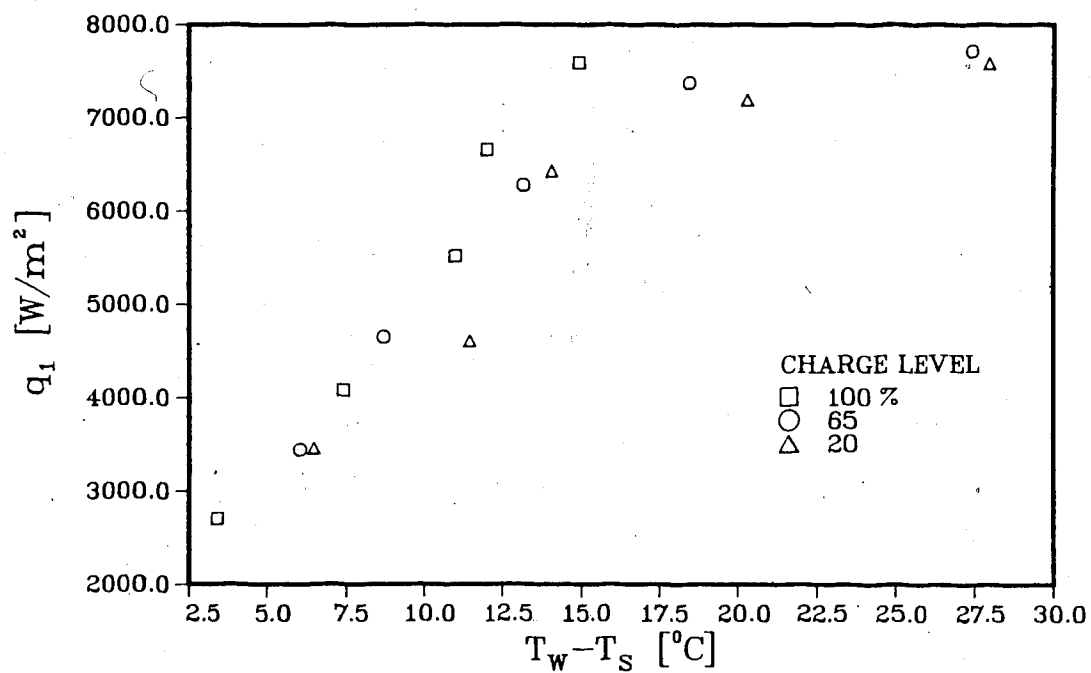


Fig. 4.10 Effect of ($T_w - T_s$) on wall heat flux with $V_c = 55$ ml/s

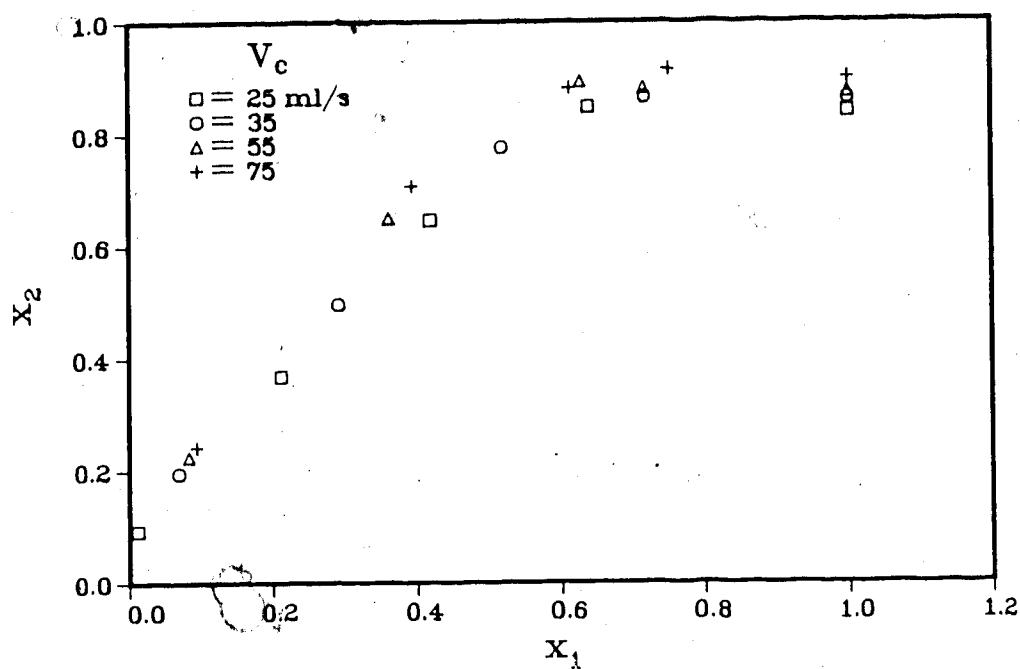


Fig. 4.11 Condenser shell side quality vs. evaporator exit quality for 100% charge level

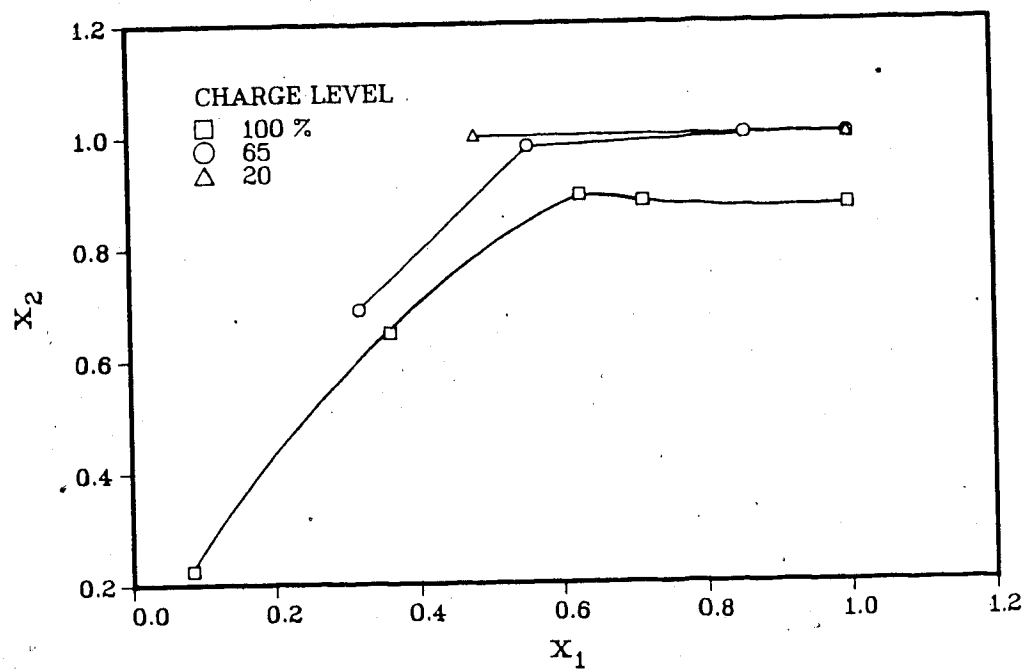


Fig. 4.12 Condenser shell side quality vs evaporator exit quality for $V_c = 55$ ml/s

and returned to the evaporator. The tapering off of the seemingly linear curve is probably a result of liquid entrainment by high speed vapor passing through the separator, as it is likely flooded for the high charge level case. The cooling water flow rate has a minimal effect and Fig. 4.12 indicates the stronger influence of charge level. Note that the 100% charge level curve shows the same drop indicated by Fig. 4.11.

The effect of condenser shell side quality on the cooling water heat extraction is shown in Figs. 4.13 and 4.14. The effect of cooling water flow rate appears to be small compared to that of the quality. The maximum heat extracted is somewhat higher for the lower charge levels, and the 20% charge level data lies entirely in the superheat region.

It is interesting to compare the separate operating systems used; that of liquid-phase thermosyphon and forced flow, two-phase water thermosyphon flow, and the two-phase R-113 system. The maximum heat transport rates for two common operating conditions between these arrangements is shown in Table 4.3.

The best performance of the natural circulation systems is achieved with R-113 as the working fluid, and this is expected for this low temperature range. The best heat extraction is obtained with the single phase forced flow situation, but requires the inclusion of a pump.

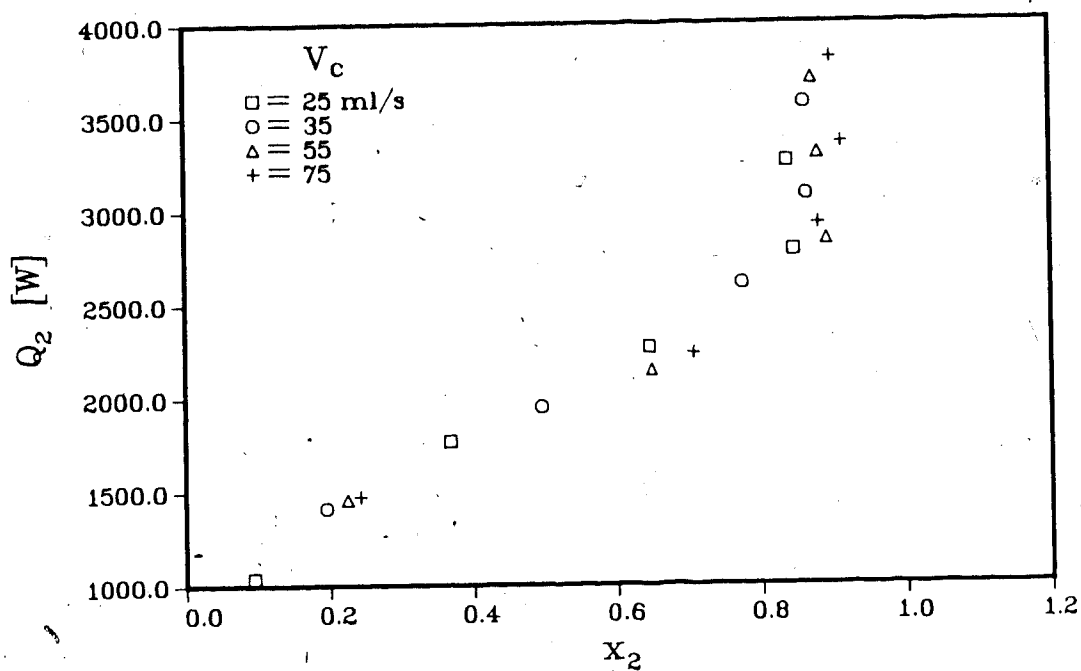


Fig. 4.13 Effect of cooling water flow rate on Q_2 vs. x_2 for 100% charge level

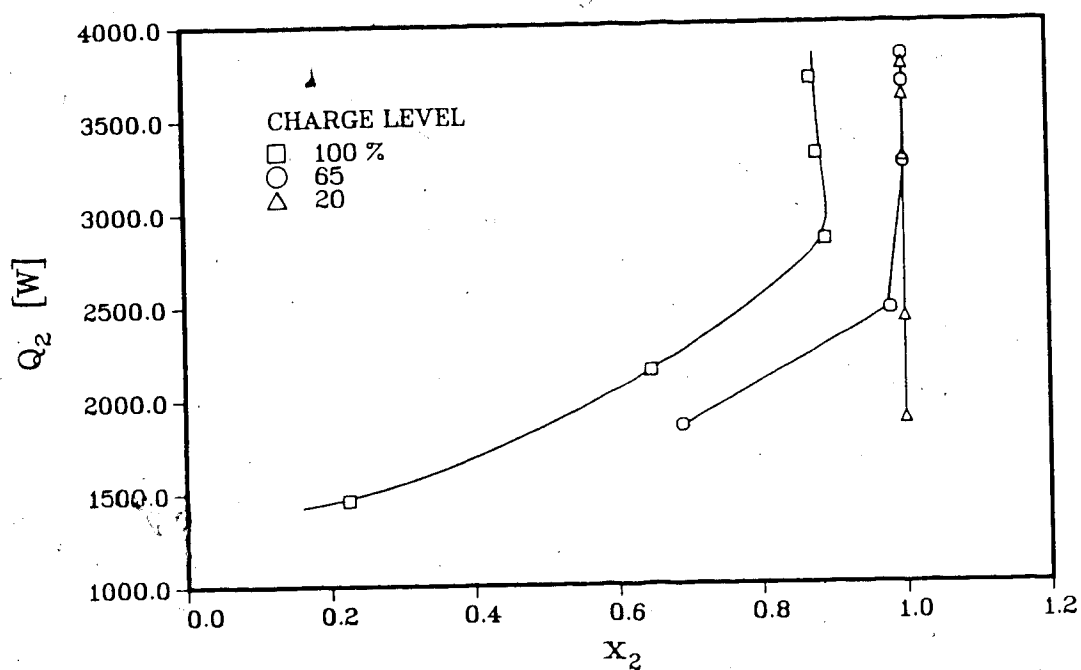


Fig. 4.14 Effect of charge level on Q_2 vs x_2 with $V_c = 55$ ml/s

Table 4.3 Heat Recovery with Different Working Fluids

Working Fluid	$T_h = 55^\circ\text{C}$	$T_h = 85^\circ\text{C}$
	Heat Recovered	(Watts)
Liquid-Phase Water	1000	3650
Two-Phase Water	1800	3800
Two-Phase Freon R-113	2250	4100
Forced Flow Water	2500	4800

note: cooling water flow rate and temperature are approximately constant for all cases.

4.5.2 System Efficiency

The overall thermodynamic efficiency of the system as calculated by Eq.(2.24) yields some important information. This is plotted against the average input heat flux in Figs. 4.15 and 4.16. Fig. 4.15 reveals that the efficiency actually falls off for high cooling water flow rate and high heat flux, and this begins to occur in a heat flux range of 6000-7000 W/m². This is the same operating region that was earlier shown to characterize superheated vapor production in the evaporator. Fig. 4.16 indicates that the lower charge levels provide better efficiency until superheating begins, but drop off more rapidly beyond that point. This is due to the higher sensitivity of the lower charge levels to superheating as was shown in Fig. 4.8 (both a lower charge level and higher cooling water flow rate increase the possibility of superheating, as discussed earlier). The low quality flow two-phase water tests showed that the efficiency increased for any increase in the input heat flux.

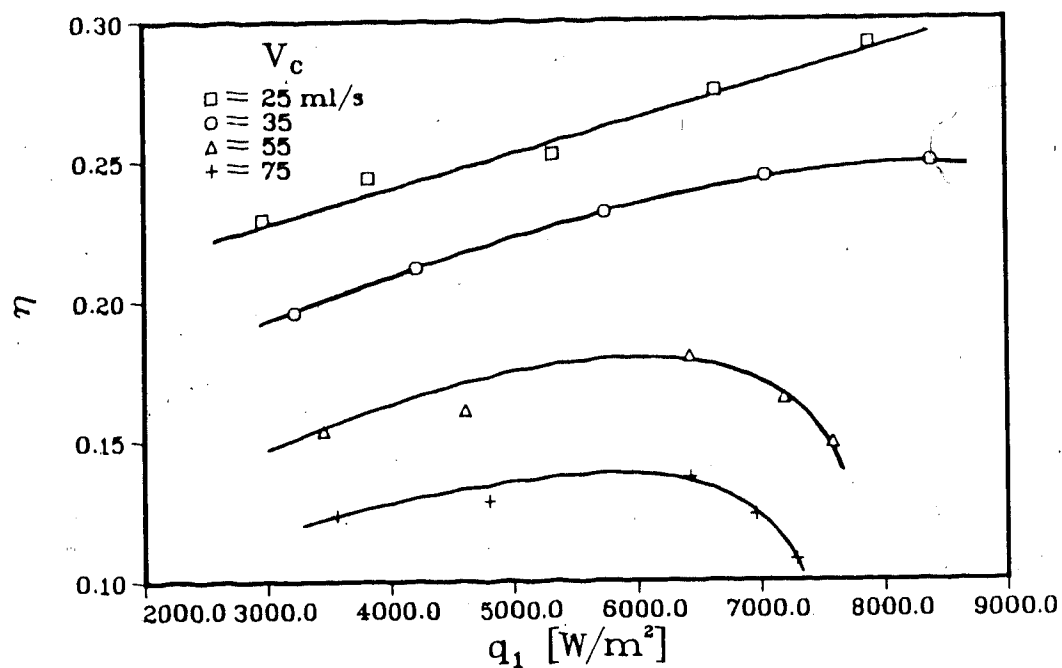


Fig. 4.15 Effect of cooling water flow rate and input heat flux on efficiency for 20% charge level

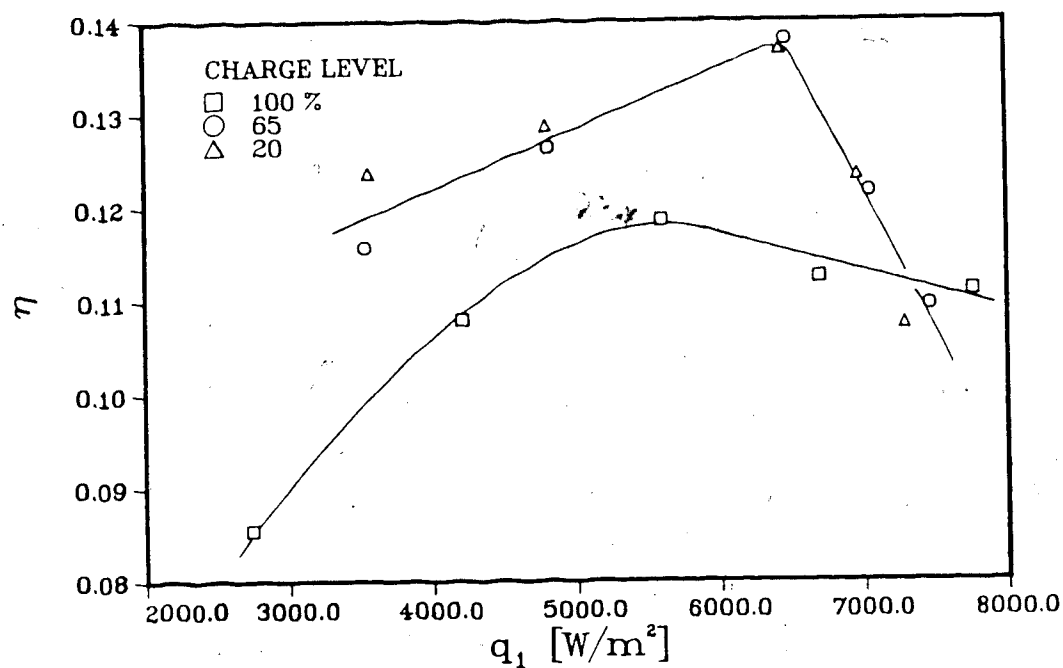


Fig. 4.16 Effect of charge level and input heat flux on efficiency with $V_c = 75$ ml/s

The effect of having superheated vapor flowing in the riser line is further illustrated by plotting the efficiency against the evaporator exit quality, as in Figs. 4.17 and 4.18. It is clear that the optimum system efficiency for a particular charge level or cooling water flow rate occurs as the evaporator exit quality approaches 1.0, or fully saturated vapor flow. Deviation from saturation into the superheated vapor region results in an immediate and rapid reduction in efficiency. This agrees with the work of McDonald, et al [17], who found that for a system with a multiple tube evaporator and condenser, that optimum performance occurred when there was no evaporator dryout.

The experimental data indicates that this system operates most efficiently in the saturation (two-phase) region of the working fluid. This means avoiding excessive subcooling of the working fluid at the condenser, or superheating at the evaporator exit. This is due to higher two-phase heat transfer coefficients, and a lower working fluid temperature which reduces heat losses.

The numerical values obtained for the efficiency of this system are quite low as compared to a single heat exchanger. As mentioned earlier, this might be improved by removing flow restrictions in the primary loop, which in this system are caused by the flow meters, piping, and fittings. An increase in the mass flow rate of the working fluid would decrease the chance of superheated vapor production in the evaporator. An ideal system with no

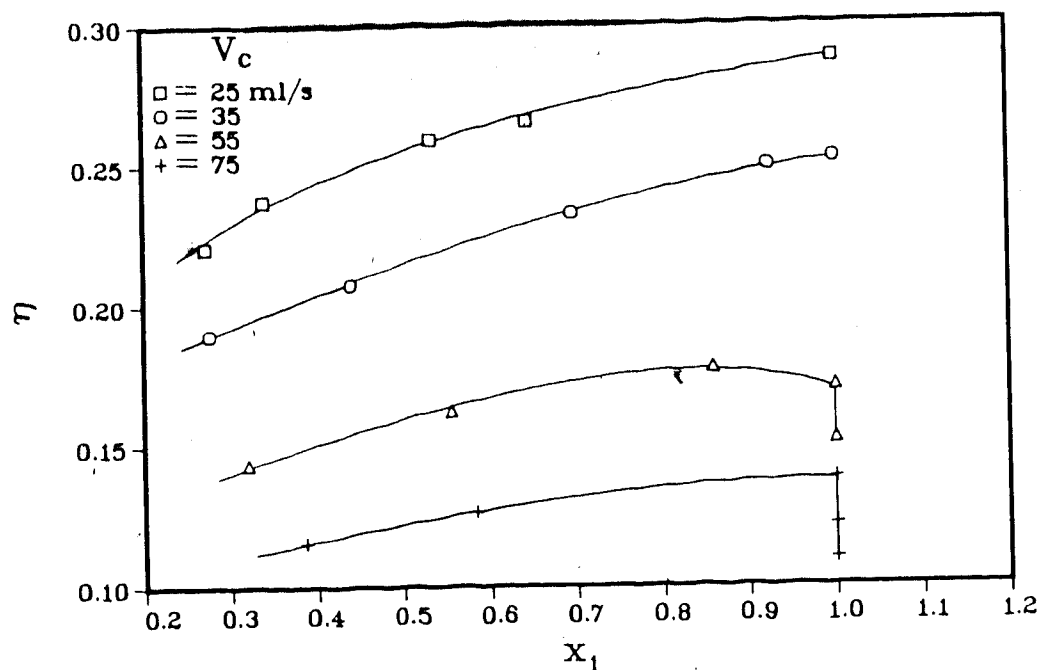


Fig. 4.17 Effect of cooling water flow rate and flow quality on efficiency for 65% charge level

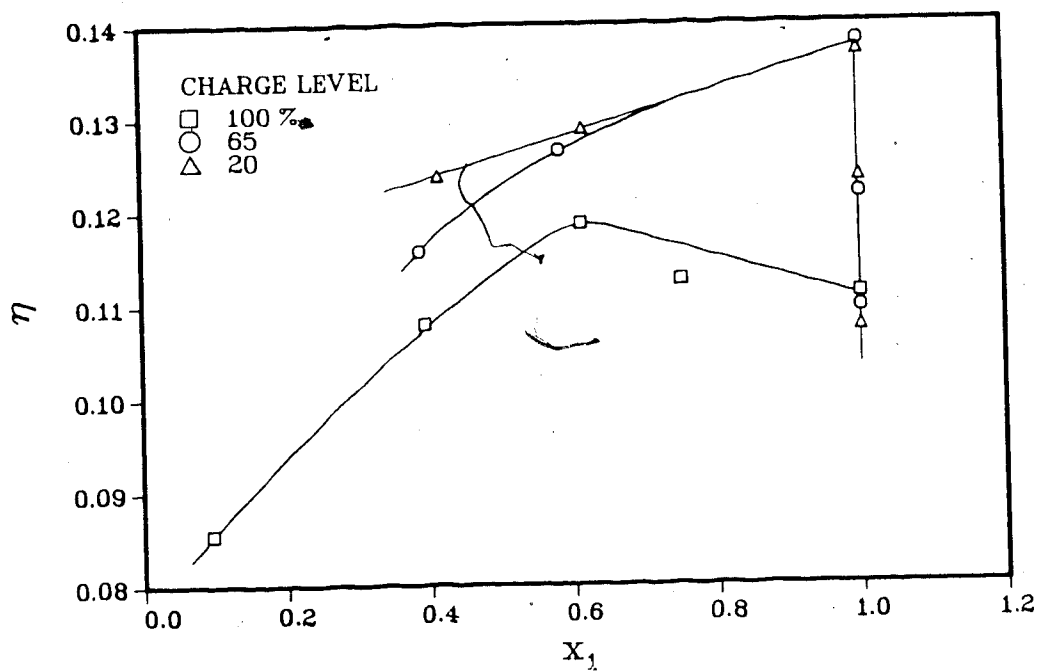


Fig. 4.18 Effect of charge level and flow quality on efficiency with $V_c = 75$ ml/s

pressure drop or heat loss might operate as illustrated on a T-s diagram as in Fig. 4.19. The evaporation process occurs from left to right in the saturation region, and the condensation process on the same line from right to left, returning to the initial point.

4.5.3 Evaporator Convective Boiling

As with the two phase water tests, the experimentally determined convective boiling heat transfer coefficient is compared with that of the turbulent liquid-phase component predicted by Eq.(3.9). The ratio of experimental to single phase coefficient is shown in Figs. 4.20 and 4.21, with inverse Martinelli parameter and Boiling number as the major parameters. The results for data lying in the saturation region only are included, as the equations fail outside the two-phase region. The results follow the expected trend as the latent component of heat transfer is much greater for higher vapor generation rates, while the liquid-phase flow and contribution to heat transfer decreases.

The experimental results for the high quality convective boiling heat transfer coefficients are compared with three separate correlation equations by Shah [31], Shrock and Grossman [32], and a recent one (1982) by Kandlikar [40].

The ratio of experimental to predicted heat transfer coefficient for the Shah correlation is plotted against the correlation's major parameter Boiling number in Fig. 4.22.

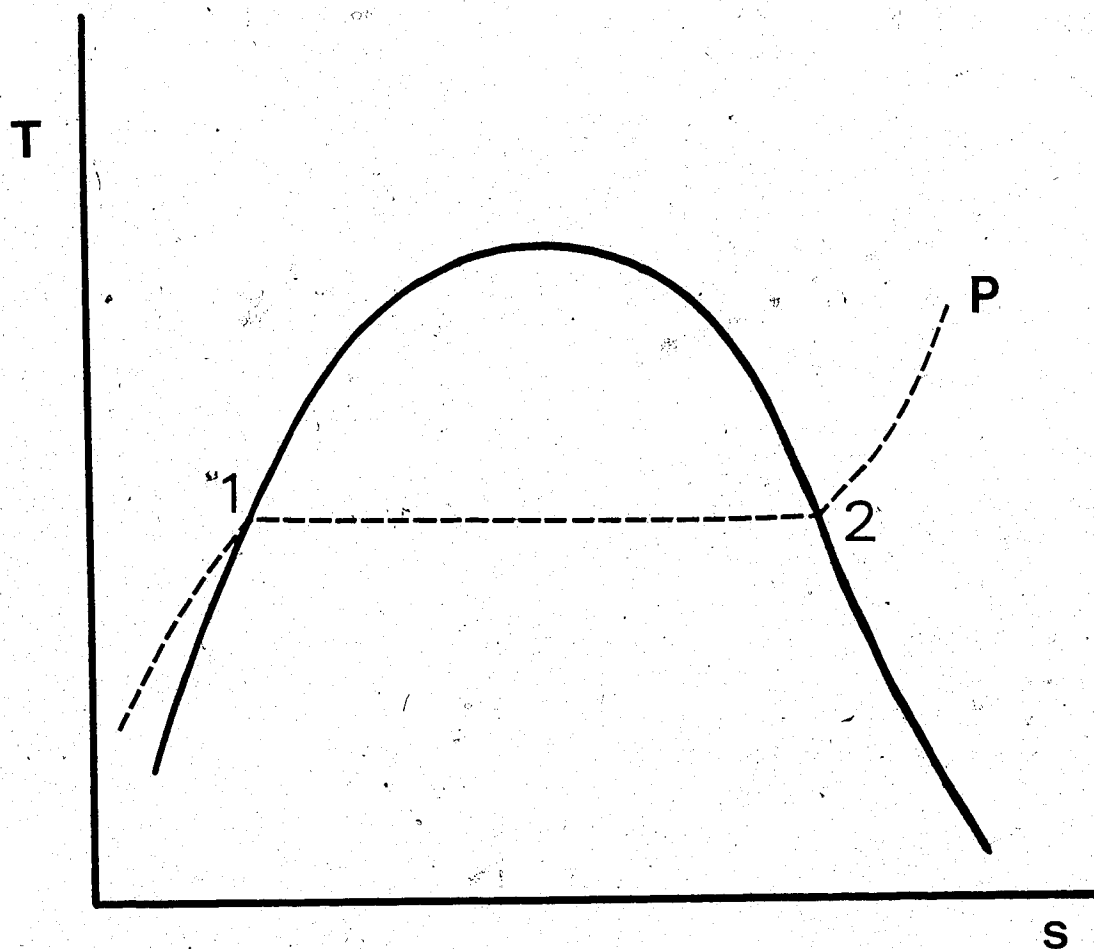


Fig. 4.19 Operating region of thermosyphon for isobaric conditions

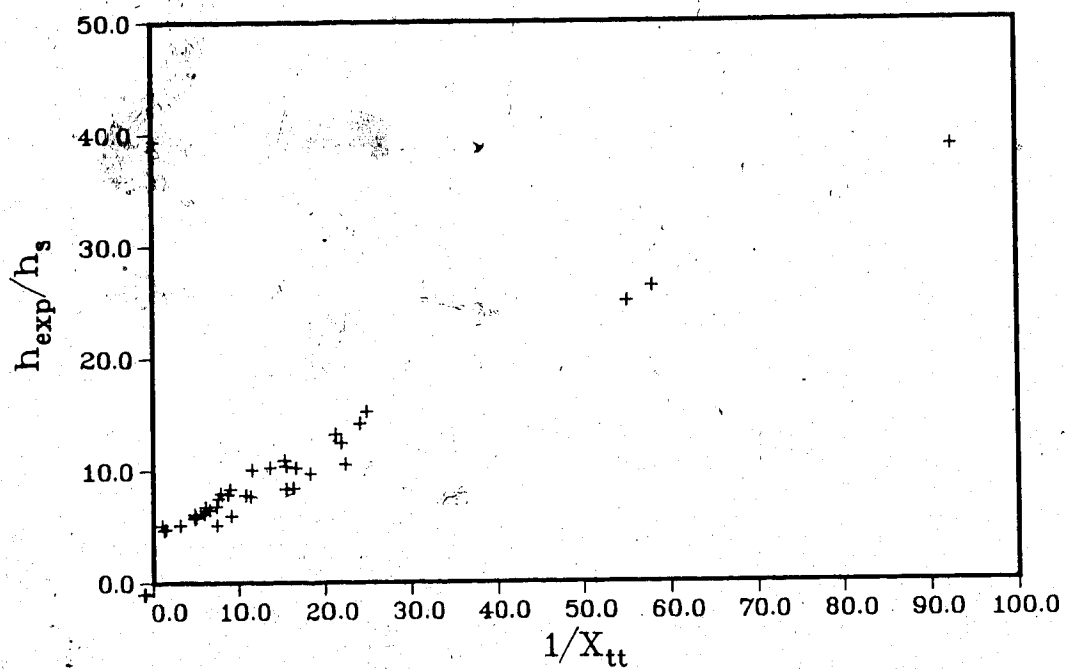


Fig. 4.20 Ratio of experimental to single phase turbulent evaporator tube heat transfer coefficient vs. inverse Martinelli parameter

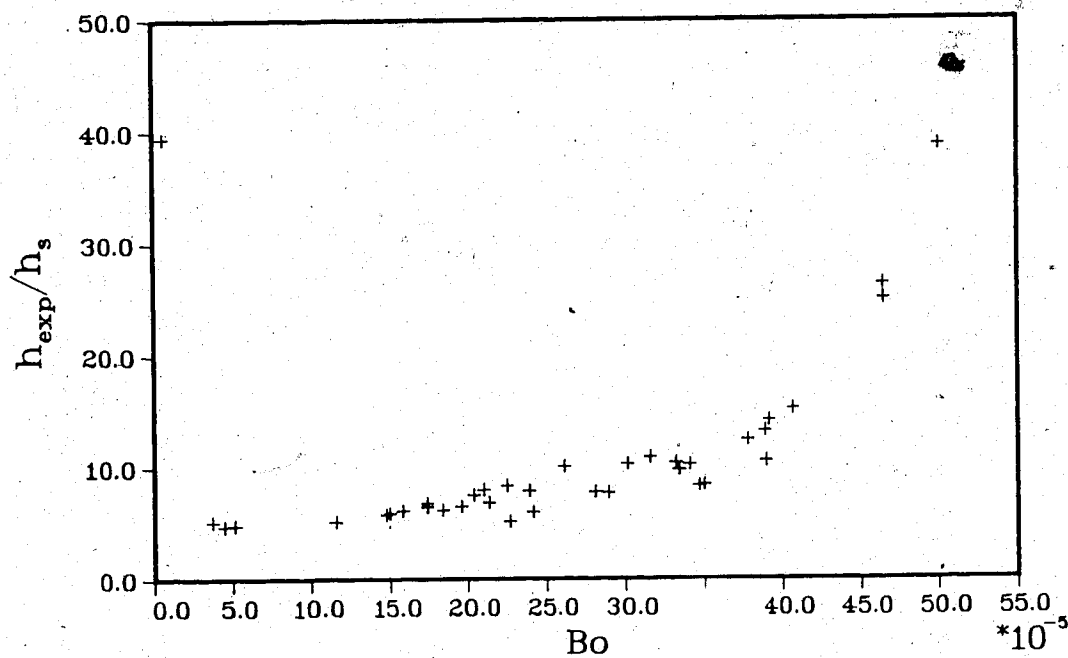


Fig. 4.21 Ratio of experimental to single phase turbulent evaporator heat transfer coefficient vs. Boiling number

Although this correlation was found to predict well for the low quality water tests, it underpredicts as vapor generation increases (increase in Bo). Although the Shrock-Grossman equation was originally specified for flow in vertical tubes, it predicts reasonably well for inverse Martinelli parameters greater than 5, as seen in Fig. 4.23.

Eq.(4.4) describes the correlation equation developed by Kandlikar for boiling flow in horizontal pipes and compares favourably with the experimental results, as shown in Fig. 4.24. The Convection number, Co , given by Eq.(4.6) is a major parameter for this correlation, and describes the convective component of the flow.

4.5.4 Primary Loop Flow and Pressure Instabilities

Interest in flow and pressure oscillations in two-phase systems has grown considerably since the 1950's due to the advent of nuclear reactors and their associated cooling problems. However, oscillatory flow instabilities may occur whenever energy is added to a flowing fluid and produces a change in volume [41]. A good review paper by Kakac and Veziroglu [42] explains the different mechanisms of flow and pressure oscillations, and sums the history and present work in this field.

The most common types of dynamic oscillations are pressure-drop oscillations, which are related to the amount of compressible volume in the system and have large time periods, and density wave oscillations, which are related to

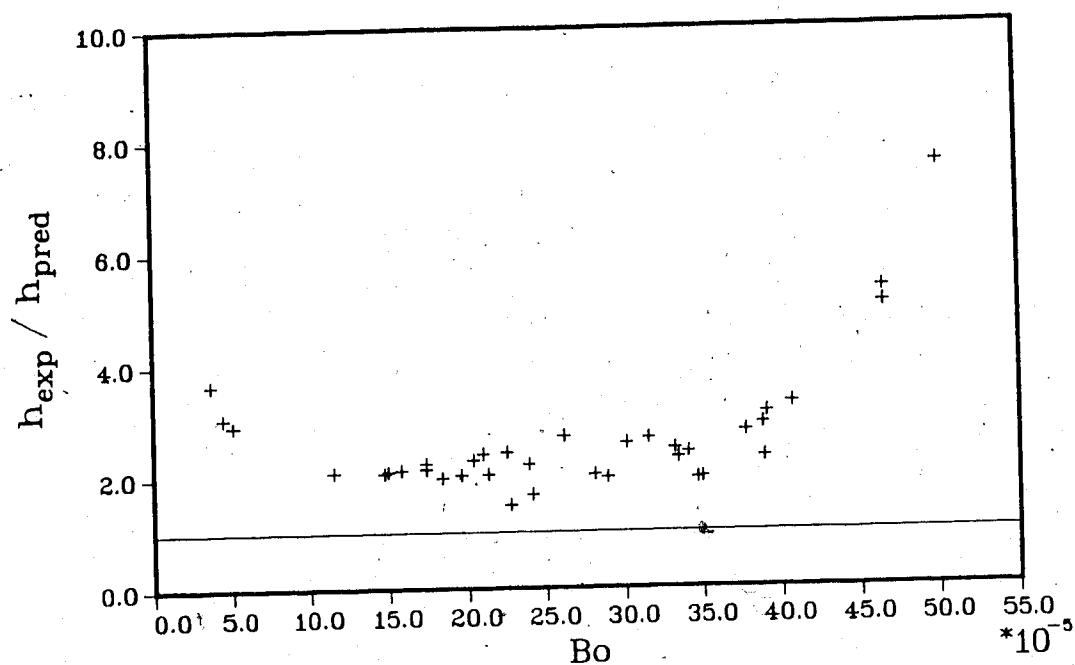


Fig. 4.22 Comparison of experimental evaporator heat transfer coefficient with Shah correlation

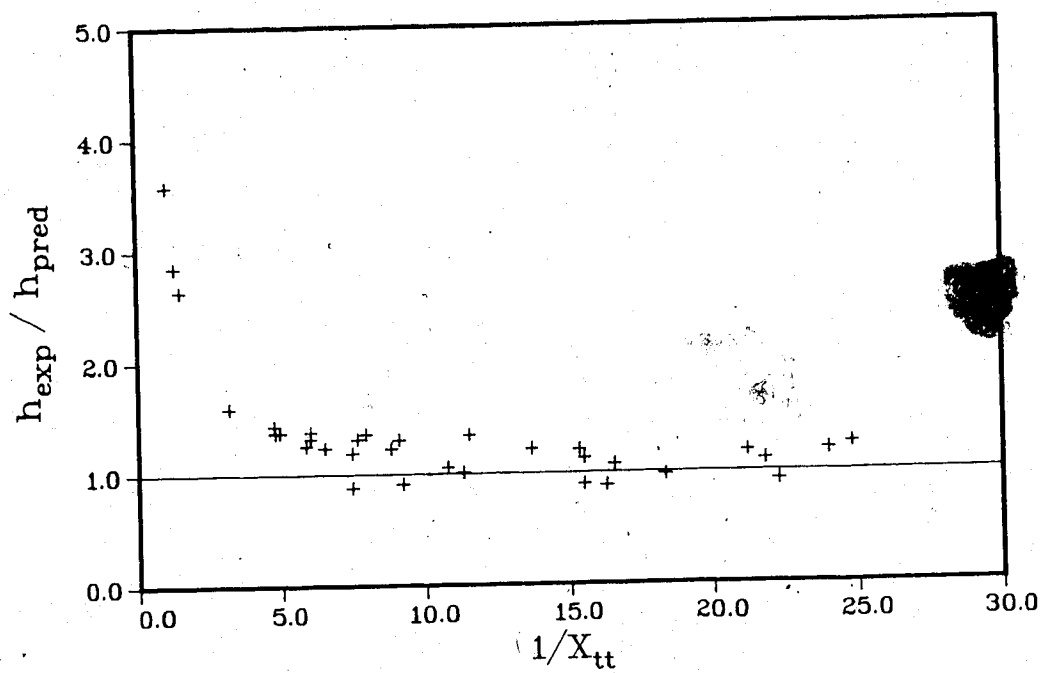


Fig. 4.23 Comparison of experimental evaporator heat transfer coefficient with Shrock-Grossman correlation

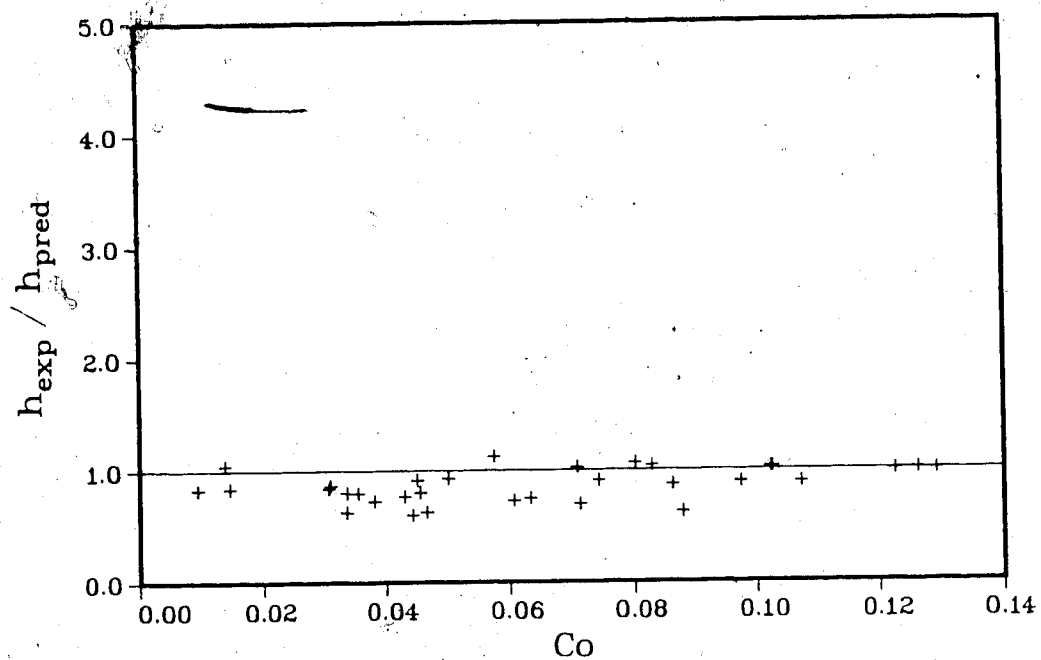


Fig. 4.24 Comparison of experimental evaporator heat transfer coefficient with Kandlikar correlation

the residence time of a fluid particle in the system, and have shorter periods. There are other types also, such as acoustic oscillations and thermal oscillations, the latter of which are related to the instabilities of the liquid film in high vapor quality flow.

These oscillations are particularly important for natural circulation systems as they may be of the same order of magnitude as the mean flow rates and pressures. This can lead to flow reversal, or fatiguing of piping and joints due to fluctuating stresses. Large, regular fluctuations in flow rates and pressure in the primary loop of the two-phase water system were noted, but it was difficult to analyze the data. For this reason, the data from the Freon system was processed with an FFT spectrum analyzer to determine the frequency content of the signals. A typical chart recorder trace of the output signals from the system pressure transducer, downcomer line flow meter, and condensate flow meter are shown in Fig. 4.25. Note that the magnitude of the condensate line fluctuations are much greater than that for the downcomer line, and this was found to always be the case over the range of tests conducted.

When the analog version of this signal is fed through the FFT, the fundamental frequencies may be identified, as in Fig. 4.26. The additional smaller peaks are the harmonics of the 0.35 cycles per second fundamental frequency. This indicates that an additional acoustic wave may be travelling around the system after the initial excitation is provided

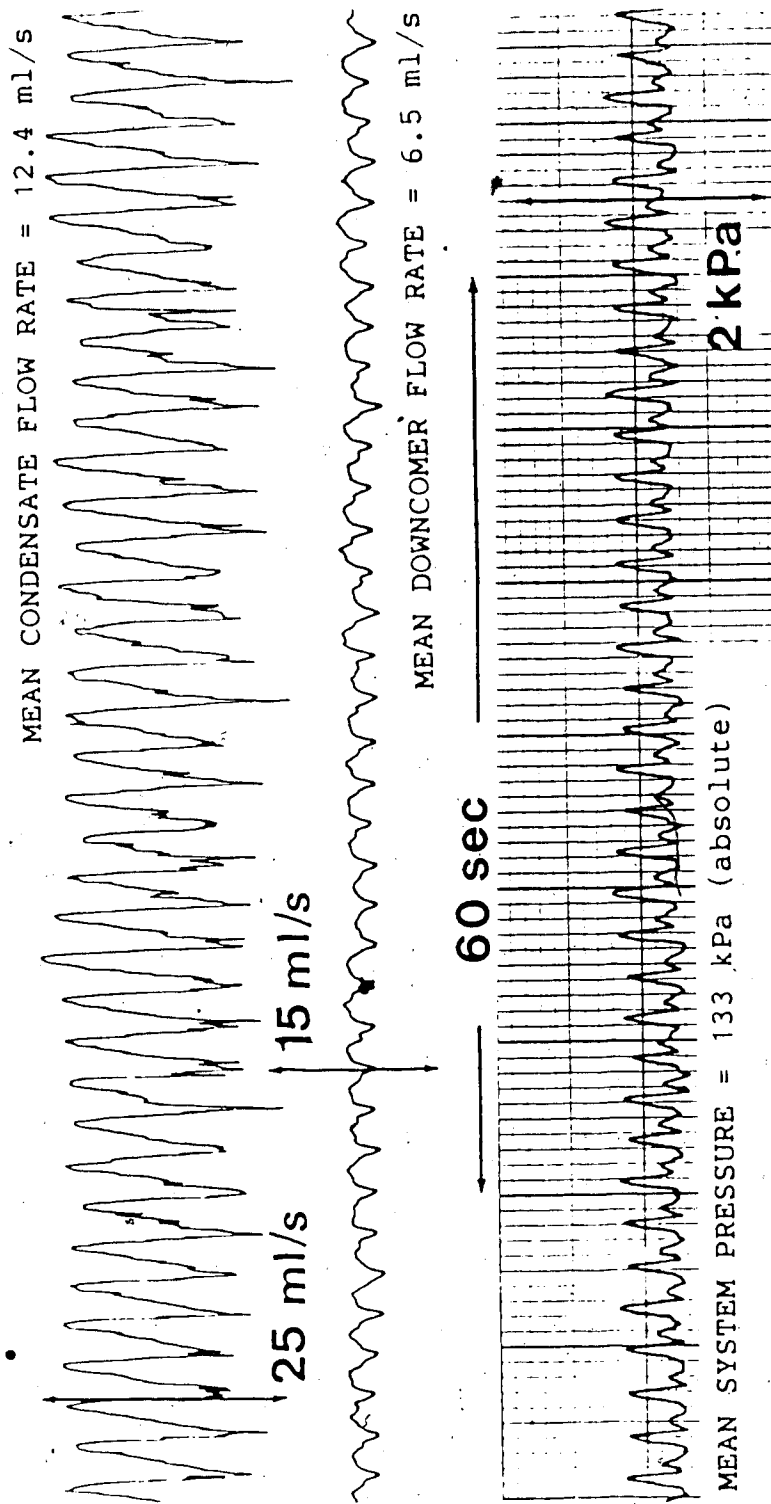


Fig. 4.25 Primary loop flow and pressure oscillations for 65% charge level, 65°C heat source temperature, and $V_C=25$ ml/s

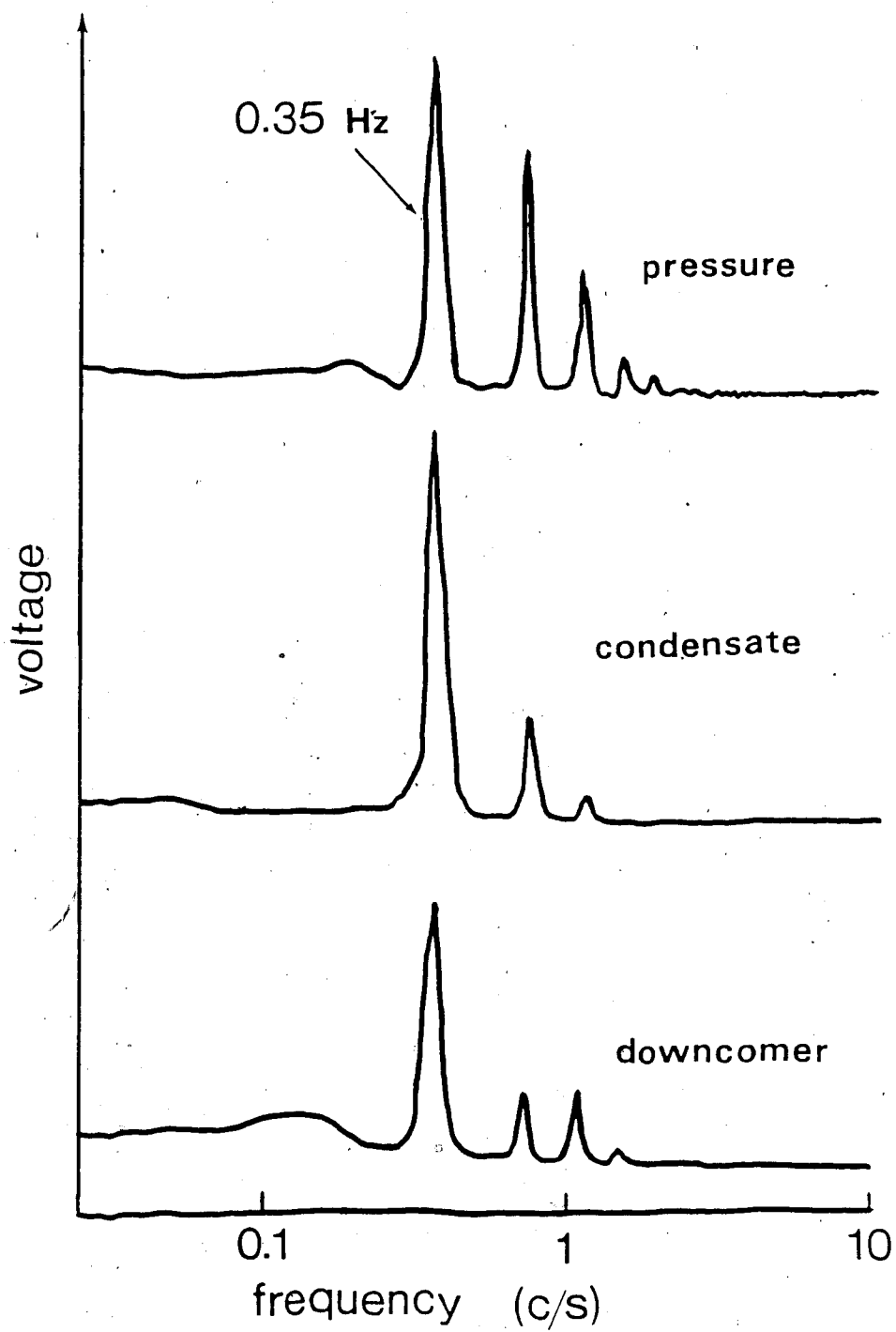


Fig. 4.26 Frequency spectrum of primary loop flow and pressure oscillations for 65% charge level, 65°C heat source temperature, and $V_C=25$ ml/s

by the fundamental. One important fact to be drawn from this figure is that all three parameters have the same frequency of oscillation, and this was found to be the case for the majority of the tests conducted. In addition, the fundamental frequency was found to be a basically constant value, varying between 0.35 and 0.375 c/s, with some data scatter. The frequencies of oscillation of the flow rates and pressures are plotted against input heat flux in Figs. 4.27, 4.28, and 4.29.

Pressure drop oscillations are of much lower frequency than 0.35 c/s, as reported in [41], and for the most part were not detected. The regularity of the oscillations for changing heat flux (thus changing vapor quality of the riser flow) indicates that they may be dependent on geometry rather than on the state of the flow. Stenning [43] indicated that the time period of density wave oscillations was of the order of the residence time of a fluid particle in the system. For an open system forced flow experiment, Verizoglu and Lee [41] found that the period of density wave oscillations was approximately 2.32 times the residence time of a particle in their heater and exit tubing, and that the frequency was in the range 0.33-0.5 c/s.

For the present closed system, a good linear relationship was not found between the oscillation periods and the time for a particle to travel around the loop. This could be due to the different sizes of tubing and fittings used, and the inability to determine the flow density at

some points. Thus the average velocity of the flow could not be accurately determined. However, the fluctuations are of the same order of magnitude as a roughly determined frequency of the flow around the loop. This, and the agreement with [41] for the frequency of density-wave oscillations indicates that this is the mechanism of the observed fluctuations, and the acoustic wave which is generated is the probable cause of the harmonics as it travels around the system and is eventually damped out.

The amplitude of the oscillating signal is important as well as the frequency. The statistical variance of the system pressure fluctuations was computed from Eq.(4.2) and the result is shown in Fig. 4.30 plotted against average evaporator heat flux. This calculation represents the deviations in the system pressure from the mean value of the fluctuations, and the figure shows that the variance increases only slightly with higher heat fluxes until a critical point is reached, at which point a dramatic increase in the variance is seen. This point is once again characterized by entry into the region of superheated vapor production in the evaporator, and this is further exemplified in Fig. 4.31, where the system pressure variance is plotted against evaporator exit quality (all data shown).

This would often cause an audible noise to emanate from the system, as well as some vibration of the primary loop tubes. This drastic effect which occurs for superheated vapor production may be caused by an increasingly unstable

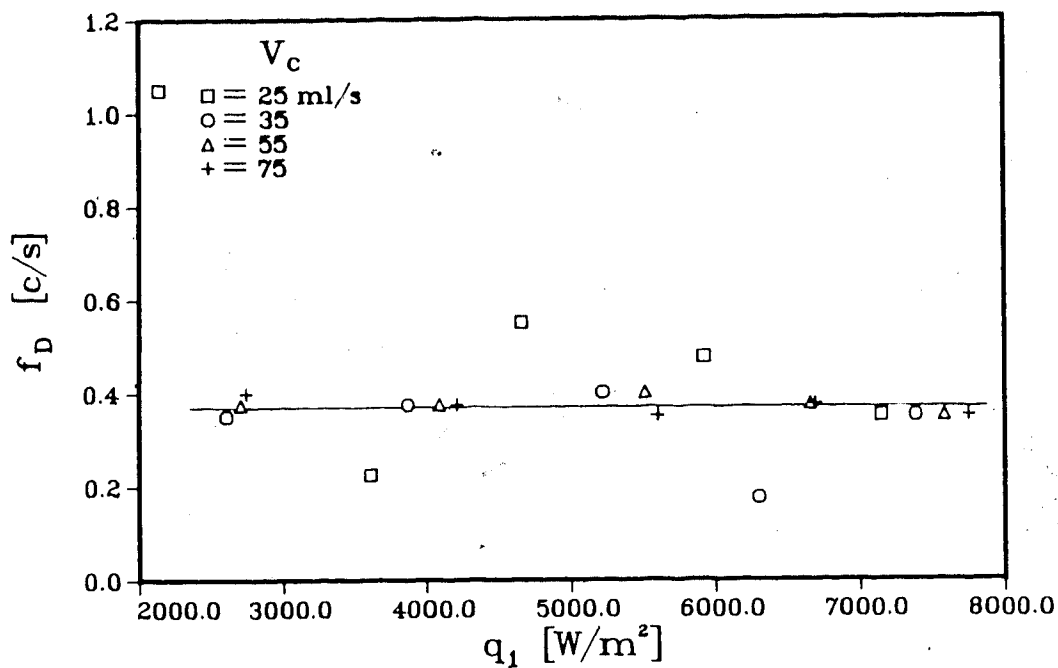


Fig. 4.27 Frequency of downcomer flow fluctuations for 100% charge level

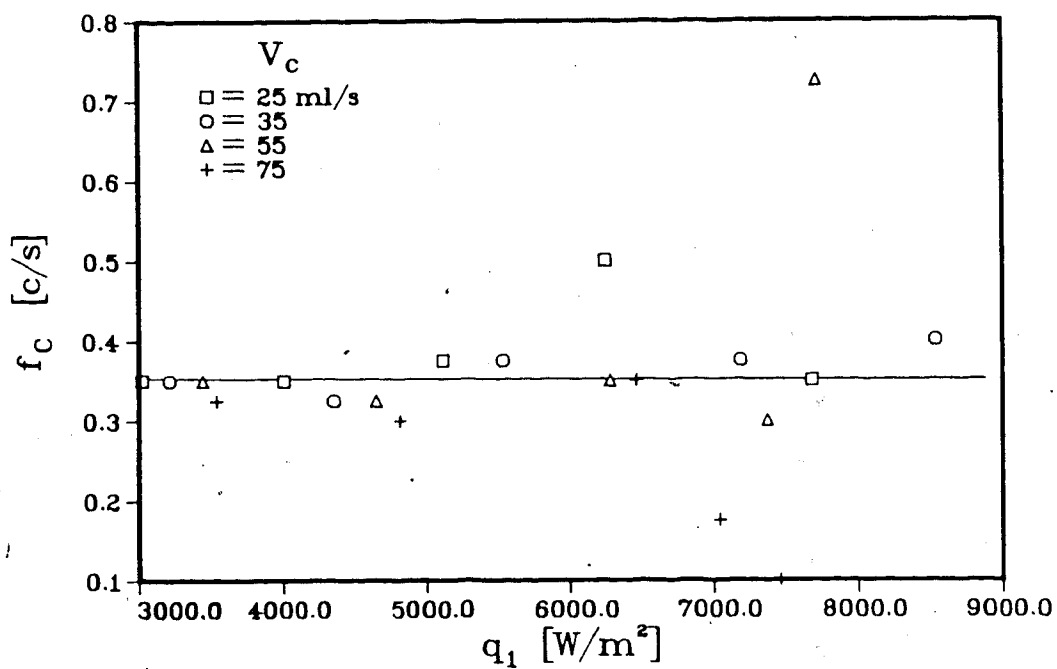


Fig. 4.28 Frequency of condensate flow fluctuations for 65% charge level

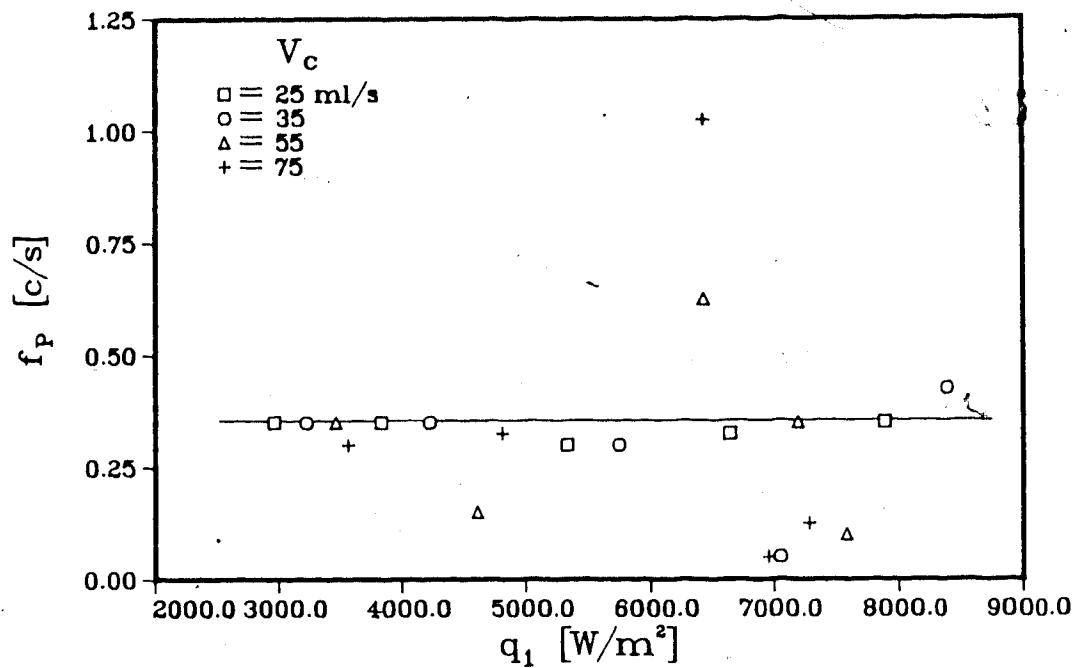


Fig. 4.29 Frequency of system pressure fluctuations for 20% charge level

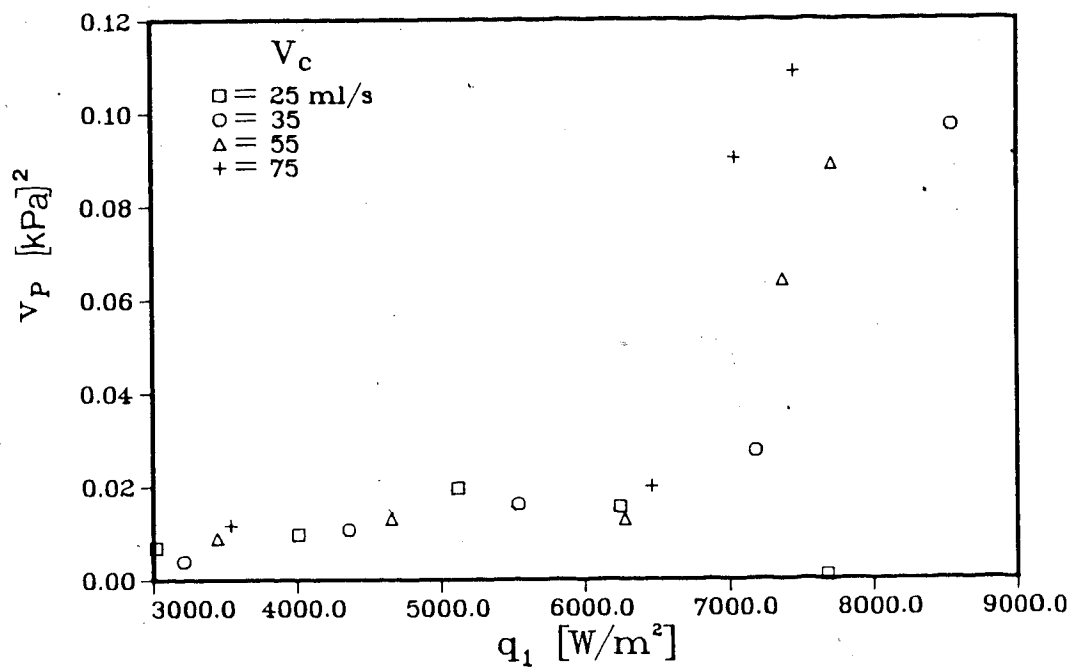


Fig. 4.30 Variance of system pressure signal for 65% charge level

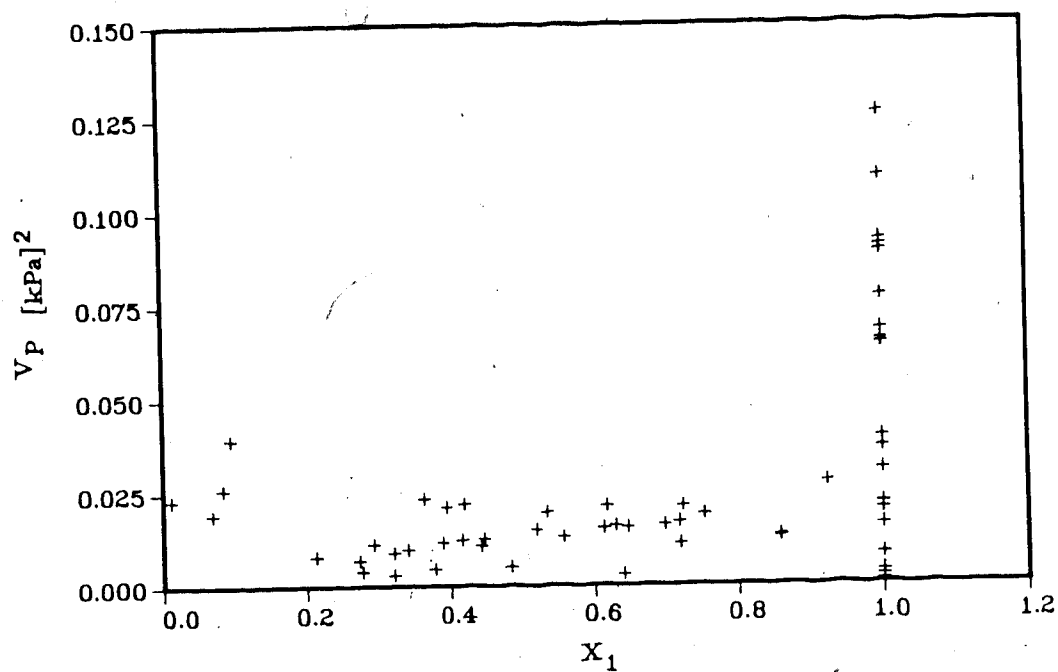


Fig. 4.31 Variance of system pressure signal with evaporator exit quality, all data

liquid film on the evaporator tube surface, or a destructive collapse of hot vapor volume as it encounters the cold surfaces and liquids in the condenser. For the particular arrangement tested, the production of superheated vapor causes mechanical effects which should be avoided.

Experiments performed with forced boiling flow in parallel channels [44] have revealed that introducing a pressure drop at the inlet to the heated section stabilizes pressure-drop and density-wave type oscillations. However, any flow restriction in the natural circulation system hinders performance, so the avoidance of mechanical problems may have to be effected through operation in the two-phase region. The system tested is the most thermodynamically efficient when superheating is avoided, which is additional incentive not to exceed saturated vapor production in the evaporator.

4.5.5 Convective Boiling Pressure Drop

Two different models are widely used to describe pressure gradients in two-phase flow, these being the homogeneous model and the separated flow model. The homogeneous model, which will be used here, assumes good mixing with equal liquid and vapor velocities, thermodynamic equilibrium between phases, and some mean property value between the two phases of the flow. The homogeneous mean absolute viscosity and density may be calculated by

$$\bar{\mu} = \left(x/\mu_g + \frac{1-x}{\mu_f} \right)^{-1} \quad (4.7)$$

$$\bar{\rho} = \left(x/\rho_g + \frac{1-x}{\rho_f} \right)^{-1} \quad (4.8)$$

When measuring the total pressure drop for the working fluid in the evaporator from an inlet static pressure tap to an outlet static pressure tap, three elements are included: the frictional, accelerational, and gravitational components. Following Shrock and Grossman [32], the accelerational pressure drop component is considered negligible. It is of primary interest to extract the frictional part of the pressure drop from the total experimental measurement. Because the heat exchanger has a 0.25 meter height, corrections for the gravity component of the reading caused by the large density change from the inlet (liquid) to the outlet (liquid-vapor) must be considered.

The pressure transducer is located in the same horizontal plane as the upper exit pressure tap, and liquid filled copper tubes connect the transducer with both pressure taps. The required correction for the gravity component is found from the density difference between the liquid filled lower pressure tap line and liquid-vapor filled evaporator tube. The flow in the evaporator tube may change from a liquid at the inlet to vapor at the outlet so

a mean density for the fluid is calculated. This is done by assuming that the flow quality varies linearly from the inlet to the outlet [13]. The density of the inlet fluid is that of liquid Freon R-113, and the density of the exit mixture is calculated from Eq.(4.8). This yields a mean evaporator tube density of

$$\bar{\rho}_m = \frac{1}{2} \left[\rho_{fi} + \left(\frac{x}{\rho_g} + \frac{1-x}{\rho_f} \right)^{-1} \right] \quad (4.9)$$

The liquid filled pressure tap line contains R-113 at room temperature (density=1569 kg/m³), so the gravitational portion of the total pressure measurement is given as

$$P_{\text{grav}} = (\bar{\rho}_m - 1569) gh \quad (4.10)$$

Finally, the friction component may be extracted from the measured pressure drop through the following equation with SI units:

$$\Delta P = P_{\text{meas}} - (\bar{\rho}_m - 1569)(9.81)(0.25) \quad (4.11)$$

The experimental two-phase frictional pressure drop will also be compared with a homogeneous model correlation. From Collier [45], the frictional pressure gradient is

$$-dp/dz = 2 f_t G^2 / \rho d \quad (4.12)$$

with f_t given by the Blasius equation assuming the boiling

flow is turbulent:

$$f_t = 0.079 (Gd/\mu)^{-0.25} \quad (4.13)$$

The total frictional pressure drop through the evaporator may then be written as

$$\Delta P_t = 2 f_t G^2 / \rho (L/d) \quad (4.14)$$

The experimentally measured friction component of pressure drop for convective boiling in the evaporator tube is plotted against the input heat flux in Figs. 4.32 and 4.33. Two data points have been eliminated from Fig. 4.32. Earlier, the total mass flow rate through the evaporator was shown to decrease and then level off for increasing heat flux. In a single phase system, this would result in a lower pressure drop over the length of the tube. Here however, the pressure drop increases in a linear fashion with increasing heat flux until a drastic reduction of the pressure loss occurs, as seen in Fig. 4.33. Note that this is for the two lower charge levels, which indicates that the superheated vapor state is being encountered. The high charge level data shown in Fig. 4.32 lie entirely in the saturation region, with a two-phase mixture being present at the evaporator exit.

The trends seen in the experimental data agree with those found in Freon R-11 tests by Kakac and Veziroglu

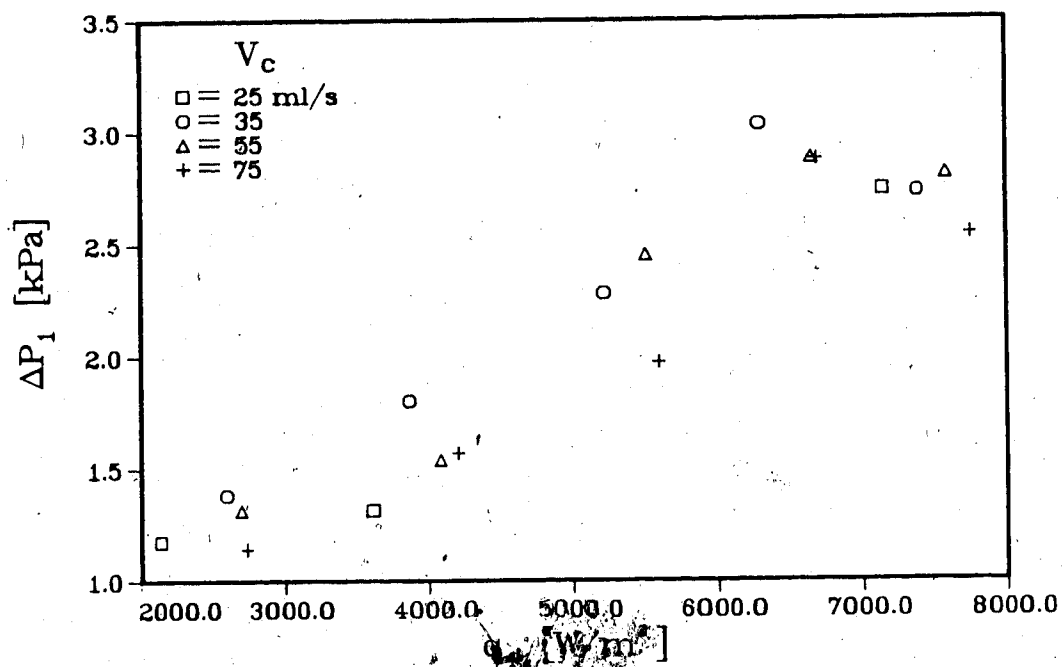


Fig. 4.32 Two-phase friction pressure drop through evaporator vs. heat flux for 100% charge level

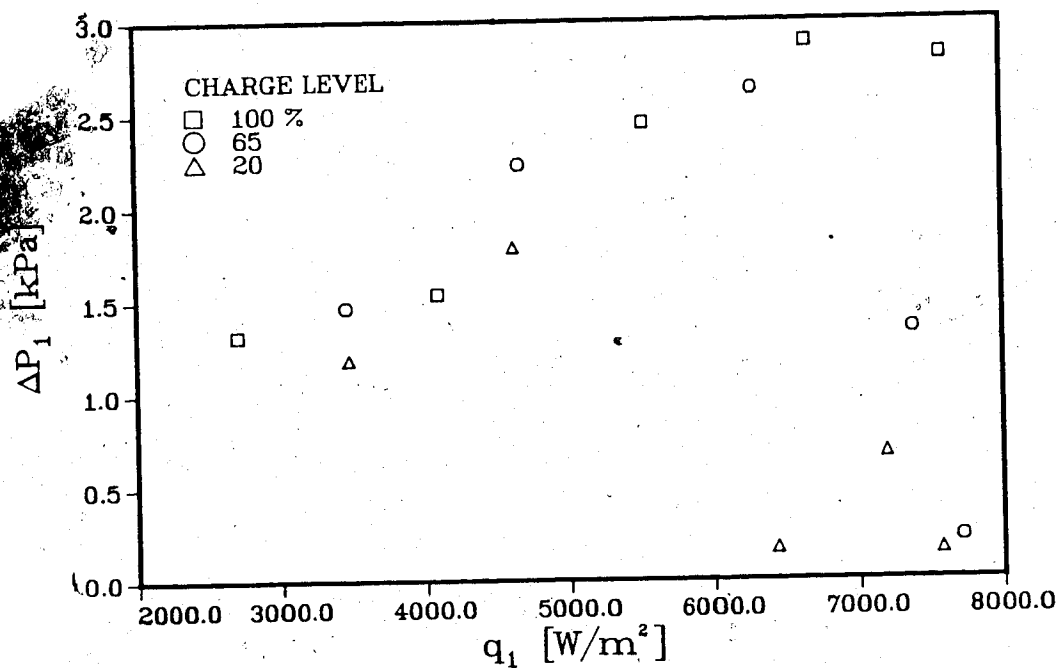


Fig. 4.33 Two-phase friction pressure drop through evaporator vs. heat flux for $V_c = 55$ ml/s

reported in [41,42] for single channel upflow boiling tests. In those experiments, the wall heat flux was held constant, and the mass flow rate varied to produce different fluid states in the boiler. It was found that when the liquid in the evaporator reached saturation, further decreases in the mass flow rate caused an increase in the pressure drop as bulk boiling commenced. Eventually the pressure drop was reduced as the mass flow rate approached zero. This type of result is to be expected, as the pressure drop caused by the turbulent mixing of a boiling fluid may offset the gain produced by lowering the mass flow rate. The volume change created by vapor generation increases the velocity of the flow which also contributes to greater friction losses.

To further illustrate the effect of the state of the fluid on the pressure drop, it is compared with the evaporator exit quality in Figs. 4.34 and 4.35. This data spans the saturation region, as well as superheated vapor production for a vapor quality of 1.0. The pressure drop increases as more of the total flow in the evaporator becomes vapor, and the mean velocity of the two-phase mixture is raised. Upon the generation of superheated vapor, the pressure drop decreases, even though the total mass flow rate does not greatly vary. For the same mass flow rate, the single phase flow exhibits a lower friction pressure drop than a two-phase mixture. Neither cooling water or charge level affect the data other than their influence on the state of the fluid in the evaporator tube.

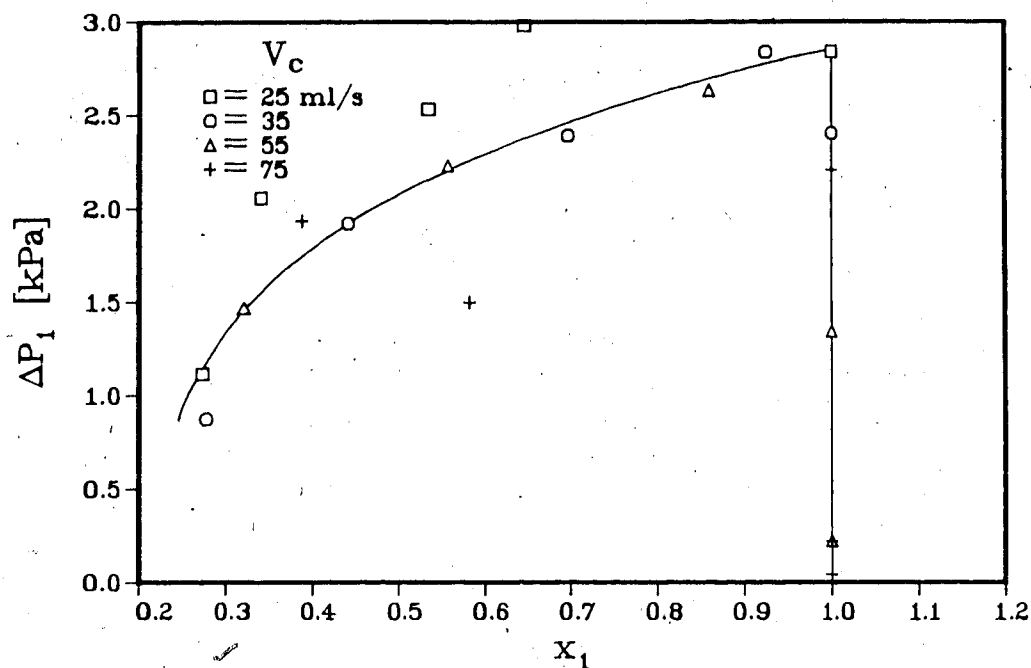


Fig. 4.34 Effect of evaporator exit quality on two-phase frictional pressure drop for 65% charge level

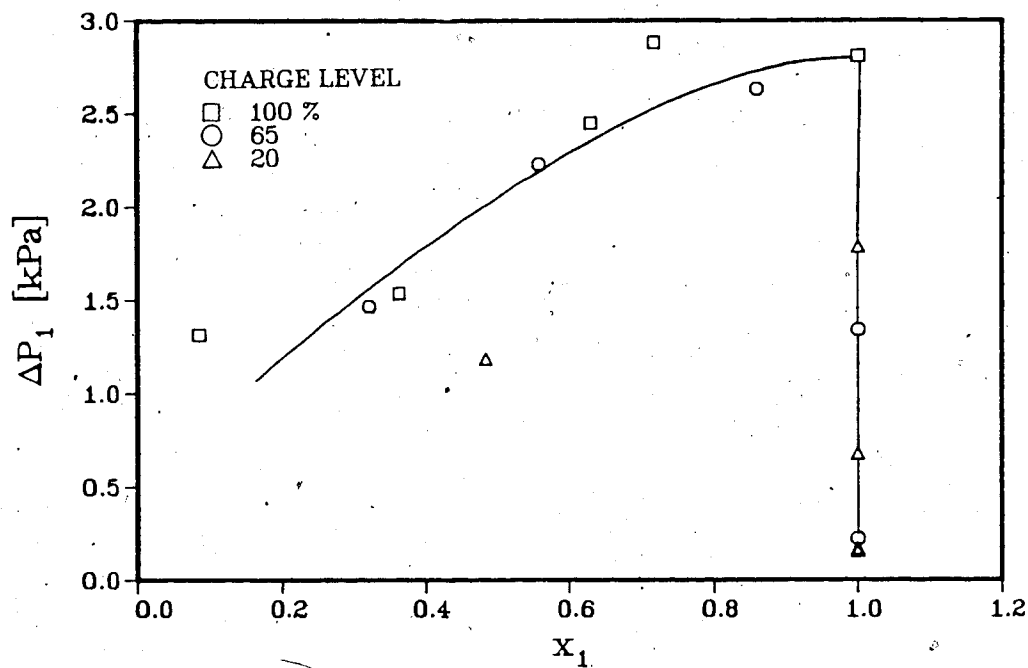


Fig. 4.35 Effect of evaporator exit quality on two-phase frictional pressure drop for $V_c = 55$ ml/s

The frictional component of pressure drop is plotted against the inverse Martinelli parameter in Fig. 4.36. The parameter is valid only for two-phase flow, so superheated data is omitted. The Martinelli parameter is the ratio of the frictional pressure gradients of liquid flowing alone to gas flowing alone and is thus a separated flow parameter. The pressure drop increases as the inverse Martinelli parameter increases, indicating again the additional pressure drop caused by the presence of vapor in the flow.

The ratio of the experimental pressure drop to that predicted by the homogeneous model of Eq.(4.14) is plotted against evaporator exit quality in Fig. 4.37. The ratio varies from 0.5 to 2 in the saturated flow region. The prediction becomes inaccurate with excessive superheating, as most of the tube length contains single-phase vapor and the correlation does not apply.

In Fig. 4.38, only the results for the two-phase mixture are shown with the ratio of experimental to homogeneous model pressure drop plotted against the inverse Martinelli parameter (two large scatter data points have been omitted). The effect of the separated flow parameter indicates that modelling of two-phase pressure drop may be better described using a combination of both the homogeneous and separated-flow techniques. Of course, no one mathematical model can be expected to account for all the physical variables encountered in real situations.

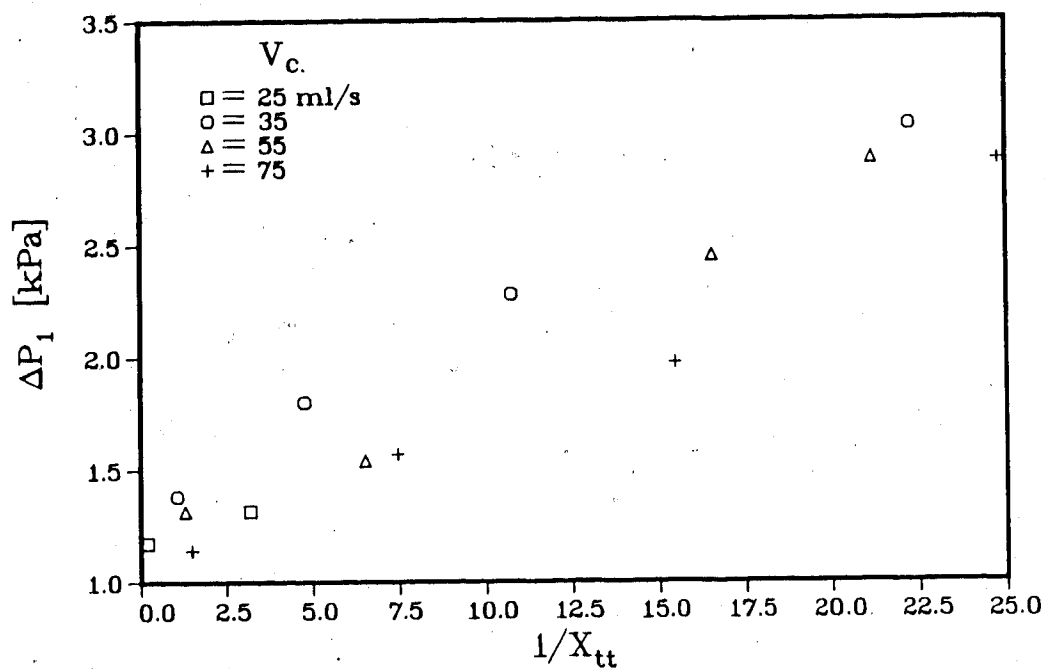


Fig. 4.36 Two-phase pressure drop vs. inverse Martinelli parameter for 100% charge level

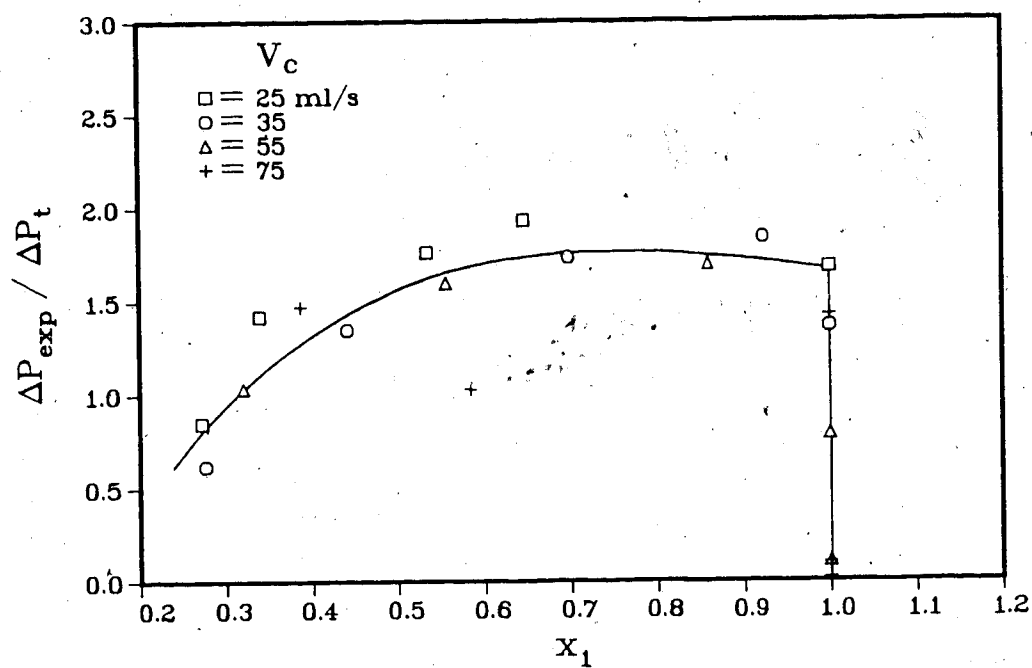


Fig. 4.37 Ratio of measured evaporator pressure drop to homogeneous model prediction vs. x_1 for 65% charge level

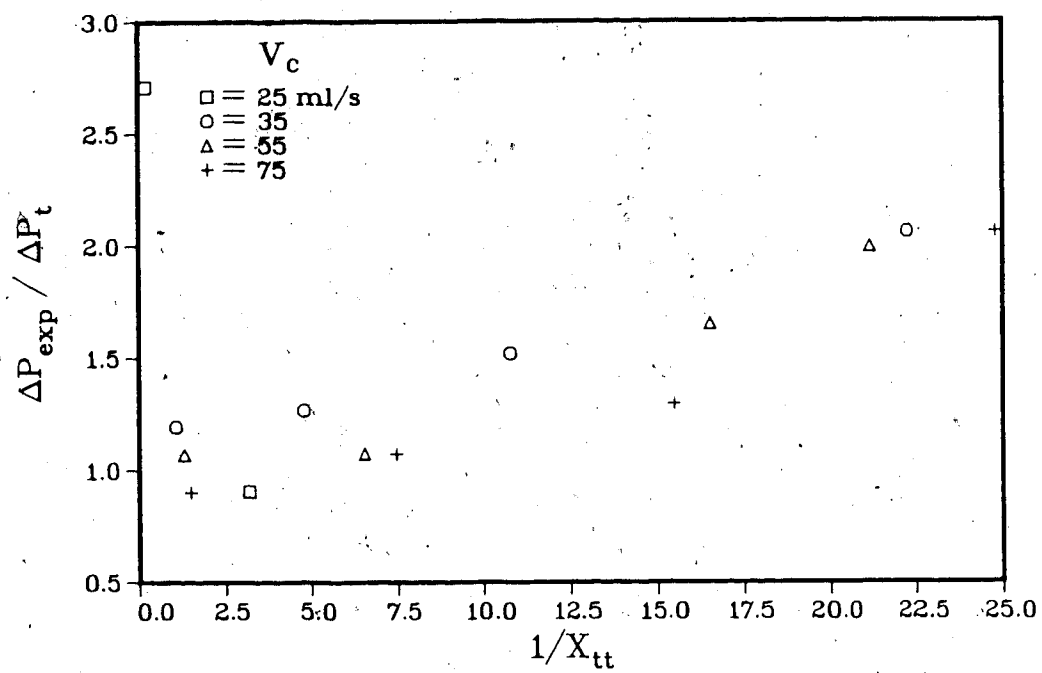


Fig. 4.38 Ratio of measured evaporator pressure drop to homogeneous model prediction vs. inverse Martinelli parameter for 100% charge level

4.5.6 Flow Visualization

The clear condenser shell and sight glass located at the evaporator exit enabled photographs of the flow patterns to be taken at these points. In the photographs, the vapor component of the two-phase mixture appears light and the liquid component somewhat darker in tone. The figures containing the photos are collected at the end of this chapter.

A time series of the flow patterns at the evaporator tube exit for a 20% charge level test are shown in Fig. 4.39. The cooling water flow rate was set at 75 ml/s, and the heating water temperature at 85°C, so that the exit state would progress from saturated liquid to superheated vapor. The first seven shots were taken over a total period of about four minutes, with a progressively longer time interval between each photograph. The liquid level at time zero is shown in (a). With the commencement of circulation of the heating and cooling fluids, low velocity bubbly flow is observed within seconds (b). In (c), the individual bubbles begin to group together, so that alternating slugs of liquid and vapor occur. Well developed slug flow did not exist for this charge level, as the flow rapidly entered the annular regime (d), with vapor flowing in the center of the tube, and a thin annulus of liquid existing around the circumference of the sight glass.

The vapor quality is increasing in (e) and (f), with only a small amount of liquid remaining in the annular

region. Here the slip velocity between the vapor core and the liquid annulus is sufficient to cause waves to appear on the inner surface of the glass. In (g), the fluid enters the superheated vapor region. The streaks which can be seen are caused by small amounts of dye trapped in the heat exchanger during the evaporation process. As the liquid containing length of the tube recedes, the non-evaporating dye is entrained by the high velocity superheated vapor. The secondary flow superimposed by the spiral geometry of the tube causes the vapor to exit the evaporator in a swirling motion, as evidenced by the patterns of the dye. The final photograph (h) is shown for the near steady state operating condition, about 20 minutes after startup.

It was found that charge level, heat source temperature, and cooling water flow rate all affect the state of the working fluid in the evaporator. Fig. 4.40 shows the combined effects of charge level and temperature as (a) occurs for steady state operation with 100% charge and a 55°C source temperature, while (b) is for 65% charge level and 85°C heat source temperature. Both have a cooling water flow rate of 25 ml/s. The effect of cooling water flow rate on the evaporator flow regime can be seen in Fig. 4.41. A change in the coolant flow from 25 ml/s to 35 ml/s for the same operating parameters of 20% charge level and 85°C heat source temperature causes the exit flow to enter the superheated vapor region as the system pressure is lowered.

A geysering phenomenon occurred for a few combinations of operating parameters. This is characterized by alternating pulses of low quality and high quality flow, at about the same frequency (manually counted) as the observed fluctuations in the system pressures and flow rates. Two instances were noticed, both for the case of 55°C heat source temperature, and 75 ml/s cooling water flow rate. Fig. 4.42(a) is for the 65% charge level condition and Fig 4.42(b) is for 100%.

The left photograph for each situation is a high quality pulse with more vapor content than on the right. The blurring of the photos on the right in both sets indicates that the flow velocity has increased, as the camera speed is the same as that for its left counterpart. The shutter speeds were 1/1000 s and 1/500 s for (a) and (b), respectively.

Photographs of the flow in the condenser shell reveal some important characteristics of the system. It was found that the condenser became flooded with liquid Freon, even for a low initial liquid charge level. With the charge level and heat source temperature fixed at 20% and 85°C, the progression of the liquid level in the condenser is seen in Fig 4.43(a-d) for cooling water flow rates of 25, 35, 55, and 75 ml/s, respectively. The liquid level in each photograph is indicated by an arrow for clarity. Steady state conditions have been achieved in each case.

At first, no flooding is observed, as the vapor generation in the evaporator is low. As the cooling water flow rate is increased, the vapor quality at the evaporator exit rises, thus displacing the liquid volume of the system into the condenser. Not much difference is observed for an increase in cooling water flow rate from 55 to 75 ml/s, as superheating does not have as great of an effect on the volume change of the vapor. Fig. 4.44(a-c) shows the same effect for the highest charge level of 100%. The initial no heating or cooling condition (a), is followed by steady state photographs for cooling water flow rates of 25 and 55 ml/s. The heating water temperature is 85°C. At this point the axial vapor dispersal tube of the condenser is completely submerged in liquid, and the heat transfer process takes on an added complexity.

With an initial liquid charge level of 65%, the condenser is flooded to the mid-plane for a heating fluid temperature of 85°C and cooling water flow rate of 75 ml/s, and the dispersal tube is partially immersed. The injection of the vapor into the liquid causes considerable splashing as seen in Fig. 4.45(a). At the other end of the condenser, an interesting phenomenon occurs at the dispersal tube inlet section. The hot vapor flowing inside the tube raises the external surface temperature to a point where bubble nucleation occurs as seen in Fig. 4.45(b), shot from below the liquid surface.

When the condenser is completely flooded, no fin surface is available for direct condensation. Rather, the process occurs as in Fig 4.46(a) for the condition of 100% charge, heat source temperature of 85°C , and cooling water flow rate equal to 35 ml/s. In 4.46(b) the cooling water flow rate is increased to 55 ml/s, and the photograph enlarged. Due to the buoyancy of the vapor phase in the liquid, immediate upflow is observed, and the vapor is almost entirely condensed before the upper finned surface is reached. The heat transfer process then relies on natural convection and conduction in the liquid to transport the heat energy to the finned cooling tube. This is no doubt less efficient than direct condensation on the metal surface, and in addition large pressure drops may be incurred by the injection of the vapor jet into the liquid phase.

It was found in [17] that condenser flooding and liquid entrainment had detrimental effects on thermosyphon performance, and the behaviour observed here helps to explain low system efficiencies through poor fin side heat transfer coefficients. Arrangements similar to the present experimental apparatus are used for phase change solar collector systems, and improved condenser design might help to make such systems more efficient by eliminating flooding caused by vapor generation in the evaporator section.

4.6 Conclusion

The refrigerant charged closed loop two-phase thermosyphon system performed well and natural circulation flow was immediately self initiating upon the application of external heating and cooling. The flow regimes in the riser line ranged from a two-phase mixture to superheated vapor. Due to the properties of the R-113 working fluid, heat transfer was found to be primarily latent, with increasing input heat flux generating vapor without raising the mass flow rate.

Optimum thermodynamic efficiency was obtained for operation in the saturation region of the refrigerant. Generation of superheated vapor in the evaporator was found to greatly decrease efficiency, while the best values were found for a flow quality of 1.0 corresponding to saturated vapor production. Both an increase in cooling water flow rate and a lower charge level were found to assist vapor generation by lowering the system pressure, and thus the saturation temperature of the working fluid.

Primary loop flow and pressure fluctuations were found to have a basically constant frequency in the range of 0.35-0.375 cycles/sec. Evidence presented by other investigators indicates that the mechanism of the instabilities is the so called density wave oscillation. The variance of the system pressure signal was found to drastically increase for superheated vapor production, which could result in mechanical problems such as fatiguing of the

pipe joints.

The recent correlation equation developed by Kandlikar for the prediction of convective boiling heat transfer coefficient was found to agree with the present experimental data. Convective boiling pressure drop in the evaporator was found to decrease when superheating was encountered. This is probably due to the absence of turbulent mixing between phases which may occur for lower quality flow.

Flow visualization photographs in the condenser shell revealed that liquid flooding was prevalent over almost the entire range of operation. This either reduced the effective condensation area, or when flooding was complete, reduced the heat transfer to a convection situation. The lower efficiency of this heat transfer process as compared to direct condensation would have detrimental effects on system performance and is an area for improvement.

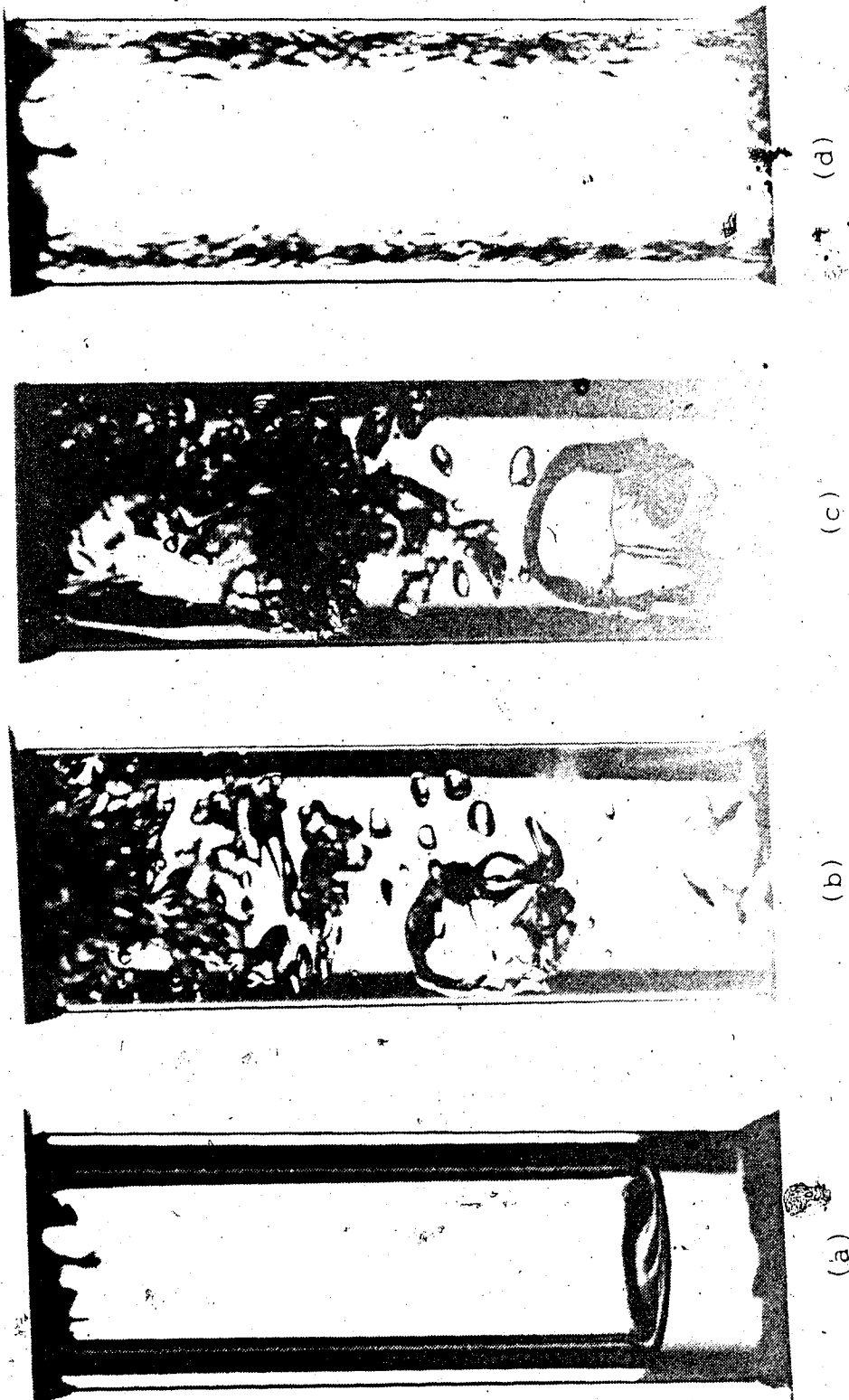
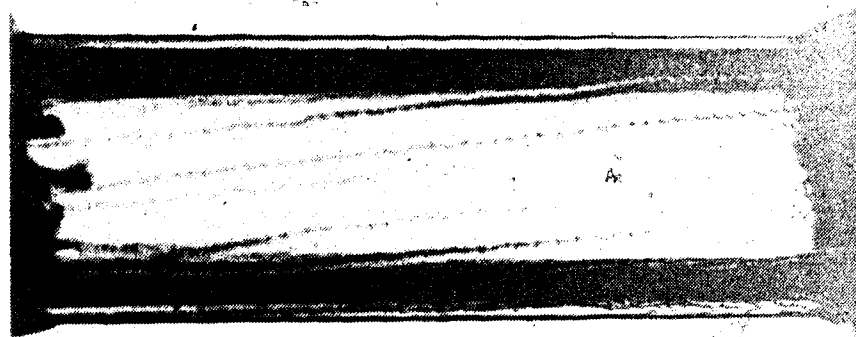
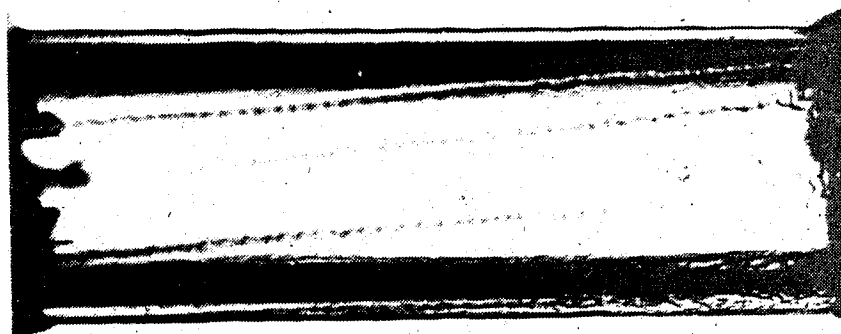


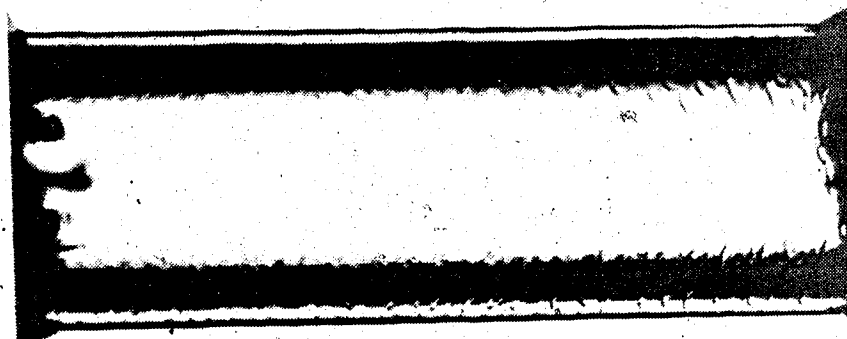
Fig. 4.39 Transient boiling flow at the evaporator exit for 20% charge level, 85°C heat source, and $V_c = 75$ ml/s



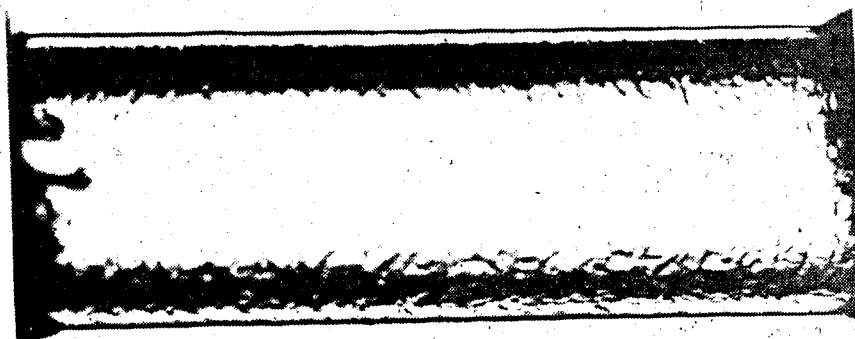
(h)



(g)

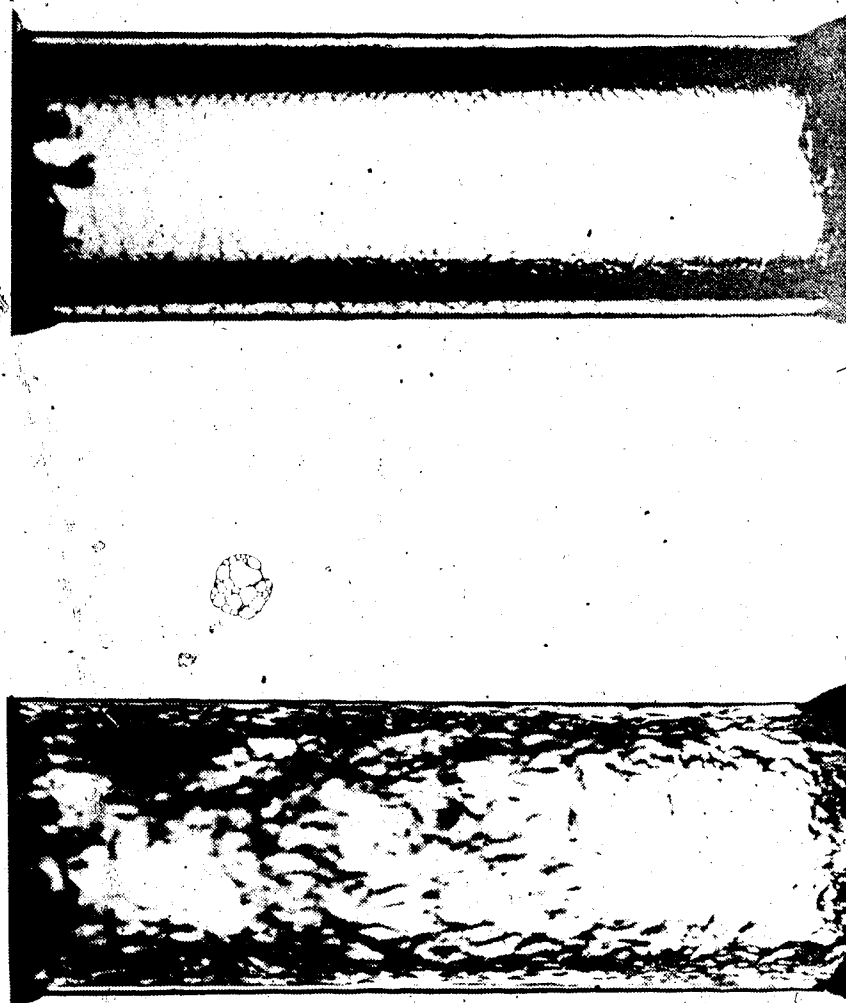


(f)

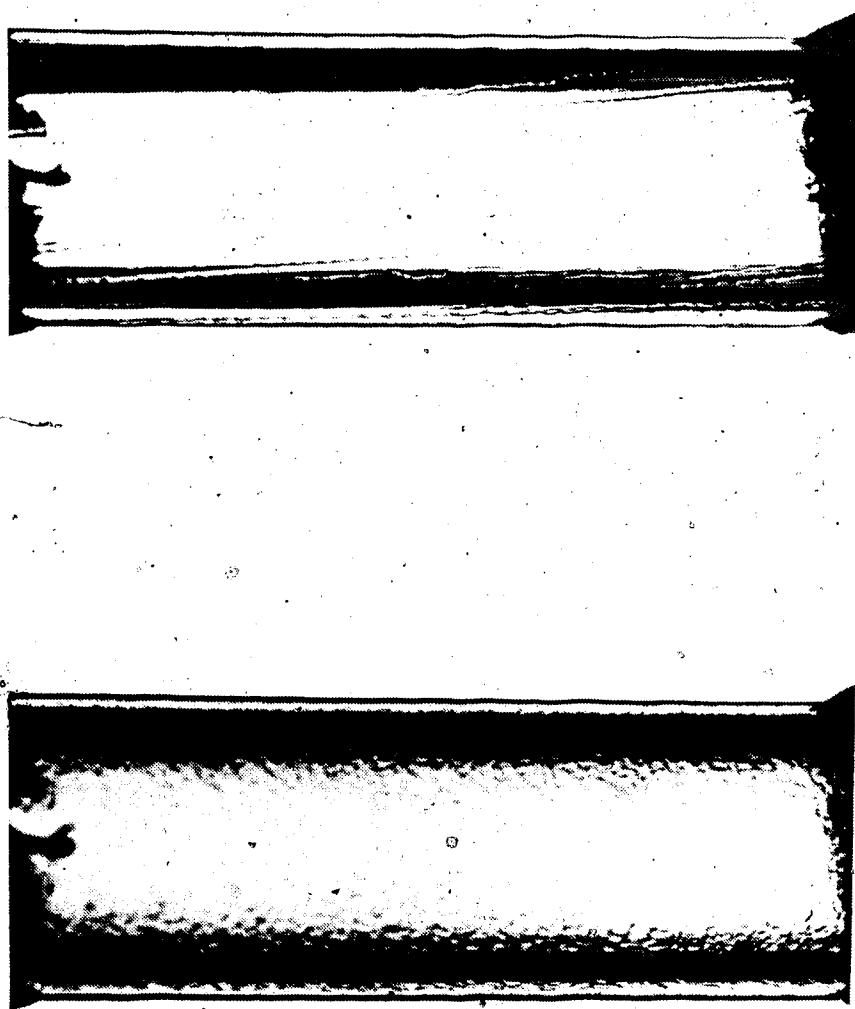


(e)

Fig 4.39 continued



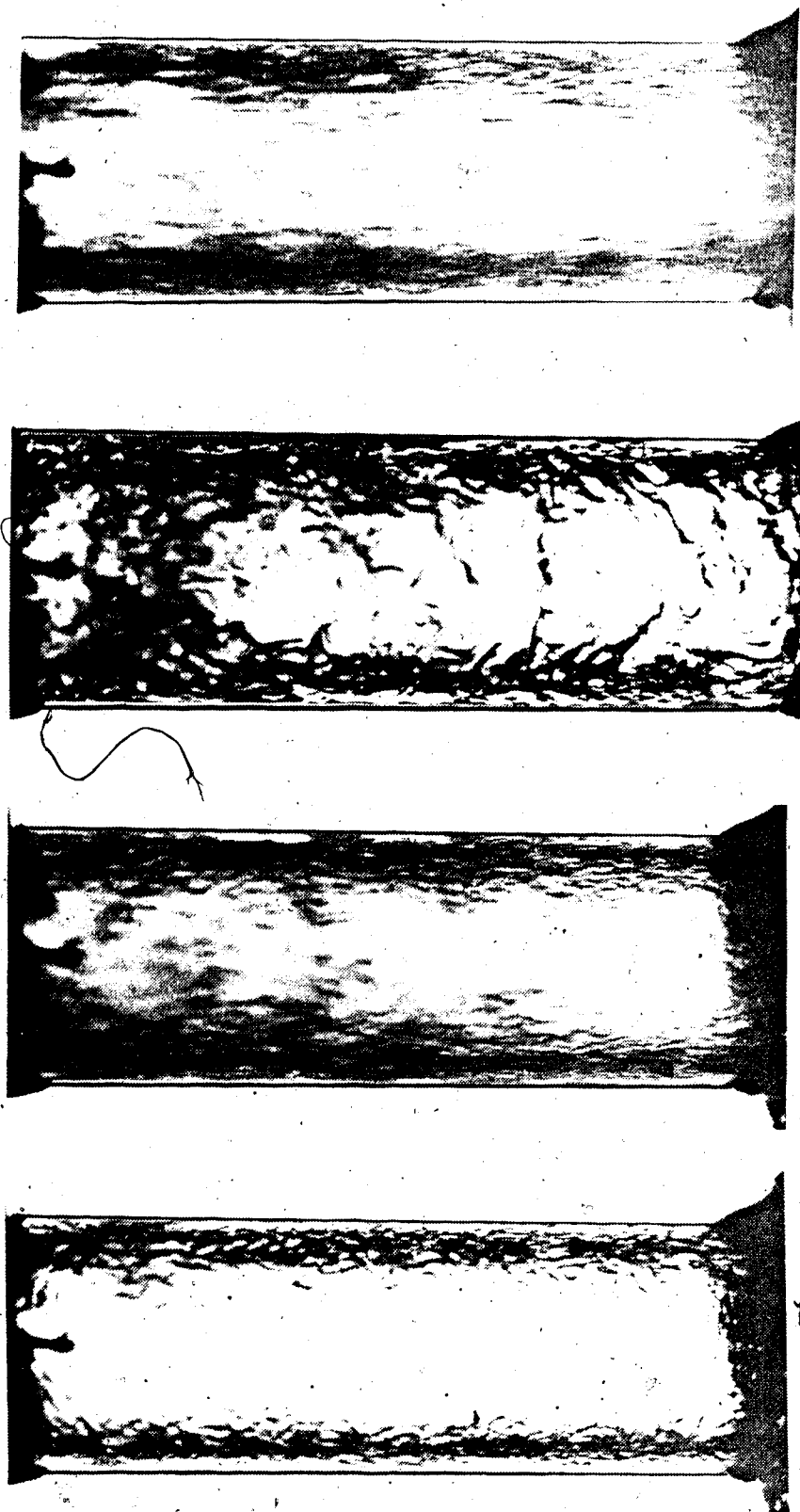
(a) 100% charge, $T_h = 55^\circ\text{C}$ (b) 65% charge, $T_h = 85^\circ\text{C}$
Fig. 4.40 Effect of charge level and temperature on evaporator
flow regimes with $V_c = 25 \text{ ml/s}$



(a) $V_c = 25 \text{ ml/s}$

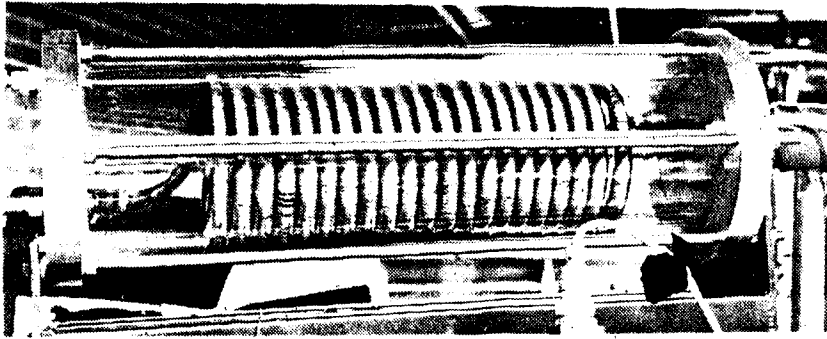
(b) $V_c = 35 \text{ ml/s}$

Fig. 4.41 Effect of cooling water flow rate on evaporator exit flow with 20% charge level and 85°C heat source

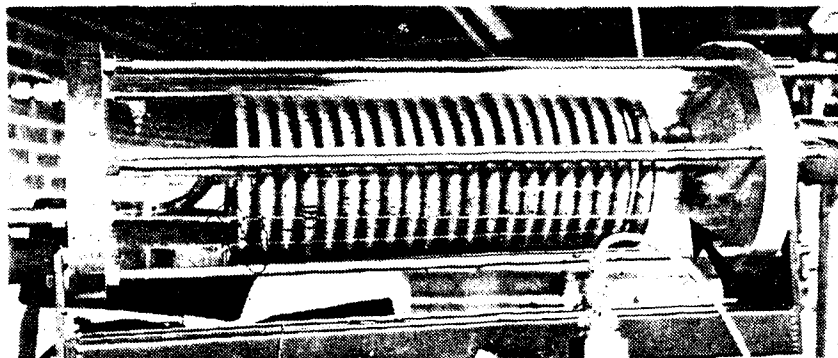


(a) 65% charge level (b) 100% charge level

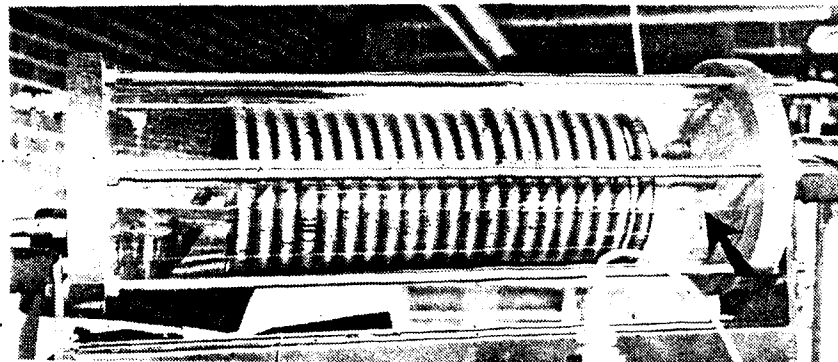
Fig. 4.42 Pulsing flow at evaporator exit with 55°C heat source and $V_c = 75$ ml/s



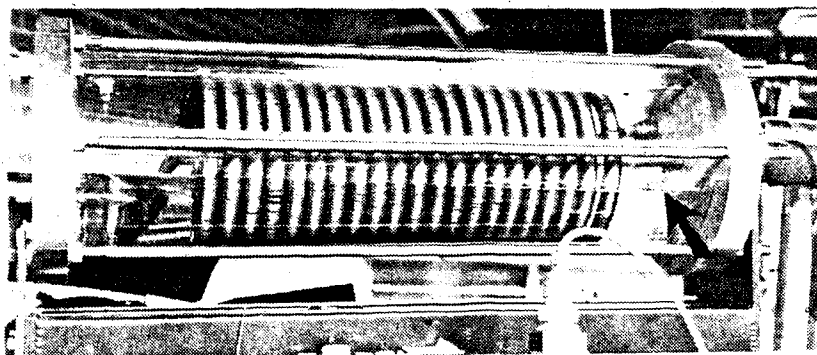
$V_c = 25 \text{ ml/s}$ (a)



$V_c = 35 \text{ ml/s}$ (b)

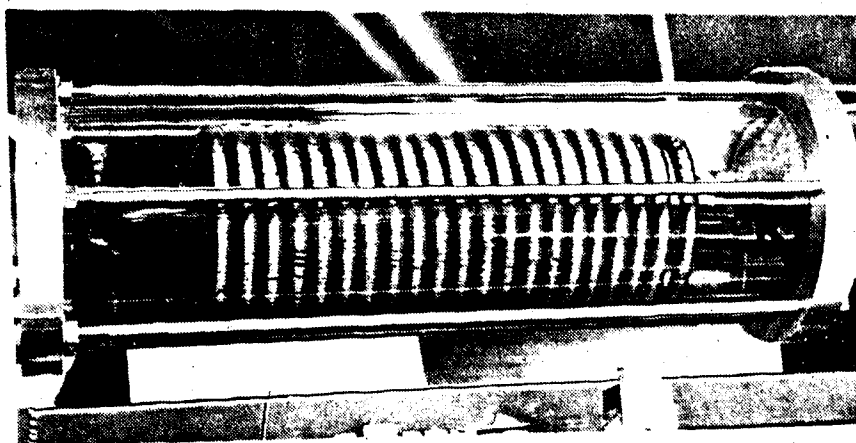


$V_c = 55 \text{ ml/s}$ (c)



$V_c = 75 \text{ ml/s}$ (d)

Fig. 4.43 Condenser flooding for 20% charge level and 85°C heat source



initial state (a)

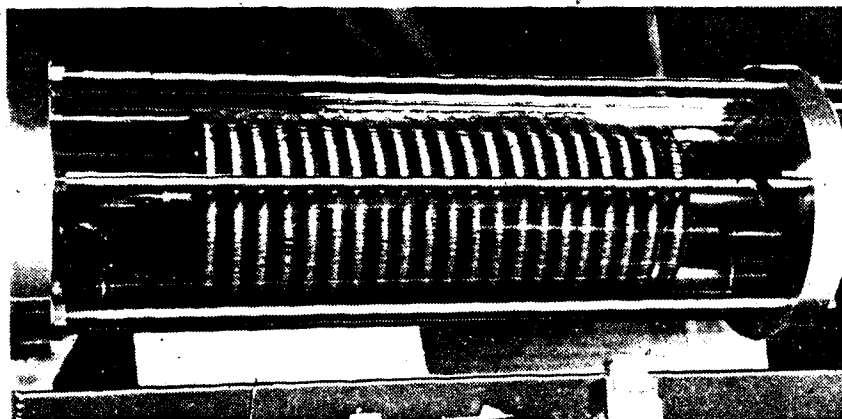
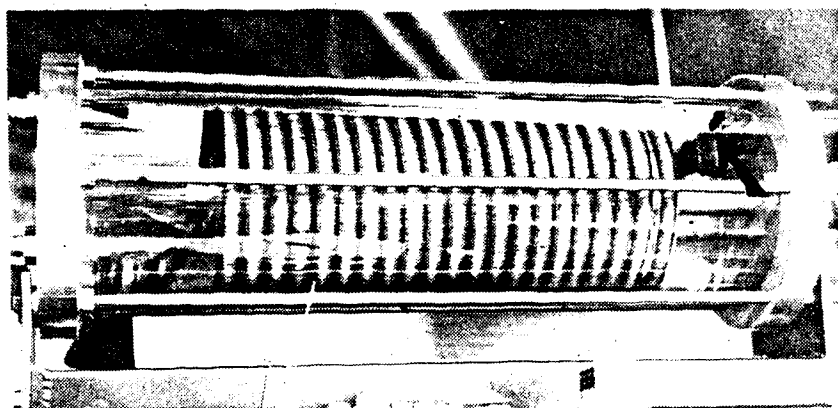
 $V_c = 25 \text{ ml/s}$ (b) $V_c = 55 \text{ ml/s}$ (c)

Fig. 4.44 Condenser flooding for 100% charge level and 85°C heat source



(a)



(b)

Fig. 4.45 Flooded condenser for 65% charge level, 85°C heat source, and $V_C = 75$ ml/s



$V_C = 35 \text{ ml/s}$ (a)



$V_C = 55 \text{ ml/s}$ (b)

Fig. 4.46 Vapor injection into fully flooded condenser for 100% charge and 85°C heat source

5. Concluding Remarks

Three different working fluids were used to study the operating and heat transfer characteristics of a closed loop two-phase thermosyphon under the influence of various external parameters. The effects of system temperature difference, cooling water flow rate, initial liquid charge level, and liquid-vapor separator were examined for a low grade energy recovery situation (heat source $<100^{\circ}\text{C}$).

The system was initially tested with liquid phase water as the working fluid to provide baseline data for future tests. External parameters which had a major effect on heat recovery were cooling water flow rate and system temperature difference. Increases in the uncontrolled variable of thermosyphon natural circulation rate were also found to improve the amount of heat transferred. The mass flow rate was found to increase with higher values of input heat flux which also corresponded to higher heat source temperature and cooling water flow rate.

The natural circulation in the primary loop set up a sympathetic link between the physically separated heat exchangers of the system. Forced flow eliminated this, and tests revealed that more heat could be transported with a pump in the system, but without an appreciable increase in thermodynamic efficiency. The single phase Nusselt number for the inner tube of the lower heat exchanger was found to be well correlated with an inverse Graetz parameter using a simple power relation.

The two-phase water system exhibited much higher mass flow rates than the single phase case, and heat recovery was improved. Parameters which contributed favourably to heat transport were high charge level, high heat source temperature, large cooling water flow rate, and the inclusion of a liquid-vapor separator in the riser line. Mass flow rates were found to increase with heat flux and vapor quality. The heat transfer processes in the evaporator and condenser were considered to be primarily single phase, enhanced by two-phase mixing with some additional latent heat transfer. The correlation of the evaporator tube Nusselt number with the inverse Graetz parameter for the low quality flow showed favourable results, indicating that future study is warranted. The condenser exhibited heat transfer coefficients far below those predicted by Nusselt theory.

The two-phase refrigerant R-113 system had a major advantage over the water charged arrangements in that self initiated natural circulation was rapid and occurred for all tests. The mechanism of heat transfer was primarily latent, as opposed to the sensible heating and cooling of the water filled loops. The total mass flow rate was found to decrease to a steady value and did not increase for higher heat flux.

Optimum efficiency was obtained when superheating of the flow at the evaporator exit was avoided, while at the same time maintaining high quality flow. Large cooling water flow rates and lower charge levels contributed to increased

vapor generation through a decrease in system pressure. The primary loop flow and pressure fluctuations were basically constant at 0.35-0.375 cycles/sec, and are believed to be the result of density wave type oscillations. Superheated vapor production resulted in a large variance of the system pressure signal which at times was physically evidenced by noise and shaking of the primary loop tubes. The convective boiling frictional component of pressure was found to decrease as superheated vapor was produced in the evaporator.

Flow visualization photographs of the shell side condensation revealed that liquid flooding was occurring, and was probably responsible for the low fin side heat transfer coefficients obtained. This could be avoided through better design of both the primary loop geometry and the condenser itself.

All three thermosyphon situations transported heat between the heating and cooling loops, with the Freon system having the best performance within the common range of operating parameters. Additional advantages of refrigerants are that they do not cause corrosion or scaling, and the type of refrigerant may be chosen to suit the desired heat source temperature range. They are however quite expensive, and the good performance of the two-phase water system suggests it to be an alternative for higher temperature operation. The single phase system performed reasonably well, but was not self starting for this particular

geometrical arrangement.

The two-phase closed loop thermosyphon is clearly suited to low grade heat recovery and transport as it is maintenance free, requires no pumps or power supplies, and will transfer heat between two independent and separated streams with a relatively low temperature difference. A current application of such a device may be found in phase change solar collector systems. It would also be suitable for gas to gas heat transfer, geothermal energy recovery, or heat recovery from contaminated waste gases or liquids.

The system tested could be improved, and one possibility would be the elimination of condenser flooding. Another unavoidable shortcoming was the flow restriction in the primary loop due to instrumentation. A similar system without large pressure drops to inhibit the thermosyphon flow would be expected to perform better. Better choice of heat exchangers for such a system would no doubt improve performance, as might the use of different working fluids. The interesting phenomena of flow and pressure oscillations in the primary loop deserve future study to further assess their physical mechanisms.

References

1. Yavuzoglu, T.N., ed., Alternative Energy Sources, Proceedings of the First-Fourth Miami International Conferences on Alternative Energy Sources, 1977-1981.
2. Wassel, A.T., Elghobashi, S.E., and Farr, J.L., "Mathematical Simulation of Ocean Thermal Energy Conversion Seawater Systems", J. Solar Engineering, Vol. 106, May 1984, pp. 198-205.
3. Mochida, Y., Kawano, S., Takahata, T., and Miyoshi, M., "Performance of the Heat Exchangers of a 100-kW (Gross) OTEC Plant", J. Solar Engineering, Vol. 106, May 1984, pp. 187-192.
4. Vandenberghe, D.G., and Vigrass, L.W., "Low-Grade Geothermal Energy: Feasibility and Demonstration at Regina, Canada", Alternative Energy Sources II, Vol. 5, 1981, pp. 2047-2070.
5. Bayley, F.J., and Lock, G.S.H., "Heat Transfer Characteristics of the Closed Thermosyphon", J. Heat Transfer 87, 1965, pp. 30-40.
6. Peace-Athabasca Delta Project Report, Intergovernmental Study Group, Dept. of the Environment, Queens Printer, Edmonton, 1972.
7. Lee, Y., and Mital, U., "A Two-Phase Closed Thermosyphon", Int. J. Heat Mass Transfer, Vol. 15, 1972, pp. 1695-1707.
8. Lee, Y., "Preservation of Permafrost by Means of Two-Phase Closed Thermosyphon", Annual Reports, DRB, 9511-96, University of Ottawa, 1969.
9. Bottum, E.W., "Refrigerant Charged Phase Change Solar Water and Space Heating Systems", ASHRAE Trans., Vol. 87(2), 1981, pp. 397-404.
10. Schreyer, J.M., "Residential Application of Refrigerant Charged Solar Collectors", Solar Energy, Vol. 26, 1981, pp. 307-312.
11. Manasse, F.K., and O'Leary, J.A., "Heliophase Solar Hot Water Heating System", Proc. of the 1978 Annual Meeting, AS/ISES, Denver, Colorado, Vol. 2.2, 1978, pp. 36-40.
12. Al-Tamimi, A.I., Performance of a Flat-Plate Solar Collector in a Closed-Loop Thermosiphon Using

- Refrigerant-11, Ph.D. Thesis, University of Michigan, 1972.
13. Lee, C.A., An Experimental Study of Refrigerant Charged Two-Phase Solar Collector Systems, M.Sc. Thesis, University of Alberta, 1983.
 14. Kissner, F., "A Passive, Refrigerant-Driven, Solar Domestic Water Heating System -- The Ultimate in Efficiency and Freeze Protection for Cold Climate", Proc. of the National Conference on Solar Energy, SESCO, Montreal, Canada, 1981, pp. 201-205.
 15. Cheng, K.C., Application of Boiling and Condensation Heat Transfer to Flat Plate Solar Collectors in Cold Region, Final Report, Alberta/Canada Energy Resources Research Fund, Contract U-79-9, 1982.
 16. Cheng, K.C., Morioka, I., Ichimiya, K., and Sadler, G. W., "Experimental Study of a Two-Phase Thermosyphon System", Alternative Energy Sources IV, Vol. 1, 1982, pp. 151-170.
 17. McDonald, T.W., Hwang, K.S., and DiCiccio, R., "Thermosyphon Loop Performance Characteristics: Part 1. Experimental Study", ASHRAE Trans. 83(2), 1977, pp. 250-258.
 18. De Paz, J.F., On the Stability of a Free Convection Loop, Ph.D. Thesis, Purdue University, 1972.
 19. El-Masri, M.A., and Bara, R.J., "Natural Circulation in a Long Vertical Loop", J. Thermal Engineering, Vol. 3, No. 2, 1983, pp. 32-44.
 20. Fujii, T., Kato, Y., and Mihara, K., "Expressions of Transport and Thermodynamic Properties of Air, Steam, and Water", Report No. 66, Institute of Industrial Science, Kyushu University, Japan, 1972.
 21. Wylen, G.J., and Sonntag, R.E., Fundamentals of Classical Thermodynamics, John Wiley and Sons, 2nd ed., 1976, pp. 99-100.
 22. Holman, J.P., Heat Transfer, McGraw-Hill, 1981, pp. 447-449.
 23. Ozisik, M.N., Basic Heat Transfer, McGraw-Hill, 1977, pp. 447-451.
 24. General Electric Corporate Research and Development: Heat Transfer and Fluid Flow Data Books, "Forced Convection", Dec. 1980, p. 21.

25. Holman, J.P., Heat Transfer, McGraw-Hill, 1981, pp. 454-456.
26. Moran, M.J., Availability Analysis: A Guide to Efficient Energy Use, Prentice-Hall, 1982, pp. 44-76 and 86.
27. McAdams, W.H., Heat Transmission, McGraw-Hill, 3rd ed., 1954, pp. 230-233.
28. Metais, B., and Eckert, E.R.G., "Forced, Mixed, and Free Convection Regimes", J. Heat Transfer, Ser. C, Vol. 86, 1964, p. 295.
29. Cheng, K.C., and Yuen, F.P., "Flow Visualization Studies on Secondary Flow Patterns in Curved Tubes and Isothermally Heated Horizontal Tubes", ASME paper 84-HT-62, 22nd ASME/AIChE National Heat Transfer Conference, Niagara Falls, New York, 1984.
30. Rohsenow, W.M., and Hartnett, J.P., Handbook of Heat Transfer, McGraw-Hill, 1973, 7-149.
31. Shah, M., "A New Correlation for Heat Transfer During Boiling Flow Through Pipes", ASHRAE Trans., Vol. 82, Part II, 1976, pp. 66-86.
32. Shrock, V.E., and Grossman, L.M., "Forced Convective Boiling in Tubes", Nuclear Science and Engineering, Vol. 12, 1962, pp. 474-481.
33. Beatty, K., and Katz, D., "Condensation of Vapors on Outside of Finned Tubes", Chemical Engineering Progress, Vol. 44, 1948, pp. 55-69.
34. Dupont of Canada, "Freon Refrigerants", Physical Properties Pamphlet, R11-371, FR-82.
35. Mastroianni, M.J., Stahl, R.F., and Sheldon, P.N., "Physical and Thermodynamic Properties of 1,1,2-Trifluorotrchloroethane (R-113)", J. Chemical and Engineering Data, Vol. 23, No. 2, 1978, pp. 113-118.
36. ASHRAE Handbook 1981 Fundamentals, pp. 17.90-17.91.
37. Fujii, T., Nozu, S., and Honda, H., "Expressions of Thermodynamic and Transport Properties of Refrigerants R-11, R-12, R-22, and R-113", Institute of Industrial Science, Kyushu University, Japan, 1977.
38. Miller, I., and Freund, J.E., Probability and Statistics for Engineers, 2nd ed., Prentice-Hall, 1977, p. 151.
39. Chen, J.C., "Correlation for Boiling Heat Transfer to Saturated Fluids in Convective Flow", Industrial and

Engineering Chemistry, Process Design and Development,
Vol. 5, No. 3, 1966, pp. 322-329.

40. Kandlikar, S.G., "An Improved Correlation for Predicting Two-Phase Flow Boiling Heat Transfer Coefficient in Horizontal and Vertical Tubes", Paper presented at the 21st National Heat Transfer Conference, Seattle, Wash., July 24-28, 1984.
41. Veziroglu, T.N., and Lee, S.S., "Instabilities in Boiling Upward Flows", Int. Symposium on Research on Co-Current Gas-Liquid Flow, 1968, pp. 303-345.
42. Kakac, S., and Veziroglu, T.N., "A Review of Two-Phase Flow Instabilities", Advances in Two-Phase Flow and Heat Transfer, Vol. II, Martinus Nijhoff Publishers, 1983, pp. 577-667.
43. Stenning, A.H., "Instabilities in the Flow of a Boiling Liquid", J. Basic Engineering, Trans. ASME, Series D, Vol. 86, 1964, pp. 213-217.
44. Veziroglu, T.N., and Lee, S.S., "Boiling Flow Instabilities in Parallel Channels", Proc Instn Mech Engrs, Vol. 184, Pt 3C, 1969-70, pp. 727.
45. Collier, J.G., Convective Boiling and Condensation, McGraw-Hill, 2nd ed., 1981, pp. 26-69

Appendix I

Sample Data Acquisition Program

THE FOLLOWING IS A DATA ACQUISITION PROGRAM
WRITTEN IN BASIC FOR AN HP-85 MICROCOMPUTER
AND HP-3497A DATA ACQUISITION CONTROL UNIT

THIS IS SPECIFIC TO THE PARTICULAR
EXPERIMENTAL SETUP AND TESTS DONE

```

10 DATA ACQUISITION PROGRAM FOR FREON R113 TESTS
20
30 DIM M(21),B(21),T(21),X(31),Z(5),C2$(100),D$(15),Z1(5)
40 DIM V1(100),V2(100),V3(100)
50 PRINTER IS 704,96
60 DEF FND9(T) = ((1+.0000087*T1.85)*.001)-1
70 DEF FNC9(T) = 4179+.000079*(T-10)2.9
80 CLEAR
90 DISP "ENTER THE DATE AND TIME OF DAY EX: AUG 3/83,H,M,S"
100 INPUT D$,H,M,S
110 SETTIME H*3600+M*60+S,0
120 PRINT USING 130 ; D$,H,M,S
130 IMAGE /5X,"THE DATE IS ",15A,"TIME IS ",2D," HOURS,
",2D," MIN, AND ",2D," SEC"
140 FOR I=1 TO 31
150 X(I)=0
160 NEXT I
170 DISP "ENTER THE LAST STORAGE IDENTIFICATION NUMBER"
180 INPUT K
190
200 ***** LINEAR CALIBRATION DATA *****
210 DATA 19049.734,19563.643,19242.378,19467.731,
19161.668,20040.256,19094.625
220 DATA 19551.966,18931.699
230 DATA .683,.343,3.261,1.374,6.928,14.881,
6.4738,11.9882,11.197
240 DATA 3.475,6.957,19552.46
250 DATA 27.995,27.484,27.696,27.528,27.726,27.534,
27.957,27.442,28.007
260 DATA .094,.005,-.059,.019,-.054,1.044,-.2364,.9795,338
270 DATA -.255,-.207,29.179
280 ***** READ THE CALIBRATION DATA *****
290
300 FOR I=1 TO 21
310 READ M(I)
320 NEXT I
330 FOR I=1 TO 21
340 READ B(I)
350 NEXT I
360 CLEAR
370 DISP "PRESSURE TRANSDUCERS MUST BE ZEROED WITH NO FLOW
RATE, INPUT ANY LETTER TO COMMENCE"
380 INPUT N$
390 IF N$="Y" THEN 400
400 FOR I=1 TO 5
410 Z(I)=0
420 NEXT I

```

```

430
440 **** OBTAINING ZERO FLOW RATE READINGS FROM PT'S ****
450 CLEAR 709
460 FOR J=1 TO 50
470 FOR I=1 TO 5
480 OUTPUT 709 ; "AC"&VAL$(I+88); "VT3"
490 ENTER 709 ; A
500 Z(I)=Z(I)+A
510 NEXT I
520 NEXT J
530 FOR I=1 TO 5
540 Z(I)=Z(I)/50
550 Z1(I)=Z(I)*M(I+9)+B(I+9)
560 NEXT I
570 PRINT USING 580
580 IMAGE /5X, "INITIAL VOLTAGES AND PRESSURES"
590 FOR I=1 TO 5
600 PRINT USING 620 ; I, Z(I), Z1(I)
610 NEXT I
620 IMAGE 5X, 2D, 3X, 2D.3D, 3X, 4D.3D
630 PRINT USING 640
640 IMAGE 2/
650 ON ERROR GOTO 2480
655 ***** PF KEY LABELLING *****
660 ON KEY# 1, "MAN" GOTO 770
670 ON KEY# 2, "FLOW" GOTO 2410
680 ON KEY# 8, "STORE" GOTO 2560
690 ON KEY# 5, "RERUN" GOTO 890
700 ON KEY# 4, "PRESS" GOTO 2240
710 ON KEY# 3, "CHK" GOTO 2330
720 ON KEY# 7, "STAT" GOTO 2680
730 CLEAR
740 KEY LABEL
750 BEEP 50, 1000
760 GOTO 760
770 CLEAR
780 DISP "ENTER THE BAROMETRIC PRESSURE IN kPA"
790 INPUT X(22)
800 DISP "ENTER THE NUMBER OF READINGS PER CHANNEL"
810 INPUT N5
820 DISP "ENTER THE REFERENCE PRESSURE IN in. Hg"
830 INPUT P3
840 DISP "ENTER THE APPROXIMATE SYSTEM PRESSURE IN in. Hg"
850 INPUT P4
860 DISP "ENTER THE CHARGE LEVEL IN %"
870 INPUT C4
880 K=K+1
890 PRINT USING 900 ; K
900 IMAGE //5X, "***** RUN NUMBER ", 3D, " *****"
910 PRINT USING 920 ; N5
920 IMAGE /5X, 3D, " READINGS PER CHANNEL"
930 GOSUB 960
940 GOTO 1360
950

```



```

960 ***** D/A WITH N5 READINGS FOR EACH CHANNEL *****
970 CLEAR DISP "ENTER THE HEATING FLUID ROTAMETER READING"
980 INPUT H4
990 FOR I=1 TO 21
1000 T(I)=0
1010 NEXT I
1020 CLEAR 709
1030 FOR J=1 TO N5
1040 FOR I=1 TO 17
1050 OUTPUT 709 ; "AC"&VAL$(I+79); "VT3"
1060 ENTER 709 ; A
1070 T(I)=T(I)+A
1080 NEXT I
1090 OUTPUT 709 ; "AC71VT3"
1100 ENTER 709 ; A
1110 T(18)=T(18)+A
1120 OUTPUT 709 ; "AC67VT3"
1130 ENTER 709 ; A
1140 T(19)=T(19)+A
1150 OUTPUT 709 ; "AC66VT3"
1160 ENTER 709 ; A
1170 T(20)=T(20)+A
1180 OUTPUT 709 ; "AC09VT3"
1190 ENTER 709 ; A
1200 T(21)=T(21)+A
1210 NEXT J
1220 T1=TIME
1230
1240 ***** AVERAGE AND CONVERT TO CALIBRATED UNITS *****
1250 FOR I=1 TO 21
1260 T(I)=T(I)/N5
1270 T(15)=H4
1280 X(I)=T(I)*M(I)+B(I)
1290 NEXT I
1300
1310 ***** ADJUST PT READINGS TO ZERO REFERENCE *****
1320 FOR I=10 TO 14
1330 X(I)=X(I)-Z1(I-9)
1340 NEXT I
1350 RETURN
1360 Q1=X(15)*.000001*FND9(X(1))*(FNC9(X(1))/2+FNC9(X(5))/2)
  *(X(1)-X(5)) HF HEAT TRANS
1370 Q2=X(18)*.000001*FND9(X(2))*(FNC9(X(2))/2+FNC9(X(6))/2)
  *(X(2)-X(6)) CF HEAT TRANS
1380 H=IP(T1/3600)
1390 M=IP(FP(T1/3600)*60)
1400 S=T1-(H*3600+M*60)
1410 PRINT USING 1420 ; D$
1420 IMAGE /5X,"THE DATE IS ",10A
1430 PRINT USING 1440 ; X(22)
1440 IMAGE 5X,"BAROMETRIC PRESSURE = ",3D.3D," KILOPASCALS"
1450 PRINT USING 1460 ; P3
1460 IMAGE 5X,"REFERENCE PRESSURE IS ",2D.D," in. Hg VAC"
1470 PRINT USING 1480 ; P4

```

```

1480 IMAGE 5X,"INITIAL EVAPORATOR GAUGE PRESSURE ",2D.D,"
in. Hg VAC"
1490 PRINT USING 1500 ; C4
1500 IMAGE 5X,"CHARGE LEVEL ",3D," %"
1510 PRINT USING 1520 ; X(21)
1520 IMAGE 5X,"ROOM TEMP ",2D.D," DEG. C"
1530 PRINT USING 1540 ; T1,H,M,S
1540 IMAGE 5X,"TIME IS NOW ",5D," SECONDS OR ",2D," HOURS,
",2D," MINUTES,AND ",2D," SECONDS" .
1550 GOSUB 1570
1560 GOTO 2010
1570 PRINT USING 1580
1580 IMAGE //5X"----- SYSTEM FLOW RATES CC/S -----"
1590 PRINT USING 1600 ; X(15)
1600 IMAGE /5X,"HEATING FLUID: ",3D.D
1610 PRINT USING 1620 ; X(17)
1620 IMAGE 5X,"WORKING FLUID THROUGH CONDENSER",3D.D
1630 PRINT USING 1640 ; X(16)
1640 IMAGE 5X,"WORKING FLUID THROUGH DOWNCOMER",3D.D
1650 PRINT USING 1660 ; X(18)
1660 IMAGE 5X,"CONDENSER COOLING FLUID: ",3D.D
1670 PRINT USING 1680
1680 IMAGE /5X,"----- SYSTEM PROPERTIES -----"
1690 PRINT USING 1700
1700 IMAGE /5X"EVAPORATOR HEATING FLUID"
1710 PRINT USING 1720 ; X(1),X(5),X(14)
1720 IMAGE " TEMP IN= ",2D.D," TEMP OUT= ",2D.D," DEG
C",4X," PRESSURE DROP= ",2D.2D," kPa"
1730 PRINT USING 1740
1740 IMAGE /,5X,"EVAPORATOR WORKING FLUID"
1750 PRINT USING 1760 ; X(4),X(7),X(11)
1760 IMAGE " TEMP IN=",2D.D," TEMP OUT= ",2D.D," DEG C",5X,"
PRESSURE DROP= ",2D.2D," kPa"
1770 PRINT USING 1780 ; X(19)
1780 IMAGE " EXIT GAUGE PRESS",4D.3D," kPa"
1790 PRINT USING 1800
1800 IMAGE /,5X,"CONDENSER COOLING FLUID"
1810 PRINT USING 1820 ; X(6),X(2),X(13)
1820 PRINT USING 1830
1830 IMAGE /,5X,"CONDENSER WORKING FLUID"
1840 PRINT USING 1860 ; X(3),X(8),X(10)
1850 PRINT USING 1860 ; X(20)
1860 IMAGE " INLET GAUGE PRESS ",4D.3D," kPa"
1870 PRINT USING 1880 ; X(9)
1880 IMAGE /,5X,"DOWNCOMER TEMP= ",2D.D," DEG C"
1890 PRINT USING 1900 ; X(12)
1900 IMAGE /,5X,"SYSTEM PRESSURE FLUCTUATION= ",2D.2D," kPa"
1910 QUALITY BASED ON MASS FLOW RATE
1920 IF X(16)<.5 THEN 1970
1930
Q3=X(17)*FND9(X(8))/(X(17)*FND9(X(8))+X(16)*FND9(X(9)))*100
1940 PRINT USING 1950 ; Q3
1950 IMAGE /5X,"QUALITY BASED ON FLOW RATE ",2D.D," %",/
1960 GOTO 1990

```

```

1970 PRINT USING 1980
1980 IMAGE /5X,"DOWNCOMER FLOW?"
1990 RETURN
2000
2010 PRINT USING 2020 ; Q1/1000
2020 IMAGE 5X,"RATE OF HEAT TRANSFER FROM HEATING
FLUID=",2D.2D," KILOWATTS"
2030 PRINT USING 2040 ; Q2/1000
2040 IMAGE 5X,"RATE OF HEAT EXTRACTION BY COOLING
FLUID=",2D.2D
2050 PRINT USING 2060
2060 IMAGE /5X,"----- SYSTEM ACQUISITION CHECK -----"
2070 PRINT USING 2080
2080 IMAGE /2X,"TC OUTPUT VOLTAGE",10X,"TEMP,DEG C"
2090 FOR I=1 TO 9
2100 PRINT USING 2120 ; T(I),X(I)
2110 NEXT I
2120 IMAGE 3X,2D.4D,22X,3D.D
2130 PRINT USING 2140
2140 IMAGE //2X,"PT OUTPUT VOLTAGE",10X,"PRESSURE DROP"
2150 FOR I=10 TO 14
2160 PRINT USING 2180 ; T(I),X(I)
2170 NEXT I
2180 IMAGE 3X,2D.3D,20X,3D.D,3X,"kPa"
2190 DISP "ENTER COMMENT"
2200 INPUT C2$
2210 GOTO 730
2220
2230 ***** ROUTINE TO CORRECT INITIAL PRESSURES *****
2240 DISP "TO BE USED FOR MANUAL INPUT OF INITIAL PRESSURES
OR RE-READING THE PRESSURES"
2250 DISP "FOR AUTOMATIC READING ENTER 'A', OTHERWISE
RETURN"
2260 INPUT N$
2270 IF N$="A" THEN 370
2280 DISP "ENTER THE INITIAL VOLTAGES AND PRESSURES ON TWO
SEPARATE LINES"
2290 INPUT Z(1),Z(2),Z(3),Z(4),Z(5)
2300 INPUT Z1(1),Z1(2),Z1(3),Z1(4),Z1(5)
2310 GOTO 570
2320
2330 ***** CHECK PROPERTIES *****
2340 N5=5
2350 GOSUB 960
2360 GOSUB 1570
2370 PRINT USING 2380
2380 IMAGE 10/
2390 GOTO 740
2400
2410 ***** CHECK FLOW RATES *****
2420 N5=1
2430 GOSUB 960
2440 DISP USING 2450 ; X(15),X(18),X(17),X(16)
2450 IMAGE /5X,"HF ",3D.D," CC/S",/5X,"CF ",3D.D,/5X,"WF

```

```

(COND) ",3D.D,/5X,"WF (DOWN) ",3D.D
2460 GOTO 740
2470
2480 ***** ERROR RECOVERY *****
2490 FOR I=1 TO 5
2500 BEEP
2510 WAIT 200
2520 NEXT I
2530 CLEAR DISP "ERROR TYPE";ERRN;" OCCURRED ON LINE";ERRL
2540 GOTO 740
2550
2560 ***** STORE DATA ONTO TAPE *****
2570 IF X(18)<10 THEN 2590
2580 GOTO 2620
2590 DISP USING 2600 ; X(18)
2600 IMAGE /,"WARNING CF FLOW=",2D.D," INPUT CORRECT VALUE"
2610 INPUT X(18)
2620 ASSIGN# 1 TO "DATA.F"
2630 PRINT# 1,K ; K,D$,H,C2$,X()
2640 ASSIGN# 1 TO *
2650 C2$=""
2660 GOTO 730
2670
2680 ***** STATISTICS *****
2690 CLEAR
2700 DISP "ENTER DOMINANT COND FREQ Hz, RMS OF TOTAL SIGNAL
V"
2710 INPUT X(23),A3
2720 DISP "ENTER DOMINANT DC FREQ ,RMS OF TOTAL SIGNAL"
2730 INPUT X(24),C3
2740 DISP "ENTER DOMINANT PRESS FREQ,RMS OF TOTAL SIGNAL"
2750 INPUT X(25),D3
2760 X(29)=A3*M(17)
2770 X(30)=C3*M(16)
2780 X(31)=D3*M(12)
2790 FOR I=1 TO 100
2800 V1(I)=0
2810 V2(I)=0
2820 V3(I)=0
2830 NEXT I
2840 CLEAR 709
2850 FOR I=1 TO 100
2860 OUTPUT 709 ;"AC96VT3"
2870 ENTER 709 ; V1(I)
2880 NEXT I
2890 FOR I=1 TO 100
2900 OUTPUT 709 ;"AC95VT3"
2910 ENTER 709 ; V2(I)
2920 NEXT I
2930 FOR I=1 TO 100
2940 OUTPUT 709 ;"AC91VT3"
2950 ENTER 709 ; V3(I)
2960 NEXT I
2970 A=0 C=0 D=0

```

```

2980 FOR I=1 TO 100
2990 A=A+V1(I)
3000 C=C+V2(I)
3010 D=D+V3(I)
3020 NEXT I
3030 A=A/100 C=C/100
3040 D=D/100
3050 A1=A*M(17)+B(17)
3060 C1=C*M(16)+B(16)
3070 D1=D*M(12)+B(12)
3080 PRINT USING 3090
3090 IMAGE //,17X,"COND",5X,"DC",5X,"PRESS"
3100 PRINT USING 3110 ; X(23),X(24),X(25)
3110 IMAGE /,5X,"DOM
FREQ",1X,2D.3D,3X,2D.3D,2X,2D.3D,3X,"Hz"
3120 PRINT USING 3130 ; X(29),X(30),X(31)
3130 IMAGE /5X,"TOTAL RMS",1X,2D.3D,2X,2D.3D,2X,4D.3D," USER
UNITS
3140 PRINT USING 3150 ; A1,C1,D1
3150 IMAGE /,5X,"MEAN VALUES ",2D.D,3X,2D.D,3X,4D.3D )
3160 A2=0 C2=0 D2=0
3170 FOR I=1 TO 100
3180 A2=A2+(V1(I)-A)2
3190 C2=C2+(V2(I)-C)2
3200 D2=D2+(V3(I)-D)2
3210 NEXT I
3220 A2=A2/99 C2=C2/99
3230 D2=D2/99
3240 X(26)=A2*M(17)
3250 X(27)=C2*M(16)
3260 X(28)=D2*M(12)
3270 PRINT USING 3280 ; X(26),X(27),X(28)
3280 IMAGE /5X,"VARIANCE",2X,2D.4D,2X,2D.4D,2X,2D.4D
3290 PRINT USING 3300
3300 IMAGE 2/
3310 PRINT USING 3340 ;
X(1),X(2),X(3),X(4),X(5),X(6),X(7),X(8),X(9),X(10)
3320 PRINT USING 3340 ;
X(11),X(12),X(13),X(14),X(15),X(16),X(17),X(18),X(19),X(20)
3330 PRINT USING 3340 ; X(21),X(22),X(23),X(24),X(25),X(26),
X(27),X(28),X(29),X(30),X(31)
3340 IMAGE 10(3D.3D)
3350 PRINT USING 3360
3360 IMAGE 5/
3370 GOTO 740
3380 END

```

Appendix II

Properties of Liquid Water

C PROPERTIES OF LIQUID WATER

C ARGUMENT OF EACH FUNCTION IS WATER
C TEMPERATURE IN DEGREES CENTIGRADE

C VALID RANGES MAY BE FOUND IN REF. [20]
C OR CHECKED FROM TABLES

C DENSITY, KG/(CU. M)
C FUNCTION WDENS(T)
C $WDENS = ((1 + 8.7E-6 * T^{1.85}) * 1.0E-3)^{-1}$
C RETURN
C END

C ABSOLUTE VISCOSITY, KG/(M S)
C FUNCTION WAVISC(T)
C $WAVISC = 2.4E-5 * 10.0^{(251.0 / (T + 135.0))}$
C RETURN
C END

C CONSTANT PRESSURE SPECIFIC HEAT, J/(KG K)
C FUNCTION WSPH(T)
C $WSPH = 4179.0 + 7.9E-5 * (T - 10.0)^{2.9}$
C RETURN
C END

C THERMAL CONDUCTIVITY, W/(M C)
C FUNCTION WCOND(T)
C $WCOND = 0.6881 - 4.0E-6 * (135.0 - T)^{2.1}$
C RETURN
C END

C COEFF. THERMAL EXPANSION, 1/K
C FUNCTION WBETA(T)
C $A1 = -0.06427E-3$
C $A2 = 8.5053E-6$
C $A3 = -6.79E-8$
C $B1 = A1 + 2.0 * A2 * T + 3.0 * A3 * T^2$
C $B2 = 1 + A1 * T + A2 * T^2 + A3 * T^3$
C $WBETA = B1 * B2$
C RETURN
C END

Appendix III

Properties of Refrigerant R-113

C PROPERTIES OF FREON R-113
C FUNCTION ARGUMENTS ARE TEMPERATURES
C IN DEGREES CENTIGRADE
C UNLESS OTHERWISE INDICATED
C VALID RANGES MAY BE FOUND IN REF. [37]
C OR CHECKED FROM TABLES

C ***** LIQUID PHASE PROPERTIES *****

C DENSITY, KG/(CU. M)
C FUNCTION FLDENS(T)
C $SV = (0.617 + 6.47E-04 * T ** 1.10) * 1.0E-03$
C $FLDENS = 1.0 / SV$
C RETURN
C END

C LATENT HEAT OF VAPORIZATION, J/KG
C FUNCTION FLATE(T)
C $FLATE = (1.611 - 3.10E-03 * T) * 1.0E+05$
C RETURN
C END

C CONSTANT PRESSURE SPECIFIC HEAT, J/(KG K)
C FUNCTION FLSPH(T)
C $FLSPH = (0.929 + 1.03E-03 * T) * 1.0E+03$
C RETURN
C END

C ABSOLUTE VISCOSITY, KG/(M S)
C FUNCTION FLVISC(T)
C $EX = 503. / (T + 271)$
C $FLVISC = 1.34E-05 * 10. ** EX$
C RETURN
C END

C THERMAL CONDUCTIVITY, W/(M C)
C FUNCTION FLCOND(T)
C $FLCOND = 0.0802 - 2.03E-04 * T$
C RETURN
C END

C ***** VAPOR PHASE PROPERTIES *****

C ABSOLUTE VISCOSITY, KG/(M S)
FUNCTION FVVIS(T)
FVVIS=(0.920+3.0E-03*T)*1.0E-05
RETURN
END

C SATURATED VAPOR DENSITY, KG/(CU. M)
C EP = ABSOLUTE PRESSURE, KPA
FUNCTION FSVDEN(T,EP)
ERP=EP/3413.0
ZS=(1.0+0.636*ERP**0.816)**(-1.0)
FSVDEN=187.39*EP*1000.0/ZS/8314.0/(T+273.15)
RETURN
END